Niobium-based bifunctional catalysts for the direct conversion of synthesis gas to dimethyl ether

Author:
David Verbart

Daily supervisor:
C. Hernández Mejía, MSc.
Project supervisor:
Prof. dr. ir. K.P. de Jong
Second examiner:
Dr. J. Zečević

Utrecht University

Inorganic Chemistry and Catalysis, Faculty of Science, Utrecht University
February 2018

Abstract

Dimethyl ether is currently used as an aerosol propellant, but has gained interest over the last decade for its use as a clean burning fuel. The most applied synthesis of dimethyl ether currently follows a two-step mechanism: first, methanol is first synthesised from synthesis gas (a mixture of CO and H_2), then this methanol is dehydrated to form dimethyl ether in a separate reactor. However, dimethyl ether can be synthesised directly from synthesis gas using a bifunctional catalyst. This catalyst contains both the methanol synthesis functionality and a dehydration functionality. For this Cu/ZnO can be combined with an solid acid such as niobic acid. Benefits of this direct synthesis method include the higher possible CO conversions that can be obtained, and the elimination of expensive methanol separation and purification steps. Much research on this direct conversion of synthesis gas to dimethyl ether focusses on the application of alumina or zeolites as solid acids, while niobic acid has proven to be extremely suited for these dehydration reactions. Various synthesis methods were used to yield niobium-based bifunctional catalysts for this reaction. The various properties of these catalysts were characterised, such as their acidic properties, surface area and spatial distribution of the different elements. Catalysts were synthesised with the aim in mind to separate the Cu/ZnO from the niobium-based solid acid from nanometer to millimeter distance. Physical mixtures, evaluated under industrially relevant conditions, showed superior activity and selectivity towards dimethyl ether. Catalysts prepared by co- or sequential precipitation, although having a closer proximity between the previously mentioned functionalities, were found to be both less active and less selective than the physical mixtures.

Contents

List of Figures

List of Tables

List of abbreviations

ANO	Ammonium niobium oxalate
BET	Brunauer Emmett Teller
BF	Bright field
CZA	Copper zinc aluminium oxide
CTY	Copper-time yield
DME	Dimethyl ether
DF	Dark field
DI	Deionized
EDX	Energy dispersive X-ray spectroscopy
FID	Flame ionization detector
FT	Fischer-Tropsch
GC	Gas chromatography
GHSV	Gas hourly space velocity
HAADF	High-angle annular dark field
H_2-TPR	Hydrogen temperature programmed reduction
ICP-MS	Inductively coupled plasma mass spectrometry
LPG	Liquefied petroleum gas
M	molar (i.e. $mol \cdot L^{-1}$)
NbO_x	Niobium oxides
NH_3-TPD	Ammonia temperature programmed desorption
NO_x	Nitrogen oxides
NPs	Nanoparticles
SO_x	Sulphur oxides
SSA	Specific surface area
STD	Syngas to dimethyl ether
STEM	Scanning transmission electron microscopy
TCD	Thermal conductivity detector
TEM	Transmission electron microscopy
TGA	Thermal gravitational analysis
TOS	Time on stream
WGS	Water-gas shift
XRD	X-ray diffraction

Chapter 1

Introduction

1.1 Background

As the energy consumption rises, and oil reserves are depleting, the need for transportation fuels derived from carbon–based feedstock other than oil (such as biomass, natural gas and coal) becomes more and more relevant[1]. From the mid-1900s onwards, petroleum derived fuels have accounted for most of the global energy consumption, however the share of oil has fallen from almost 50% to little over 30% from 1973 to 2016[1]. With oil prices varying largely over time, mostly due to political events as can be seen in Figure 1.1, the decrease of reliance on oil exporting countries can be seen as a national security strategy and has economical benefits[2].

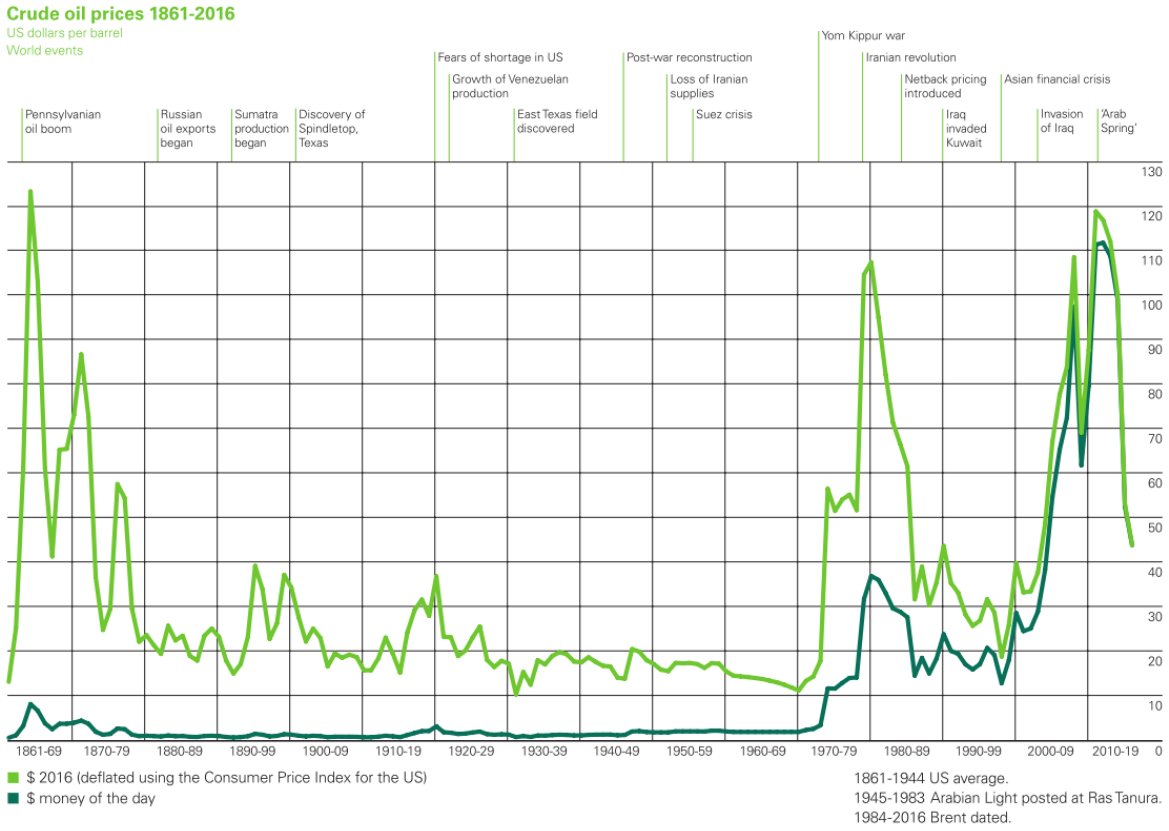

Figure 1.1: The evolution of oil prices from 1861–2016, in light green the prices adjusted for inflation. Image reproduced from[1]

Although petroleum-derived fuels are of great importance to our society, their use comes with negative effects. Due to impurities in the hydrocarbon feedstock used, nitrogen oxides (NO_x), sulphur oxides (SO_x) are amongst the combustion products, as well as particulate matter. These nitrous and sulphuric oxides cause acid rain, which in turn damages soil, causes deforestation and disrupts the ecosystem. Particulate matter in the air has a significant effect on global health, mostly in urban areas, and it is estimated to be responsible for many diseases and deaths related to respiratory issues every year[3].

The transition of petroleum derived fuels towards sustainable energy sources that are completely carbon neutral, can be bridged by using fuels that can be derived from alternative carbon feedstock. This can thus be expected to have many advantages, both economical and environmental. Using established processes, such as the Fischer–Tropsch (FT) process, hydrocarbons can be derived from a mixture of carbon monoxide and hydrogen gas (CO and H_2, also called synthesis gas or syngas for short)[4]. This synthesis gas can be derived from carbon-based feedstock such as biomass, coal and natural gas. Recently, other chemicals are gaining attention for their use as a sustainable energy source, one example of such a chemical is dimethyl ether (DME, CH_3OCH_3)[5–8]. While DME already knows many applications, both in the personal care (as an aerosol propellant) and chemical industry, it is currently being investigated for its use as a clean fuel.[9;10].

Dimethyl ether is a relatively clean fuel with only CO_2 and H_2O as combustion products, since DME is free of sulphur/nitrogen contaminations[11;12]. Particulate matter is not generated upon combustion, as DME lacks C–C bonds. DME can also serve as a hydrogen carrier, by reformation to CO and H_2, for fuel cell applications. The currently existing infrastructure for liquified petroleum gas (LPG, a mixture of mostly propane and butane) can be used for the storage and transportation of DME with little adaptions, due to their similar physical properties. The use of DME as cooking fuel has many benefits over coal and methane. Cooking with solid fuels, which are extensively used in rural areas in countries such as China, leads to health-damaging effects due to high concentrations of pollutants[13]. DME is considerably less harmful to the environment than methane, as it breaks down within 3–30 hours by a photochemical reaction to CO_2 and H_2O[14], whereas unburned methane (CH_4) has a greenhouse potential far higher than CO_2[15].

Today, the conventional way of producing DME is an indirect method, consisting of two separate steps: 1, the synthesis of methanol from synthesis gas, or syngas, (a mixture of CO and H_2, often containing small amounts of CO_2); 2, the dehydration of purified methanol over a solid acid catalysts in a second reactor[8]. In recent years the direct synthesis of dimethyl ether from syngas (STD, syngas to dimethyl ether) has gained considerable attention[8]. In this direct method, synthesis gas is converted into methanol and subsequently dehydrated to DME, in the same reactor, combining two distinct catalysts[16]. The cost of methanol separation and preparation for the DME synthesis feed are hereby avoided[17]. Another benefit of this direct synthesis method is that the thermodynamically limited methanol synthesis reaction can be shifted towards higher syngas conversion by consuming methanol to form DME[18;19].

1.2 Indirect synthesis method

1.2.1 Methanol synthesis

Background

The first process in the synthesis gas to dimethyl ether (STD) reaction is the methanol synthesis from syngas, for which the main reactions that are involved are the hydrogenation of CO, CO_2 and the water gas shift reaction, these are listed in Equations 1.1, 1.2

and 1.3 respectively[17]. As these reactions are exothermic and result in volumetric contraction, according to Le Chatelier's principle low temperatures and pressures are the preferred reaction conditions. For this process, the earliest developed catalysts consisted of zinc oxide (ZnO) and chromium oxide (chromia, Cr_2O_3). As this catalyst was not very active, high temperatures of 200–600 °C and pressures exceeding 50 bar were needed[20]. More active catalysts, mainly consisting of copper, were developed later on, but these were more susceptible for poisoning due to sulphur contaminations[21–23]. Synthesis gas derived from natural gas contains less of these sulphur contaminants than synthesis gas derived from coal. Therefore, a shift in syngas derived from coal to syngas derived from natural gas meant less poisons and increased the economic viability of copper-based catalysts for methanol synthesis[23]. The first industrial application of these copper-based catalysts was the low-pressure methanol process, introduced by Imperial Chemical Industries in the 1960s. This process could be operated at pressures as low as 30 bar and temperatures ranging from 220–300 °C[23;24]. These milder conditions resulted in the reduced formation of by-products, and a methanol selectivity greater than 99% could be reached[23]. Modern catalysts for methanol synthesis still consist mainly of copper, zinc and aluminium (CZA), but are improved by adding trace amounts of promotors such as magnesium[23]. Typical weight ratios of $CuO/ZnO/Al_2O_3$ found in catalysts used in industry are $\sim 60/30/10$[24].

$$CO + 2H_2 \rightleftharpoons CH_3OH \quad \Delta H_{298K} = -90.4 \text{ kJ/mol} \tag{1.1}$$

$$CO_2 + 3H_2 \rightleftharpoons CH_3OH + H_2O \quad \Delta H_{298K} = -49.4 \text{ kJ/mol} \tag{1.2}$$

$$CO + H_2O \rightleftharpoons CO_2 + H_2 \quad \Delta H_{298K} = -41.0 \text{ kJ/mol} \tag{1.3}$$

The active site

The active site and exact mechanism of methanol synthesis over these CZA-catalysts has been greatly investigated[25;26]. Among the proposed active sites are: metallic copper (Cu^0)[27;28], Cu^+ ions[29;30] and Cu^- ions, residing at the copper-zinc oxide interface[31;32]. Other reports ascribe the methanol formation to a strong metal-support interaction (SMSI)[33–38]. The term "strong metal-support interaction" is used to describe the changes in bonding onto the metals that are supported on reducible metal oxides[39;40]. Although this SMSI can give rise to various effects, and is a very interesting phenomenon, an in-depth review of this effect is beyond the scope of this research. Aside from the metal-support interaction between copper and zinc oxide, zinc oxide has promoting effects within these CZA-catalysts. The presence of zinc oxide as a structural promotor is clear as it results in an increased dispersion of copper, thus preventing the sintering of copper particles[41]. Additional promoting effects of zinc oxide have been ascribed to the formation of highly active copper surfaces[42;43]. It has been concluded that a close proximity between metallic copper step sites and zinc oxide is essential for methanol synthesis using the CZA-catalysts[25]. These promoting effects (i.e. more active and more stable catalysts) of zinc oxide are as beneficial for methanol synthesis from syngas as they are for the direct synthesis of dimethyl ether from syngas.

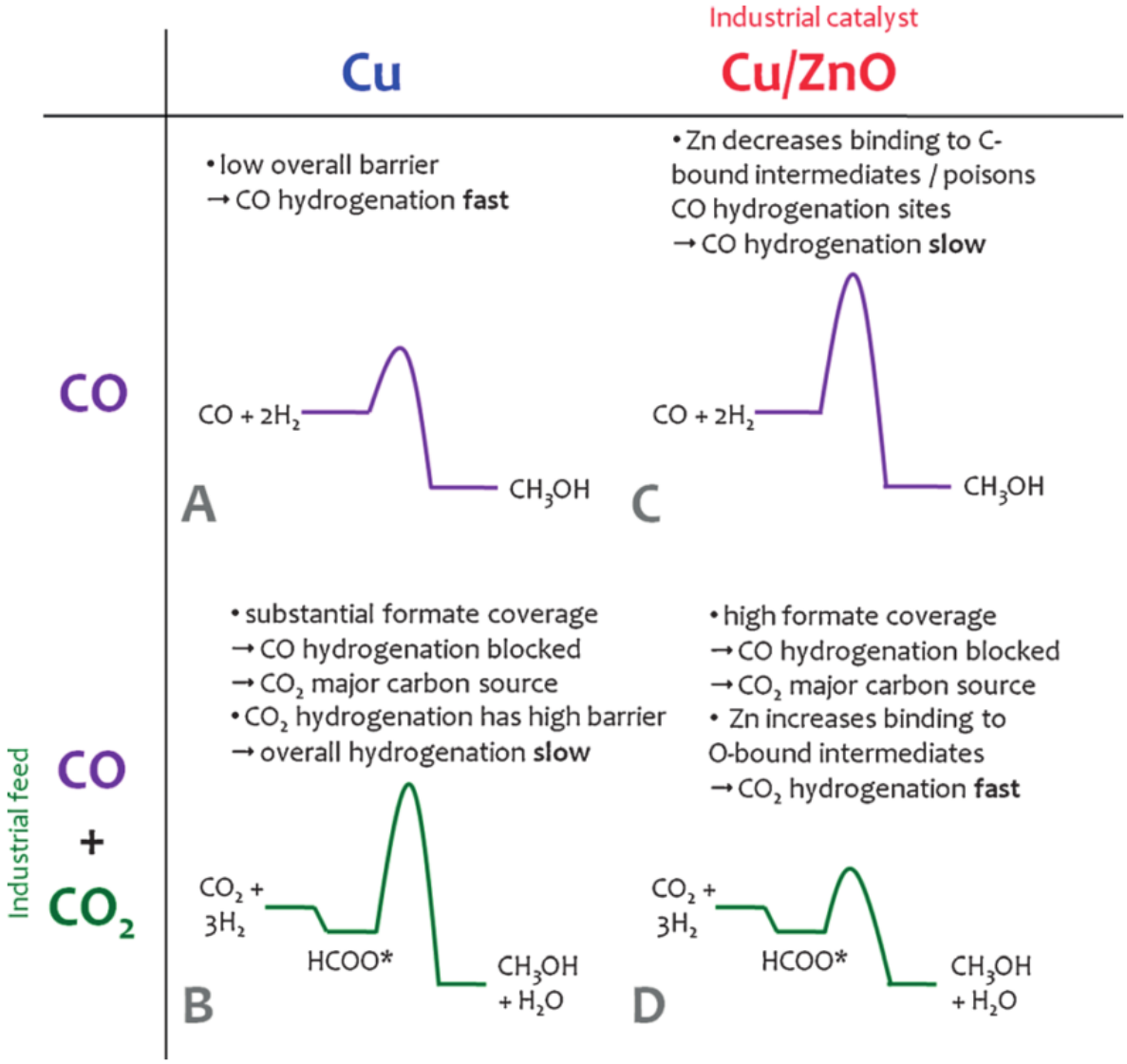

Figure 1.2: Mechanism of syngas hydrogenation to methanol over Cu and Cu/ZnO catalysts. **A**, hydrogenation of CO to methanol over metallic Cu; **B**, hydrogenation of the industrial feed, containing both CO and CO_2, over metallic Cu; **C**, hydrogenation of CO over the industrially used catalysts containing Cu/ZnO; **D**, hydrogenation of the industrial feed over the industrially used catalysts. Image reproduced from [26]

The role of CO and CO_2

Whether methanol is formed by the hydrogenation of carbon monoxide (Eq. 1.1) or carbon dioxide (Eq. 1.2) has been researched extensively [22]. The presence of CO_2 in the syngas used was found to have no influence in the methanol synthesis process at first, when a ZnO/Cr_2O_3 catalyst was used, operated at high pressures and temperatures [22]. Because of this, CO was long thought to be the main carbon-source in methanol synthesis. Only when copper-based catalysts were used, it was found that the presence of small amounts of CO_2 was beneficial to methanol synthesis [44]. Radioactive labelling studies

later on confirmed that CO_2 was indeed hydrogenated to methanol over these kind of catalysts[45;46]. However it took some time to accept these findings, as CO_2 was also found to poison copper-catalysts that didn't contain any zinc oxide[47]. Later studies, combining theoretical calculations and experimental results, have shown that the hydrogenation of CO or CO_2 is preferred over copper and copper-zinc oxide catalysts respectively[26]. Figure 1.2 schematically illustrates the difference in four distinct cases of syngas hydrogenation to form methanol. The hydrogenation of CO over a Cu catalysts is shown to be fast, due to its low energy barrier (case **A**). However, CO hydrogenation over an industrial catalyst consisting of Cu/ZnO is slow (shown in case **C**), as the presence of zinc results in a decreased binding of the intermediates. An industrial feed, containing CO and CO_2, results in a slow overall hydrogenation when a Cu catalyst is used (case B). This is due to a substantial formate coverage that blocks the CO hydrogenation. When the industrial feed and Cu/ZnO catalyst are used however, the presence of Zn in the catalysts increases the binding to oxygen-bound intermediates and the high formate coverage results in high overal hydrogenation of CO_2 (case D).

Catalyst preparation

The synthesis of an active, selective, and stable CZA-catalyst for methanol synthesis has been extensively researched[22;48–53]. The conventional way of catalysts preparation for these kind of catalysts is co-precipitation[49]. In this technique, the precursor salts of the active metal and support are dissolved in the same solution, and the solid precursor to the active metal and support is obtained in a single step[54]. Benefits of this technique are the high metal loadings (more than 70 wt.%) and small particle sizes that can be achieved simultaneously. Small particle sizes are often desired due to their high surface to volume ratios, effectively resulting in more active sites per weight of metal, thus resulting in more active catalysts. The formation of these small particles is a direct result of the degree of supersaturation: a very high degree of supersaturation will result in a high nucleation rate for all components and at the same time[54;55].

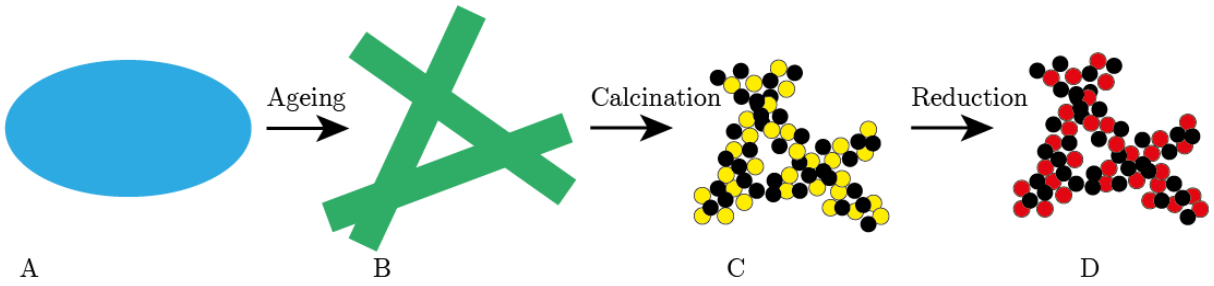

Figure 1.3: Illustration of a catalysts for methanol synthesis prepared by co-precipitation. The amorphous co-precipitate (A) chrystallizes during aging (B). Subsequent calcination yields (C) crystalline metal oxide nanoparticles (yellow) on a support (black). Prior to reaction, the metal oxides are reduced to form (D), with metallic nanoparticles (red). Image adapted from[56]

As previously mentioned, copper-based catalyst for methanol synthesis mostly contain copper, zinc oxide and aluminium oxide (CZA-catalysts). Copper and zinc molar ratios of ∼70:30 are among the most frequent encountered catalysts as this results in the formation of porous aggregates consisting of Cu/ZnO nanoparticles (NPs)[25]. Increasing the Cu content even further results in much larger CuO particles, and thus a significant decrease of the Cu surface area[57]. First, the metal nitrate salts are dissolved in their corresponding ratios, to yield one aqueous solution. Precipitation is induced by addition of a base, sodium carbonate is amongst the most used for this purpose. The presence of sodium is undesired in the final catalyst as this makes the reduction of CuO to metallic Cu difficult[58], so extensive washing steps are needed for its removal. The use of ammonium bicarbonate instead of sodium carbonate reduces the amount of water needed for the washing steps, making it a greener (i.e. more sustainable) synthesis method[53]. Many factors determine the catalytic performance of the obtained catalysts, including the pH of the solution during the synthesis[49;56;59] and the pH/temperature of the aging period[56;60]. The catalyst precursor is then dried and calcined at 600-700 K[56]. This causes the decomposition of the precursor, yielding metal oxide nanoparticles. As the previously described active site in methanol synthesis consists of metallic copper and zinc oxide, the copper oxide needs to be reduced to metallic copper. Prior to reaction the CuO/ZnO is reduced to yield the active catalyst. These steps are schematically represented in Figure 1.3.

1.2.2 Dimethyl ether synthesis

After the formation of methanol, the second distinguishable step in dimethyl ether synthesis is the dehydration of methanol, shown in Equation 1.4[17]. This dehydration is usually executed over a solid acid catalyst[61], and favoured at lower temperatures as it is an exothermic process. At higher temperatures, the formation of unwanted by-products such as olefins or hydrocarbons becomes more significant[62].

$$2CH_3OH \rightleftharpoons CH_3OCH_3 + H_2O \quad \Delta H_{298K} = -23.0 \text{ kJ/mol} \tag{1.4}$$

The active site

Suggested reaction mechanisms of this reaction follow either Langmuir-Hinshelwood kinetics or Eley-Rideal kinetics[8]. Langmuir-Hinshelwood kinetics are schematically represented in Figure 1.4. The individual steps of this reaction mechanism can be distinguished as: adsorption of methanol to the catalytic surface (Fig. 1.4 **A** & Eq. 1.5 and 1.6), reaction on the catalytic surface forming the DME and H_2O (Fig. 1.4 **B** & Eq. 1.7) and desorption of these products (Fig. 1.4 **C** & Eq. 1.8). Evidence that the solid acid catalysed methanol dehydration follows this type of reaction can be found in literature[63;64].

$$A + * \rightleftharpoons A* \tag{1.5}$$

$$B + * \rightleftharpoons B* \tag{1.6}$$

$$A* + B* \rightleftharpoons AB* + * \tag{1.7}$$

$$AB* \rightleftharpoons AB + * \tag{1.8}$$

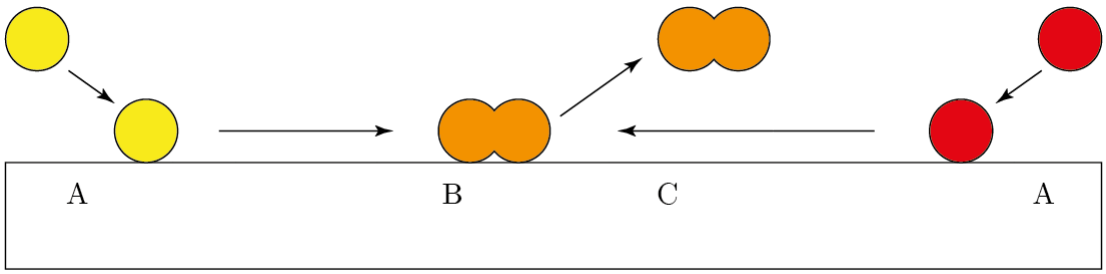

Figure 1.4: Generalised illustration of Langmuir-Hinshelwood kinetics. The individual steps are: **A** adsorption of one of the reagents (yellow or red) to the catalytic surface; **B** reaction of the adsorbed reagents (yellow and red) with one another, forming the reaction product in the process (orange); **C** desorption of the formed product.

Eley-Rideal kinetics are schematically represented in Figure 1.5. In this model, first one molecule of methanol adsorbs on the catalytic surface (Fig. 1.5 **A** & Eq. 1.9). The other molecule then, while not being adsorbed to the surface, reacts with its adsorbed counterpart, creating DME and H_2O (Fig. 1.5 **B** & Eq. 1.10). In the final step, the products desorb from the surface (Fig. 1.5 **C** & Eq. 1.11). Evidence that methanol dehydration to dimethyl ether over a solid acid follows a likewise mechanism is indicated by Kiviranta-Pääkkönen et al. and Lei et al.[65;66].

$$A + * \rightleftharpoons A* \tag{1.9}$$

$$B + A* \rightleftharpoons AB* \tag{1.10}$$

$$AB* \rightleftharpoons AB + * \tag{1.11}$$

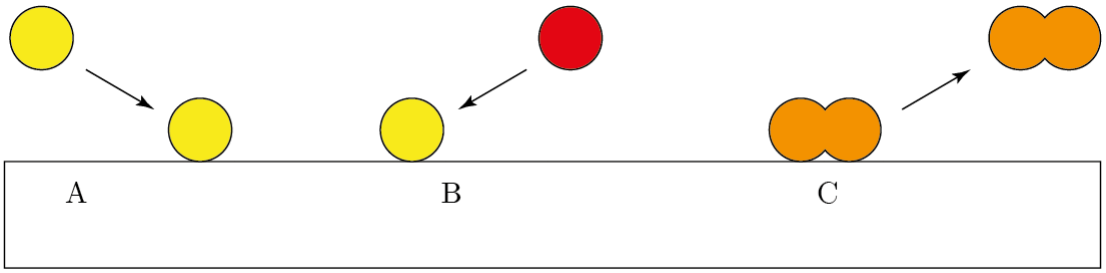

Figure 1.5: Illustration of Eley-Rideal kinetics. The individual steps are: **A** adsorption of one of the reagents (yellow) to the catalytic surface; **B** reaction of the adsorbed reagent (yellow) with another reagent that is not adsorbed to the catalytic surface (red), forming the reaction product in the process (orange); **C** desorption of the formed product.

The dehydration of methanol to form DME can occur over Lewis acid-base pairs[67–69] and Brønsted acid-Lewis base pairs[64;70;71]. Although acid sites are essential for this dehydration reaction, the presence of too strong acid sites was found to have a negative effect on the catalytic performance. Catalysts containing weaker acid sites show higher selectivity towards DME, while the presence of strong acid sites results in significant formation of by-products such as light olefins and heavy hydrocarbons[72;73]. The solid acid best suited for this dehydration is not dependent solely on the acidity. The stability of the catalyst used, its side product formation and the costs are all important factors.

Solid acids

As one of the reaction products is water, the catalyst's tolerance for water is of great importance for its application in the methanol dehydration reaction. Many solid acids have been investigated for their application in this reaction, including (modified) alumina, ion-exchange resins, titania-zirconia (TiO_2−ZrO_2) and various zeolites.[17;66;74–79]. The most studied solid acids for the methanol dehydration reaction towards DME are γ-alumina and various zeolites, due to their well know properties.

The application of aluminium-based compounds (e.g. Al_2O_3) for the dehydration of methanol to form DME has already been known for a long time[80]. The benefits of using (modified) alumina include its high mechanical and thermal stability. γ-Al_2O_3 contains mainly Lewis-acid sites, and shows high selectivity towards DME when applied as a methanol dehydration catalyst. However, water is strongly adsorbed to these acid sites, resulting in a loss of activity[78;81]. Aluminium phosphate ($AlPO_4$) or alumina modified with phosphate shows stronger acidity, and thus show higher activity for the methanol dehydration, than regular γ-Al_2O_3[82–85].

Zeolites such as H-ZSM-5 and Faujasite (zeolite-Y) are know for their Brønsted-acid character, and are extensively researched for their application as methanol dehydration catalysts[75;79]. The acidic character of zeolites results in high methanol conversion and high DME yields, even at low temperatures. The diffusion of DME through the small zeolite pores is restricted, increasing the chances of subsequent dehydration. The dehydration of DME results in the formation of hydrocarbons and coke, deactivating the zeolite catalyst in the process. To prevent this deactivation, zeolites can be treated to deactivate these strong acid sites[72].

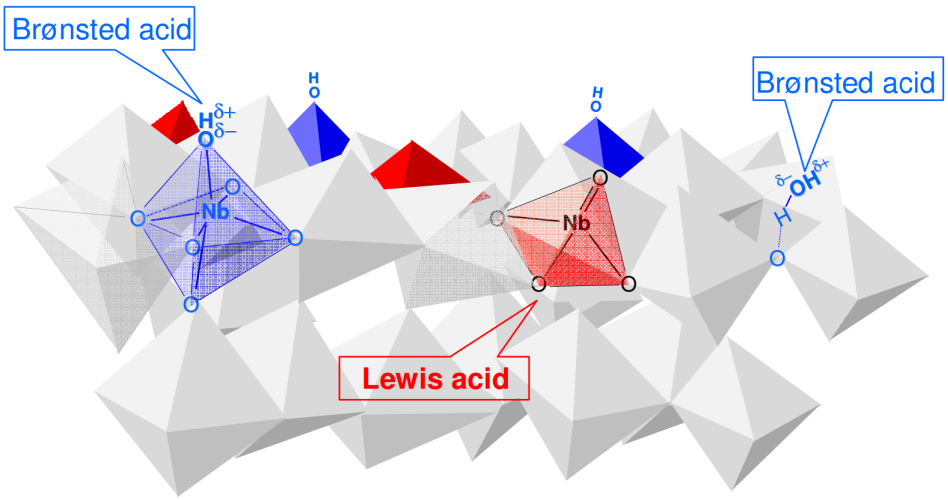

Figure 1.6: Schematic structure of niobic acid, with Brønsted and Lewis acid sites illustrated. Reproduced from[86]

Niobium-based materials, such as niobium pentoxide (Nb_2O_5), are well known for their acidic properties and show great potential for catalytic applications[87–89]. The hydrated form of niobium pentoxide (niobic acid, $Nb_2O_5 \cdot nH_2O$) is a well know solid acid, containing both Brønsted and Lewis acid sites[90]. The surface acidity of niobic acid corresponds to an acidity of 70% sulphuric acid[87;88]. Niobium phosphate, $NbOPO_4$, showed more and stronger acid sites than niobic acid[90]. Niobium-based compounds have been extensively researched for their application in the dehydration reaction of methanol to form DME[89–94]. Metal oxides typically show a loss in activity in dehydration reactions, as the formed water can inhibit the active (Lewis acid) sites[95–97]. For niobic acid however, it has been

shown that its Lewis acid sites can still be catalytically active while in the presence of water[98]. The lewis acid sites of niobic acid originate from NbO_4 tetrahedra on the surface, forming NbO_4-H_2O adducts upon the inhibition of water. Unlike many other metal oxides, such as γ-Al_2O_3 this does not result in complete deactivation, as the acid sites are still accessible[86]. This exceptional quality makes niobic acid very suitable for the methanol dehydration reaction[90;91]. A visual representation of the acid sites of niobic acid are represented in Figure 1.6[86]. The vast research on niobium-based compounds has lead to the discovery of unique qualities, and they have found their application as a catalyst for many different reactions[99] (e.g. isomerisation, polymerisation, dehydration[100–102], esterfication[87], hydration[103] and oxidation[104]). Examples of this include novel materials with various applications[105–108], tuning the surface acidity of Al_2O_3 with deposition of Nb_2O_5[92;109–111], and as support/promotor for many reactions[112–114].

1.3 Direct synthesis method

The synthesis of dimethyl ether from syngas in one step is known as the direct synthesis method. In this reaction, syngas is fed and converted to methanol which is subsequently dehydrated over a solid acid catalyst. The basic reactions that are involved in this direct STD reaction are Eq. 1.1 - 1.4.

Upon dehydration of methanol to DME (Eq. 1.4), the equilibrium of Equation 1.1 and 1.2 shifts in favour of methanol formation[18;19]. The water generated in this process will be removed from the system by the water-gas shift reaction (Eq. 1.3). This shift in equilibrium can be clearly seen in Figure 1.7. Calculated equilibrium compositions are given in Figure 1.8. From these calculation we can clearly see that DME is the main product of this reaction. However, the formation of water upon methanol dehydration is responsible for the considerable amount of CO_2 being formed due to the water-gas shift reaction. As higher conversions are the main benefit of this direct synthesis method, additional benefits include the price independence of DME to methanol. Methanol purification and separation steps can be avoided, making this synthesis method economically more favorable than the two-step process[12;17;95;115;116].

In this reaction, both methanol synthesis and dehydration need to be facilitated. Catalyst containing multiple functionalities, thus catalysing multiple kinds of reactions, are so-called bifunctional catalysts. As previously mentioned, most of the recent research focus on this method of dimethyl ether synthesis[8]. The commonly applied methanol synthesis catalysts are the previously mentioned CZA-catalysts, and many different solid acids are being used for the subsequent dehydration of methanol[72;73;79;95]. Niobium-based materials, such as modified γ-Al_2O_3, outperforms regular γ-Al_2O_3 as dehydration catalyst in these bifunctional materials[92;93].

1.3.1 Catalyst deactivation

As water is a dominant product of the dimethyl ether synthesis, this have a significant effect on the performance of the bifunctional catalyst. Water can react according to

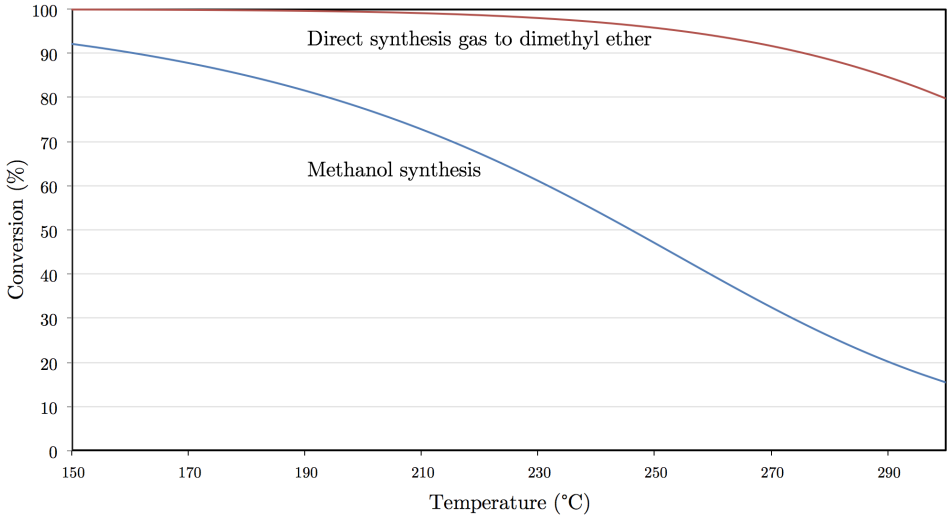

Figure 1.7: CO conversions of methanol synthesis from syngas (blue) and direct dimethyl ether synthesis from syngas (red). Calculations were performed at 40 bar total pressure, in the temperature range from 150–300 °C, $H_2/CO=2$. Calculated using the HSC software from Outotec, v 7.14.

Equation 1.3, forming CO_2. However, high amounts of water present can result in catalyst deactivation. Either by deactivation of the CZA catalyst, as it assists the sintering of copper particles[117;118]. The solid acid can deactivate by adsorbing water too strongly, thus no longer being able to catalyse the dehydration of methanol, or dehydrating DME to form hydrocarbons and carbonaceous materials[119].

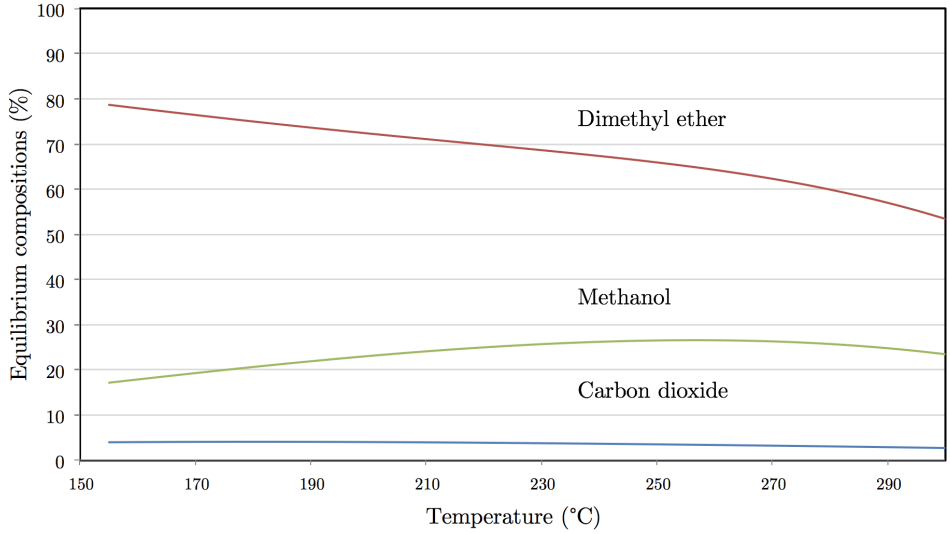

Figure 1.8: Equilibrium compositions of the synthesis of DME from syngas. DME selectivity in red, methanol selectivity in blue, CO_2 selectivity in green. Calculated at 40 bar total pressure, in the temperature range from 150–300 °C, $H_2/CO=2$. Calculated using the HSC software from Outotec, v 7.14.

1.3.2 Proximity effect

In bifunctional catalysts, the distance between the two functionalities can be anywhere in the nanometer to micrometer range. The importance of this proximity was first described in 1962 by P.B. Weisz, and has been investigated for many bifunctional catalytic reactions since[120–125].

For hydrocracking catalysts, the (de)hydrogenation reactions are catalysed by metal sites, while the isomerization and cracking reactions are catalysed by acid sites. Both de ratio of metal to acid sites and their relative proximity are of great importance to these reactions[120;126]. In this bifunctional reaction, the reaction intermediate has to diffuse between the two different active sites. Too low diffusivity and too large distances will result in lower activity due to the formation of concentration gradients. Not just activity, but also selectivity have found to vary, depending on this intimacy. For this specific reaction (the hydrocracking reaction) the general belief has been that closer proximity is better, while new research is changing this by showing contradictory proof[127]. While multiple hydrocracking occurrences on one very long chain hydrocarbon are not uncommon, further dehydration of DME is unwanted as this might form hydrocarbons or coke. An increased distance between acid sites can be expected to be beneficial to the selectivity towards DME, as this reduces the possibility of subsequent dehydration. Pd/zeolite bifunctional systems have been investigated for their conversion of syngas into DME, methanol and hydrocarbons. For these systems, DME conversion on (Brønsted) acid sites results in the formation of olefins (alkenes) that can be hydrogenated on the Pd sites to form paraffins (alkanes). This process effectively stops the chain growth. For this system, the selectivity toward branched products was found to decrease with increased proximity between the Pd/acid sites[121]. However, (long chain) hydrocarbons are not expected to be main products in the syngas to DME reaction over CZA/niobic acid-catalysts, nor is Cu a very active (de)hydrogenation catalysts compared to Pd. Therefore the proximity effect can be very different from the Pd/zeolite system.

1.4 Research aim

The goal of this research is to gain insight in niobium-based bifunctional catalysts for the direct conversion of synthesis gas to dimethyl ether. For this, two main research questions have been lined out.

1. How does the synthesis procedure relate to the proximity between different functionalities in these catalysts?

2. How does the synthesis procedure relate to the characteristics of these bifunctional catalysts?
   e.g. the acidic properties, crystallite phases present and surface area

To answer these questions, various synthesis methods to create niobium-based bifunctional catalysts were devised. The proximity between the different functionalities was studied using advanced microscopy techniques. As the acidic functionality is of great importance in the STD reaction, quantification of acid sites was evaluated using temperature programmed desorption of basic probe molecules. For the evaluation of the catalytic performance, synthesised catalysts were submitted to industrially relevant conditions. The catalysts' activity, selectivity towards certain products, and stability (loss of activity or selectivity over time) were evaluated. The structure-performance relationships were elucidated by combining the information obtained about these catalysts. The eventual goal of this project was to effectively combine both the methanol synthesis and methanol dehydration components without losing one functionality. This is of great importance in order to answer the research questions listed above with certainty.

In **Chapter 2**, the synthesis methods and characterisation techniques will be described. The results of these characterization methods will be discussed in **Chapter 3, Chapter 4 and Chapter 5**, in these chapter the catalytic performance will also be evaluated. **Chapter 3** will first discuss the various methanol synthesis catalysts, then the solid acid catalysts and lastly the physical mixtures thereof. In **Chapter 4** the catalysts that were prepared by co-precipitation will be discussed. The catalysts that were prepared by sequential precipitation will be discussed in **Chapter 5**. The results will be correlated to answer the research questions in **Chapter 6**. Proposed future work will be discussed in **Chapter 7**.

Chapter 2

Experimental methods

2.1 Catalyst preparation

2.1.1 Chemicals used

In Table 2.1 detailed information is listed on the chemicals that were used during the preparation of different catalysts. Chemicals were used without further treatment or purification.

Chemical	**Formula**	**Supplier**	**Quality**
Copper-based catalyst for methanol synthesis	$CuO/ZnO/Al_2O_3/MgO$	Alfa Aesar	
Ammonium bicarbonate	$(NH_4)HCO_3$	Acros Organics	
Copper nitrate trihydrate	$Cu(NO_3)_2 \cdot 3\,H_2O$	Acros Organics	≥99%
Zinc nitrate hexahydrate	$Zn(NO_3)_2 \cdot 6\,H_2O$	Sigma Aldrich	≥99%
Aluminium nitrate nonahydrate	$Al(NO_3)_3 \cdot 9\,H_2O$	Acros Organics	
Ammonium niobium oxalate hydrate	$NH_4[NbO(C_2O_4)_2(H_2O)]_2 \cdot nH_2O$	CBMM	
Niobic acid	$Nb_2O_5 \cdot nH_2O$	CBMM	
Oxalic acid dihydrate	$C_2H_2O_4 \cdot 2\,H_2O$	Sigma Aldrich	≥99%
Acetone	CH_3COCH_3	VWR	≥99%
Water	H_2O	Millipore	Type 1

Table 2.1: Chemicals used

The catalyst from Alfa Aesar was supplied as pellets, with dimensions of 5.4 by 3.6 mm, but crushed and sieved (38–150 μm) prior to use. The composition of this catalyst was determined by Alfa Aesar at 10.1 wt.% Al_2O_3, 63.5 wt.% CuO, 24.7 wt.% ZnO and 1.3 wt.% MgO (product number 45776; lot number I06Z036). One batch of niobic acid was calcined at 400 °C, this was used later on. Deionized water was supplied by the in-house Direct-Q® 3 UV system, from Millipore. Type 1 water indicates a resistivity of 18.2 MΩ·cm at 25 °C.

2.1.2 Physical mixtures

Physical mixtures were prepared in order to obtain bifunctional catalysts, in which the aimed distance between the two functionalities (i.e. methanol synthesis and dehydration sites) are separated in the micrometer range. For these physical mixtures first the individual catalysts need to be prepared. After synthesis of these catalysts, the two components were ground together using a mortar and pestle. If necessary, the mixture was compressed and crushed again in order to obtain the desired amount in the desired sieve fraction. The mixed catalysts were subsequently sieved and kept in order to evaluate their catalytic performance.

Using this procedure, different methods can be distinguished in the prepared physical mixtures:

1. Catalysts prepared from combination of commercially available methanol synthesis catalyst and niobic acid.
2. Catalysts whose precursors were precipitated by using ammonium (bi)carbonate as a precipitating agent.
3. Catalysts whose precursors were precipitated by using oxalic acid as a precipitating agent.

The reasoning behind choosing these different precipitating agents will be explained later on in this section.

Precipitation using ammonium bicarbonate

As previously mentioned, extensive research has been done on the synthesis of a CZA-catalyst for methanol synthesis. These syntheses make use of the co-precipitation method, in which the metal nitrates salts are first all dissolved in the same aqueous solution. Precipitation is induced by the addition of a base, often sodium carbonate, effectively raising the pH. The precipitate is washed to remove residual sodium and nitrate ions as this can poison the catalysts[55]. Controlling the conditions (e.g. temperature, pH and concentration) during the precipitation and ageing process is essential when preparing the catalysts precursor. The desired catalyst precursor is zincian malachite ($(Cu,Zn)_2(OH)_2CO_3$ with a copper content of 73-100%), this has been shown to yield the most active CZA-catalyst upon thermal decomposition[22]. To reduce the amount of washing steps needed to obtain a poison-free catalyst, the use of other bases as precipitating agent has been investigated. Ammonium bicarbonate ($(NH_4)HCO_3$) was used as a base, as this easily decomposes at moderately elevate temperatures[53]. The copper catalyst for methanol synthesis and niobium-based solid acid were synthesized separately.

Methanol synthesis catalyst

The CZA-catalyst for methanol synthesis was synthesized as described in literature[49]. Copper nitrate trihydrate, zinc nitrate hexahydrate and aluminium nitrate nonahydrate were used. A solution of these salts was prepared by dissolving these in deionized (DI) water in a 66:17:17 molar ratio, with a total metal ion concentration of 1.1468 $mol \cdot L^{-1}$. Precipitation was induced by raising the pH to $\sim$7 using an aqueous solution of ammonium bicarbonate (1.44 $mol \cdot L^{-1}$). This solution was added dropwise using a Pasteur pipette. The precipitate was separated from the supernatant using a Büchner funnel and subsequently washed with DI water. After this, the product was dried at 80 °C for 3 hours and subsequently calcined at 400 °C for 2 hours, using a heating rate of 5 $°C \cdot min^{-1}$, in a muffle oven.

Niobium-based solid acid catalyst

Many niobium precursors show a low solubility in water and readily decompose, forming gases and toxic substances[128]. Ammonium niobium oxalate (ANO) shows a relatively high solubility in water, ranging from 60 to 160 grams of niobium per liter (between 20 and 80 °C)[128;129]. The chemical formula and structure of ANO are shown in Table 2.1 and Figure 2.1 respectively. 250 mL of 0.01444 mol·L^{-1} ANO in DI water solution was prepared. The aforementioned ammonium (bi)carbonate solution was added using a syringe pump (∼50 mL, 2 mL·min^{-1}) to raise the pH to ∼7, resulting in a white precipitate. This precipitate was separated from the supernatant using a Büchner funnel and washed with DI water. The product was dried at 120 °C for 3 hours and subsequently calcined at 400 °C for 2 hours, with a heating rate of 5 °C·min^{-1} in a muffle oven.

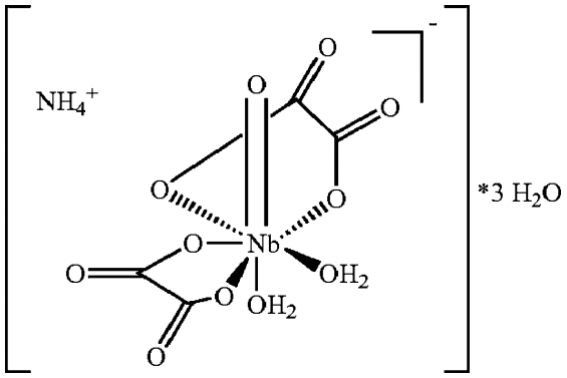

Figure 2.1: The molecular structure of ammonium niobium oxalate, reproduced from[129].

Precipitation using oxalic acid

As the most active precursor for a CZA-catalyst is zincian malachite, as previously mentioned, precipitation of the metal nitrate salt is induced by the addition of a base. However, this is not the only precipitation method available. When combined with an oxalic acid solution, poorly soluble copper and zinc oxalates are formed, which can be easily separated from the supernatant. An excess (2:1 molar ratio of oxalic acid:copper and zinc) solution of oxalic acid in acetone was used to precipitate copper and zinc oxalate. This method was applied in order to obtain well dispersed metal/niobia particles, as reported in literature[113]. In order to compare catalysts to the highest extend possible, this method was also applied in the synthesis of the individual components, and not just for the bifunctional catalysts.

Methanol synthesis catalyst

The CZA-catalyst for methanol synthesis was synthesized using an adapted method of those described by Xiang et al.[113], consisting of copper and zinc, instead of copper and cobalt. An aqueous solution was prepared of copper nitrate and zinc nitrate, in a 2.1:1 molar ratio. In total, 0.05928 moles of metal nitrate was dissolved in 25 mL DI water and 0.10699 moles of oxalic acid was dissolved in 350 mL acetone. Under constant stirring

the metal nitrate solution was added to the oxalic acetone solution and a precipitate was formed. The precipitate was separated from the supernatant by centrifuging, and washed with acetone. The products were dried at 60 °C overnight and subsequently calcined at 400 °C for 2 hours, with a heating rate of 5 °C·min^{-1} in a muffle oven.

Niobium-based solid acid catalyst

The niobium-based solid acid was synthesized using an adapted method of that described by Xiang et al.[113], i.e. the niobium precursor was precipitated by injection of an aqueous ANO solution into acetone. After precipitation of the niobium precursors, it was separated from the supernatant by centrifuging, and washed with either acetone. The products were dried at 60 °C overnight and subsequently calcined at 400 °C for 2 hours, with a heating rate of 5 °C·min^{-1} in a muffle oven.

2.1.3 Sequential precipitation

In this method, as the term indicates, the two active precursors are precipitated in a sequential manner. Because of this, the active components are expected to be less separated than the physical mixtures. Jeong et al. have published a take on this method in which they use this method, instead of the conventional co-precipitation, to modify the properties of the final catalyst (e.g. increasing the selectivity of a CZA-catalyst to produce more DME)[130]. Precipitation of the copper and zinc precursor, followed by the precipitation of the niobium precursor, was adapted from this method.

The first of the catalysts prepared by sequential precipitation were prepared by first precipitating the copper and zinc precursors, subsequently adding the ANO solution and again inducing precipitation, all by raising the pH with ammonium (bi)carbonate. Catalysts with different ratios were prepared according to the following method: First a copper and zinc nitrate solution was prepared by dissolving these salts in DI water yielding a ∼1.2M total metal ion concentration. This solution was diluted in a double walled, baffled vessel using DI water in order to monitor the pH and temperature of the solution. Under constant stirring and at 70 °C, the pH was slowly raised to ∼7 using the aforementioned ammonium bicarbonate solution to precipitate the copper and zinc precursor. After a short ageing period of 1 hour, the (acidic) ANO solution was added, decreasing the pH in the process. Again, ammonium (bi)carbonate was added to raise the pH to ∼7 as to precipitate the niobium precursor. After precipitation the product was separated from the supernatant by centrifuging and dried at 60 °C for multiple days. The final catalyst was obtained after calcination at 400 °C for 2 hours, with a heating rate of 5 °C·min^{-1} in a muffle oven.

The second way of catalyst preparation using this method is adapted from the method described by Xiang et al.[113] Two solutions were prepared, on of copper and zinc nitrate in DI water in a 2.3:1 molar ratio, and one of ANO in DI water. The exact concentrations and amounts varied depending on the desired ratio of Cu/Zn to Nb in the final product. This solution was poured into a solution of oxalic acid in acetone, at room temperature and under constant stirring at 400 rpm using an overhead stirring setup. After the near

immediate precipitation of the copper and zinc oxalates, the ANO solution was poured into the dispersion within seconds of the first addition. After precipitation, the precipitate was separated from the supernatant by centrifuging, and washed with acetone. The products were dried at 60 °C overnight, and subsequently calcined at 400 °C for 2 hours, with a heating rate of 5 °C·min^{-1} in a muffle oven.

2.1.4 Co-precipitation

Co-precipitation of the copper and zinc precursor with the niobium precursor was investigated, using the two different precipitation methods as previously mentioned. Co-precipitation was expected to yield the closest proximity between the two active components in the final products. In one method, the two precursor solutions (i.e. the aqueous copper/zinc nitrate solution and aqueous ANO solution) were added and precipitation was induced by the addition of an ammonium (bi)carbonate solution. In the other method, the two precursor solutions were added simultaneously into a solution of oxalic acid in acetone.

A copper/zinc nitrate solution was prepared by dissolving the salts into DI water, in a 2.3:1 molar ratio, yielding a 1M (total metal ion concentration) solution. Ammonium niobium oxalate was dissolved in DI water (the exact amount was dependent on the desired ratio of Cu/Zn to Nb) and an aqueous solution of ammonium bicarbonate was added to raise the pH to ∼7. The Cu/Zn nitrate solution was added dropwise to the ANO solution, 2 mL·min^{-1} using a syringe pump. The exact amounts that were used were dependent on the desired ratio of Cu/Zn to Nb. Precipitation occurred immediately upon addition of the Cu/Zn nitrate solution, while the pH decreased. The pH was increased again to 7, by dropwise addition of the ammonium bicarbonate solution. During the synthesis the temperature was kept constant at 65 °C using an oil bath, and the solution was stirred at 400 rpm using a stir bar. The resulting dispersion was left to age, typically for 1.5 h, until the pH remained stable. Products were obtained by filtration using a Büchner funnel, and washed twice with DI water. After drying the obtained product at 120 °C overnight they were calcined at 400 °C for 2 hours, with a heating rate of 5 °C·min^{-1} in a muffle oven.

The second way was adapted from the previously mentioned method as described by Xiang et al.[113] Instead of two separated additions, a dual syringe pump was used to add both solutions simultaneously. One syringe was filled with an aqueous solution of copper and zinc nitrate, the other was filled with an aqueous ANO solution. Concentrations of these solutions were dependent on the aimed final composition. The two solutions were simultaneously added (0.5 mL·min^{-1} per syringe, in total 1 mL·min^{-1} of volume was added) to a baffled vessel containing a solution of oxalic acid and acetone. After precipitation, the products were dried at 60 °C overnight. The final catalysts were obtained after thermal decomposition at 400 °C for 2 hours, with a heating rate of 5 °C·min^{-1} in a muffle oven.

2.2 Characterization

2.2.1 Powder X-ray diffraction

Powder X-ray diffraction (XRD) is used to determine the crystallite phases present in a system, as a qualitative bulk technique. X-ray photons are scattered by atoms in a periodic lattice. When these scattered photons are in phase the result is constructive interference, according to Bragg's equation (Equation 2.1)[131].

$$n\lambda = 2d\sin\theta \ ; \ n = 1, 2, 3, \ldots \tag{2.1}$$

In this equation, n is an integer, the order of reflection, λ is the wavelength of the used radiation, d the lattice plane distance, and θ the angle between the lattice plane and the incoming X-rays. In Figure 2.2 a schematic representation of X-ray diffraction is given.

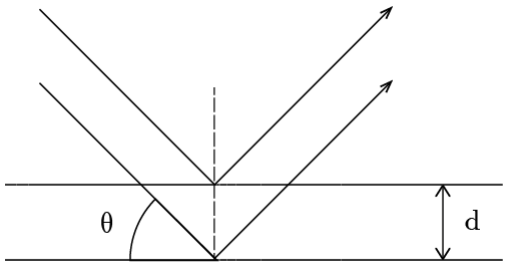

Figure 2.2: A schematic representation of X-ray diffraction by two lattice planes

Samples were analysed using a Bruker-AXS D2 Phaser, equipped with a Co Kα radiation source (λ = 1.79026 Å). The crystal phases expected in the synthesised catalysts (after calcination, prior to reduction) were CuO and ZnO, as niobic acid ($Nb_2O_5{\cdot}nH_2O$) is amorphous.

The Scherrer equation (Equation 2.2) can be used to determine the crystallite size from the obtained XRD data. For analysis of diffractograms the DIFFRAC.EVA and TOPAS by Bruker software were used. Diffraction patterns were obtained from 2θ = 10 to 80°, with a step size of 0.05 °and a time of 0.5 seconds per scan.

$$\tau = \frac{K\lambda}{\beta\cos\theta} \tag{2.2}$$

- τ is the mean size of the crystalline domain
- K is the dimensionless shape factor
- λ is the wavelength used by the X-ray diffractometer
- β is the line broadening at half the maximum (FWHM, full width at half maximum)
- θ is the Bragg angle in degrees

2.2.2 Nitrogen physisorption

Physisorption is a much used technique to characterize the specific surface area and porosity of materials[132;133]. Molecular nitrogen is very suited for this application, due to its physical properties such as small size and chemical inert nature. Due to nitrogens natural abundance in the atmosphere, an additional benefit is that it is relatively cheap. During physisorption experiments, the pressure is slowly increased from vacuum to the condensation pressure $p/p_0 = 1$. This causes nitrogen to physically adsorb to the surface of the sample, yielding the so-called adsorption isotherm in the process. Slowly decreasing the pressure from $p/p_0 = 1$ to vacuum causes nitrogen to desorb from the sample, yielding the desorption isotherm in the process. Using the method developed by Brunauer, Emmett and Teller (BET), the specific surface area of a sample can be determined from the obtained isotherms. The method developed by Barrett, Joyner, and Halenda can be used to determine the mesoporosity of the sample[133].

Nitrogen physisorption experiments were performed using a Micrometrics® TriStar 3000 system. Samples were typically dried under nitrogen flow at 200 °C for a full day prior to evacuation at 300 °C overnight and subsequent cooling to 77 K.

2.2.3 Electron microscopy

Electron microscopy (EM) is a very insightful technique that is used to visualize objects that are too small to see with a regular optical microscope. Whereas an optical microscope uses light to create enlarged images, an electron microscope uses an electron beam, causing the detection limit to be in the nanometer range, and even in the sub-nanometer range[134]. When used in transmission mode (transmission electron microscopy, TEM), the focussed electron beam is partially transmitted through the sample, generating an image on a detector. The average particle size can be determined from the obtained images by randomly measuring 200 particles or more. As this is a local technique, the more particles measured the more accurate the analysis is.

TEM images were obtained on a Philips/FEI Tecnai T12 instrument, with a max operating voltage of 120 kV. High-angle annular dark-field scanning transmission electron microscopy (HAADF-STEM) was also used, in combination with energy-dispersive X-ray spectroscopy (EDX) for elemental mapping. HAADF-STEM EDX images were obtained on a FEI Thalos™ F200X TEM, operated at 200 kV. Figure 2.3 is a schematic representation of electron microscopy (adapted from[132]). If the sample thickness is sufficiently small, a portion of the electrons will pass through the sample without losing their energy. The extinction of the beam is dependent on the density and thickness. These transmitted electrons will form a two-dimensional image of the sample when they are detected. As the incident electron beam can excite an electron in an inner shell, an electron hole is created where this electron previously was. Electrons from an outer shell, higher in energy can subsequently fill this hole. The excess energy may be released in the form of an X-ray. These X-rays are characteristic of the energy difference in these shells and thus reveal information about the atomic structure in the sample[132]. Samples for EM were prepared by adding small amounts to isopropanol, using an ultrasonic bath particles were dispersed in the solution. A drop of the dispersion was subsequently placed on the TEM grid. A

conventional copper grid was used for regular TEM analysis, whereas a nickel grid was used for STEM-EDX analysis.

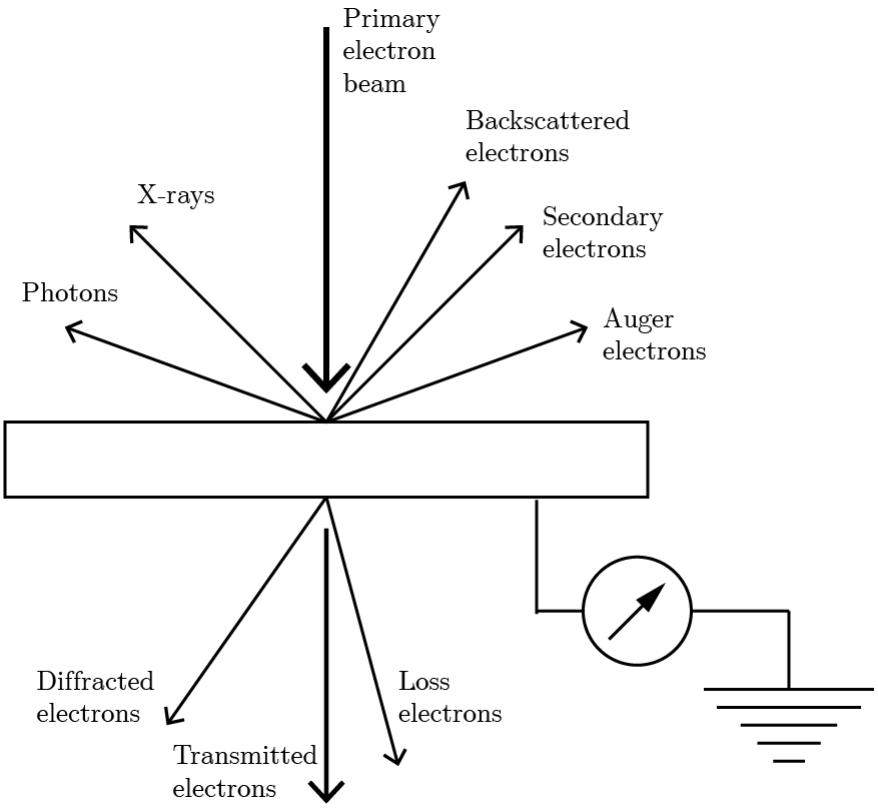

Figure 2.3: A schematic representation of electron microscopy, adapted from[132]

2.2.4 Ammonia temperature programmed desorption

A quick and efficient way to determine the presence of acid sites is ammonia temperature programmed desorption (NH_3-TPD). Prior to these experiments the samples are dried under nitrogen or helium flow at a sufficiently high temperature. A mixture of ammonia in helium is then pulsed multiple times over the sample until it is saturated. The temperature is kept at 100 °C during the saturation of the sample with ammonia to minimise the physisorption. As a result, the ammonia only chemisorbs to the (Brønsted and Lewis) acid sites in the sample. Due to the small size of the ammonia molecules, they are able to enter porous systems quite easily and cover most of the acid sites in the sample. The sample is then heated in a constant manner in an inert flow to allow for the desorption of the ammonia. Ammonia can be chemisorbed to both Brønsted and Lewis acid sites. Of these two, there is more energy required to break the ammonia bonded to Brønsted acid sites than to Lewis acid sites. Therefore, ammonia that is chemisorbed on Lewis acid sites will desorb at lower temperatures. The amount of ammonia can be quantified by using a thermal conductivity detector (TCD) upon desorption. The working mechanism of this method is that the current in the detector is constantly being measured. A flow of ammonia through the detector results in a higher current, as there are molecules that can

conduct electricity. By calibrating the equipment with a known concentration of ammonia the integral of the TCD can be directly correlated to an amount of ammonia.

TPD experiments were done using a Micrometrics AutoChem™ II 2920 system, equipped with a thermal conductivity detector. Quartz U-tubes were prepared by creating a bed of sample (typically 100 mg) between two plugs of quartz wool. Samples were dried at 100 °C, with a heating rate of 10 °C min^{-1} for 15 minutes. A mixture of ammonia in helium (1 or 10%, depending on availability) was pulsed until saturation. The amount of these pulses was dependent on the gas mixture used. Once the sample is saturated with ammonia, the sample is heated to a pre-set temperature of 400 °C. This heating was done in helium flow with a heating rate of 5 °C min^{-1}. The sample was kept at 400 °C for 25 minutes to allow for complete desorption of ammonia.nThe obtained desorption profiles were analysed using the provided software of Micrometrics. Using the integrated peak editor, peak boundaries were manually selected; the integral was related to a calibration run to quantify the amount of ammonia that was adsorbed to the sample.

2.2.5 Temperature programmed reduction

The conditions needed for complete reduction of CuO to Cu are of great importance for the methanol synthesis catalyst. Temperature programmed reduction (TPR) is a conventional technique in order to determine these conditions. In this technique, dried samples are subjected to a reducing atmosphere (usually a mixture of hydrogen in an inert gas) as the temperature is slowly increased. Hydrogen uptake is monitored and can be correlated to the reduction state of the catalyst. As Nb_2O_5 will be reduced at temperatures around 850 °C, hydrogen uptake in this region is also an indication of its presence.

As with the temperature programmed desorption, a Micrometrics AutoChem™ II 2920 equipped with a thermal conductivity detector was used. Quartz U-tubes were prepared by creating a bed of sample (typically an amount corresponding to a metal loading of 20 mg) between two plugs of quartz wool. Prior to TPR experiments, the samples were dried at 120 °C for 15 min, with a heating rate of 5 °C min^{-1}. After drying the samples were heated to 1000 °C with a heating rate of 5 °C, under a 5% H_2 in Ar flow. The obtained hydrogen uptake profiles were analysed using the provided software of Micrometrics. Using the integrated peak editor, peak boundaries were manually selected.

2.2.6 Thermal gravimetric analysis

The metal oxides (CuO, ZnO and Nb_2O_5) can be obtained after thermal decomposition of the precipitated precursors. IUPAC defines "calcination" as "heating to high temperatures in oxygen or air". Many factors of this calcination treatment (e.g. the heating rate, final temperature, total time and composition of the atmosphere/flow used) can influence the decomposition process of the precursors. These effects can be investigated using thermal gravimetric analysis (TGA), which can be coupled to a mass spectrometer (TGA-MS). For this, some sample was weighed into a platinum cup connected to a spring. As the sample is heated in a specific air composition, the mass is constantly monitored. The mass loss can

be plotted against the time or temperature and gives useful insight in the decomposition. When coupled to a mass spectrometer, the species that are generated upon decomposition can be monitored. For example, the thermal decomposition of nitrates will form NO_x in the process, while carbonates will form CO_2 when decomposed.

TGA experiments were performed using a TA Instruments TGA Q50, in an air flow of 60 $mLmin^{-1}$. Samples were heated from ambient temperature to 1000 °C with a heating rate of 15 °Cmin^{-1}. TGA-MS was performed using a Perkin Elmer Pyris 1 TGA, equipped with a Omnistar™ Pfeiffer Vacuum mass spectrometer. First, samples were dried at 50 °C for 19 minutes, under a nitrogen flow of 20 $mLmin^{-1}$. After drying the sample was heated from 50 °C to 600 °C, with a heating rate of 5 °Cmin^{-1} under oxygen rich atmosphere.

2.2.7 Inductively coupled plasma mass spectrometry

Analysis of elements in solid samples can be done by laser ablation inductively coupled plasma mass spectrometry (LA-ICP-MS). Many elements of the periodic table can be determined with great accuracy, even below the 100 parts per million range. In this technique, a high power laser of $> 1 \cdot 10^{10}$ Wcm^{-2} is shined upon the sample. Solid particles are physically ablated from the surface, and are carried in a stream of helium or argon into an argon plasma. In the plasma the particles are ionised before being measured in a mass spectrometer[135].

The experiments were performed on either a ThermoFischer Scientific Element 2 magnetic sector ICP-MS and a Geolas 193 nm excimer laser ablation system, or on a ThermoFischer Scientific X-series quadrupole ICP-MS. All experiments, including sample preparation was done at the petrology lab of Utrecht University by Ms. Helen de Waard[136].

2.2.8 Catalytic performance

Catalytic performance was evaluated using an Avantium Flowrence® 16 parallel reactor system. The (stainless steel) reactors were loaded with typically 100–250 mg of calcined catalyst (38–150 μm) diluted with typically 200 mg of SiC (212–425 μm) to prevent the formation of hotspots in the reactor. Catalysts were reduced at 250 °C for 2.5 h prior to reaction, under a 20% H_2/Ar flow at atmospheric pressure. In all cases, synthesis conditions were at 40 bar total pressure and a H_2/CO ratio of 2 was used. The temperatures used were always in the range from 280 °C to 320 °C. Products were analysed using an on-line Agilent 7980A gas chromatograph from Agilent Technologies. Permanent gasses were separated on a micropacked ShinCarbon ST column and quantified with a thermal conductivity detector (TCD) against helium, the internal standard used. Hydrocarbons were separated on an Agilent J&W PoraBOND Q column and detected by a flame ionization detector (FID). The products were quantified against the TCD signal of the internal standard, helium.

Chapter 3

Results and discussion - physical mixtures

3.1 Synthesis and characterisation of physical mixtures

3.1.1 Methanol synthesis catalysts

The composition, by weight, of the commercial copper-based catalyst for methanol synthesis used was 63.5% CuO, 24.7% ZnO, 10.1% Al_2O_3 and 1.3% MgO. This information was provided by Alfa Aesar, product number 45776, lot number I06Z036.

Prior to *in situ* reduction of copper-based catalysts various crystal phases are present in the prepared catalysts, which can be distinguished using powder X-ray diffraction. The X-ray diffraction patterns of various catalysts are presented in Figure 3.1. Catalysts were prepared by following one of the previous described methods for precipitation of the precursor salts. Peaks at 2θ values of 41.5, 45.5, 57.5, 63, 69, 73 and 78 ° result from the presence of crystalline copper(II) oxide phases. Peaks at 2θ values of 37, 40, 42, 56, 67, 75 and 78 ° result from the presence of crystalline zinc oxide phases. Peaks due to crystalline ZnO can be clearly seen to be more prevalent in catalysts prepared by co-precipitation, using a solution of oxalic acid in acetone. Moreover, the broadening of the peaks upon the addition of aluminium oxide (as seen in **C**) can be explained by the loss of crystallinity. As aluminium oxide acts as a structural dispersant more, smaller, particles are formed.

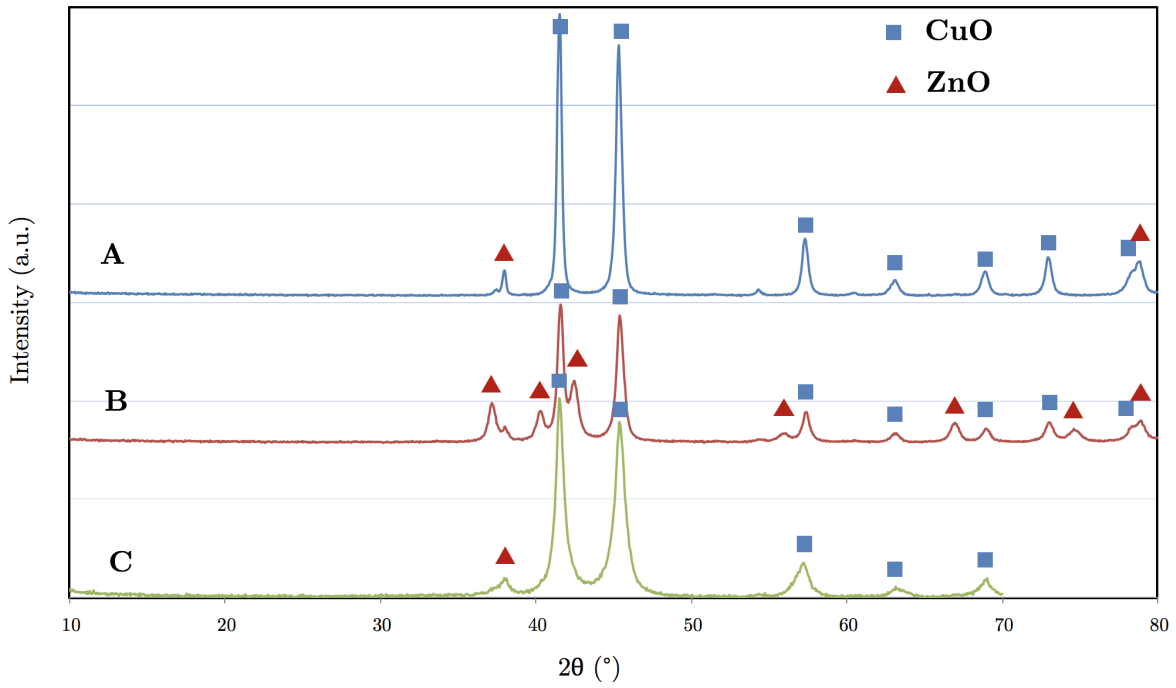

Figure 3.1: XRD patterns of various methanol synthesis catalysts consisting of copper and zinc oxide (**A** and **B**) and aluminium oxide (**C**) prepared by various synthesis methods. **A**, prepared by co-precipitation, using an aqueous solution of ammonium (bi)carbonate; **B**, prepared by co-precipitation, using a solution of oxalic acid in acetone; **C**, a conventional methanol synthesis catalyst, prepared by co-precipitation using an aqueous solution of ammonium (bi)carbonate.

3.1.2 Niobium-based solid acid

From literature it is known that thermal treatment of $Nb_2O_5 \cdot nH_2O$ yields a pseudo-hexagonal Nb_2O_5 structure at temperatures around 500 °C[114]. Increasing the temperature further will cause a phase transition towards orthorombic Nb_2O_5 (700-800 °C) and monoclinic Nb_2O_5 (1000 °C)[108]. Calcination at 400 °C however does not cause this crystallisation of niobia, which thus remains amorphous. Characteristic for the amorphous character of $Nb_2O_5 \cdot nH_2O$ are the two broad 'peaks' in the area from 2θ values of 20–45 ° (with a shoulder around 40 °, and 50–80 °. which can be seen in Figure 3.2. These broad 'peaks' are due to the presence of long range order in the amorphous sample. The only significant difference in these diffractograms is the presence of a small peak around 28 ° in **B**. This small peak cannot be due to the presence of CuO, ZnO (Fig. 3.1 or crystalline niobia[114] and is therefore attributed to a contamination.

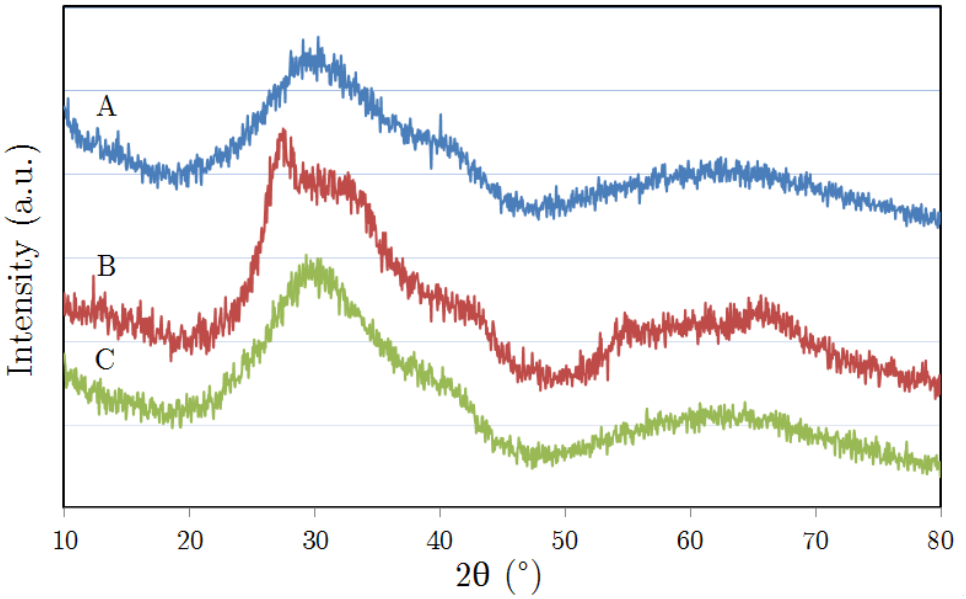

Figure 3.2: XRD of Nb_2O_5. **A**, $Nb_2O_5 \cdot nH_2O$ calcined at 400 °C, supplied by CBMM (HY-340); **B**, Nb_2O_5 prepared by precipitating ANO from aqueous solution using ammonium carbonate solution; **C**, Nb_2O_5 prepared by injecting an aqueous solution of ANO into a solution of oxalic acid in acetone.

The specific surface area (SSA) of the calcined niobic acid was determined to be 92.2 m^2/g, which is in line with previous reported values in our group[114]. Quantification of acid sites was performed using ammonia temperature programmed desorption (NH_3-TPD), assuming a one-on-one ratio between adsorbed ammonia molecules and acid sites. For niobic acid calcined at 400 °C, the amount of adsorbed ammonia was determined to be 0.78 mmol/g sample. The very broad TPD profile can be explained due to the presence of different types of acid sites, as niobic acid contains both Lewis and Brønsted acid sites.

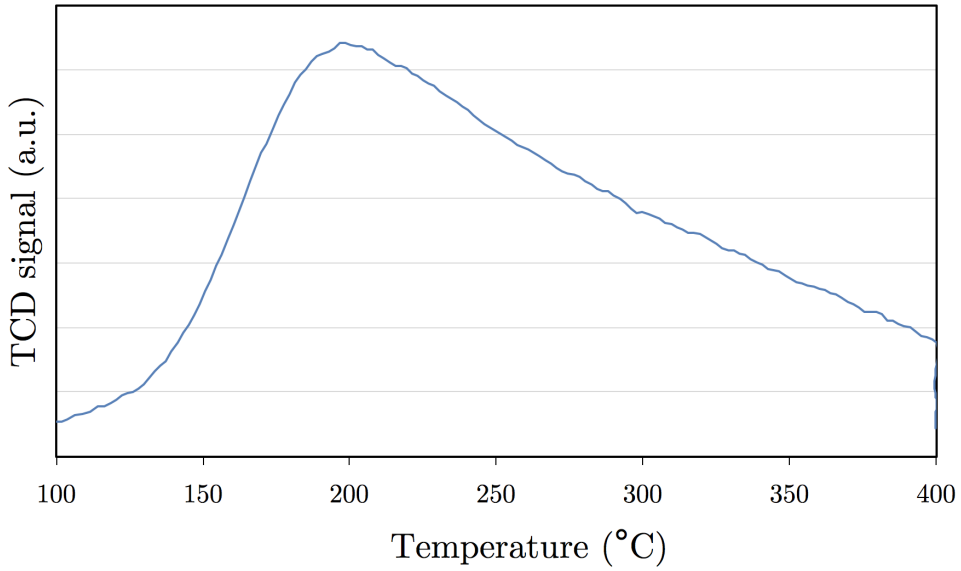

Figure 3.3: NH_3-TPD profile of $Nb_2O_5 \cdot nH_2O$ calcined at 400 °C.

3.2 Catalytic performance

3.2.1 Activity

The activity of physical mixtures with various niobia weight loadings was compared to a commercial methanol synthesis catalyst (CZA-catalyst). Activities are plotted as copper time yield (CTY) per time on stream (TOS). This CTY is the amount of CO converted per g of metallic copper per second ($mol_{CO}\ g_{Cu}^{-1}\ s^{-1}$). This is done so that differences due to varied loadings are not cause for different activities. As the reactor was loaded with an amount corresponding to ∼50 mg of CZA-cat, the amount of catalyst mixture (both CZA and niobic acid) in the reactor varied from ∼75 to ∼200 mg. This difference in actual catalyst loading is cause for the gas hourly space velocity (GHSV, defined as the total gas flow divided by the catalyst volume per hour) to be inconsistent.

As can be seen in Figure 3.4 is the proximity between the CZA-catalyst and solid acid already sufficient to shift the thermodynamic equilibrium towards higher CO conversions. The increase in CTY is already visible at low concentrations of niobia. With the tested weight ratios, ranging from 1:2 to 3:1 niobia to CZA catalyst, no maximum has been reached. From the visible decrease in CTY over time (as visible in Fig. 3.4) it can be concluded that there is a minimal difference in catalyst deactivation. Physical mixtures seem to deactivate slightly faster than the commercial CZA-catalyst, however this does not seem significant.

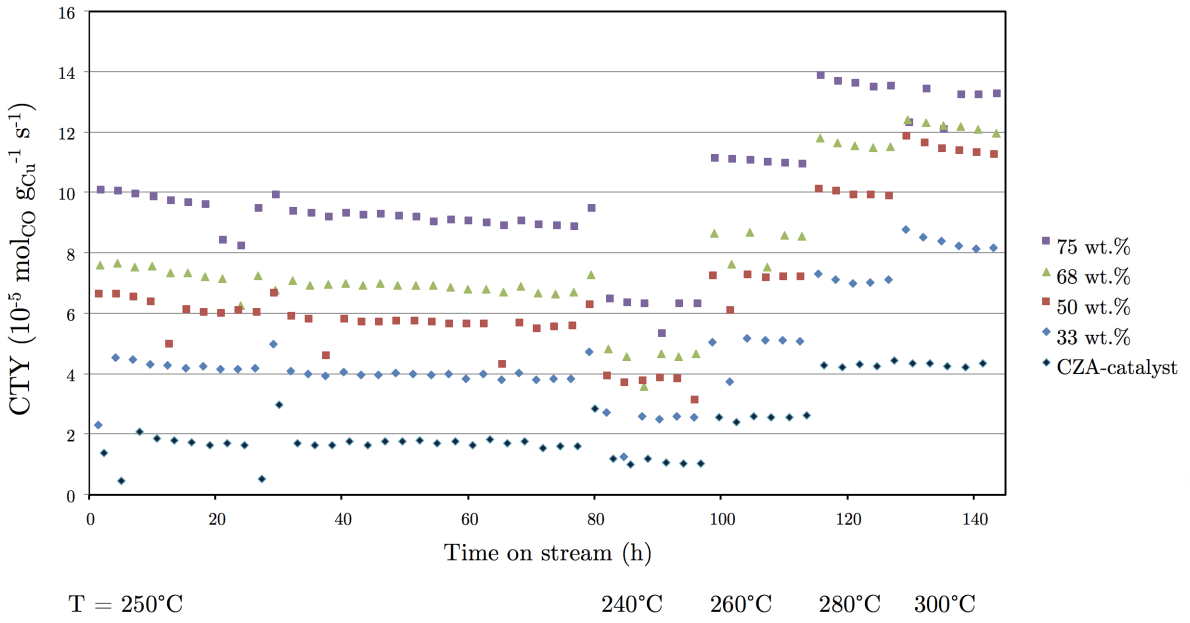

Figure 3.4: Activity of commercially available methanol synthesis catalyst and various physical mixtures of this catalyst with niobic acid. Reaction at 250 °C, with 40 bar total pressure, a H_2/CO ratio of 2, GHSV = 2200–7900 h^{-1}. After 80 h TOS, temperatures were varied stepwise.

3.2.2 Selectivity

The selectivity of physical mixtures with various niobia weight loadings (Figure 3.6 to 3.9) was compared to a commercial CZA catalyst for methanol synthesis (Figure 3.5). The selectivity of the commercial methanol synthesis catalyst towards methanol decreases at higher temperatures. At 300 °C the formation of other products becomes significant. Small amounts of DME are produced, and about 15% of other products, unidentifiable by the GC due to its apolar column. However we can reason that possible products that encompass these fraction of 'Others' are most likely not fully hydrogenated CO/CO_2 species, such as formaldehyde. Physical mixtures with low loadings of niobia (e.g. 33 wt.%) produce significant amounts of methanol and other products, even at elevated temperatures. With increasing weight loadings of niobia, the product distribution clearly shifts towards dimethyl ether formation, even at lower temperatures (such as 260 and 280 °C). Even at a weight ratio of 3:1 (niobia:CZA catalyst) not all methanol is dehydrated at lower temperatures, but temperatures of 260 °–280 °C are preferred, as there seems no significant difference in product distribution when the temperature is increased from 280 to 300 °C. The formation of 'Other' products decreases with the temperature, contrary to the commercial catalyst. Identification of these products is essential for complete understanding of this process.

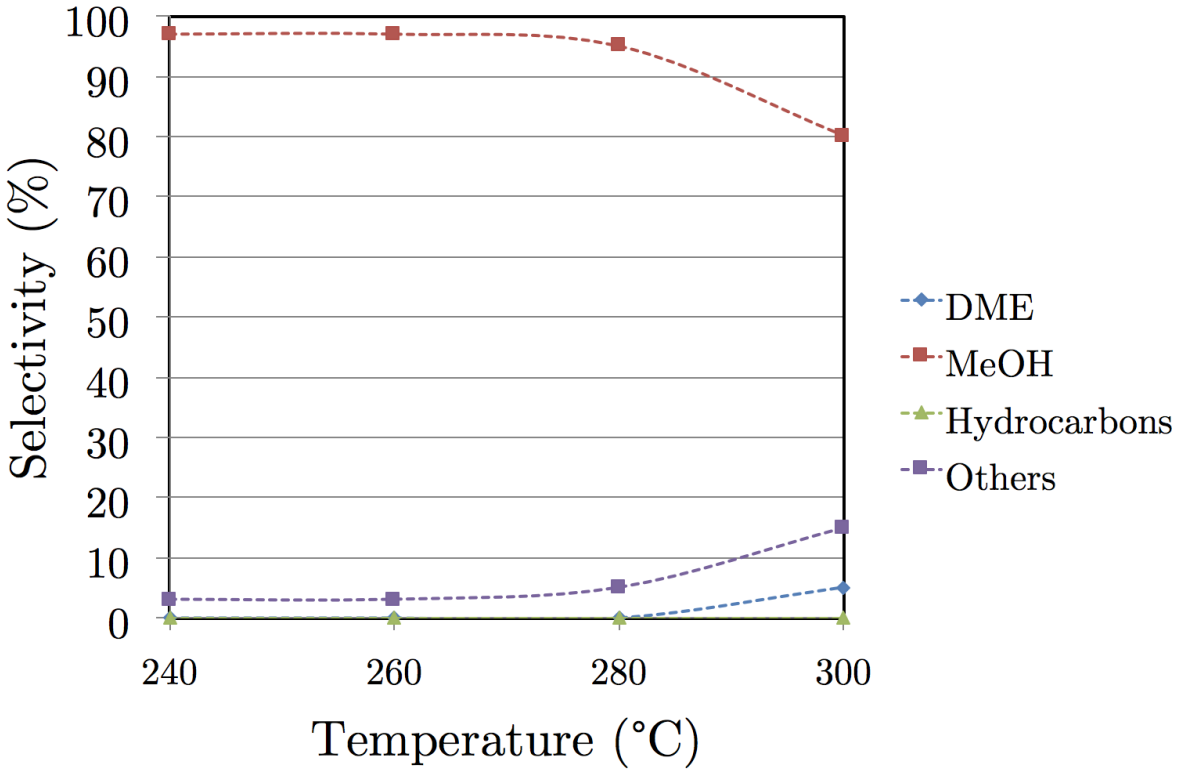

Figure 3.5: Selectivity of a commercially available methanol synthesis catalyst consisting of $CuO/ZnO/Al_2O_3$ and MgO promotor.

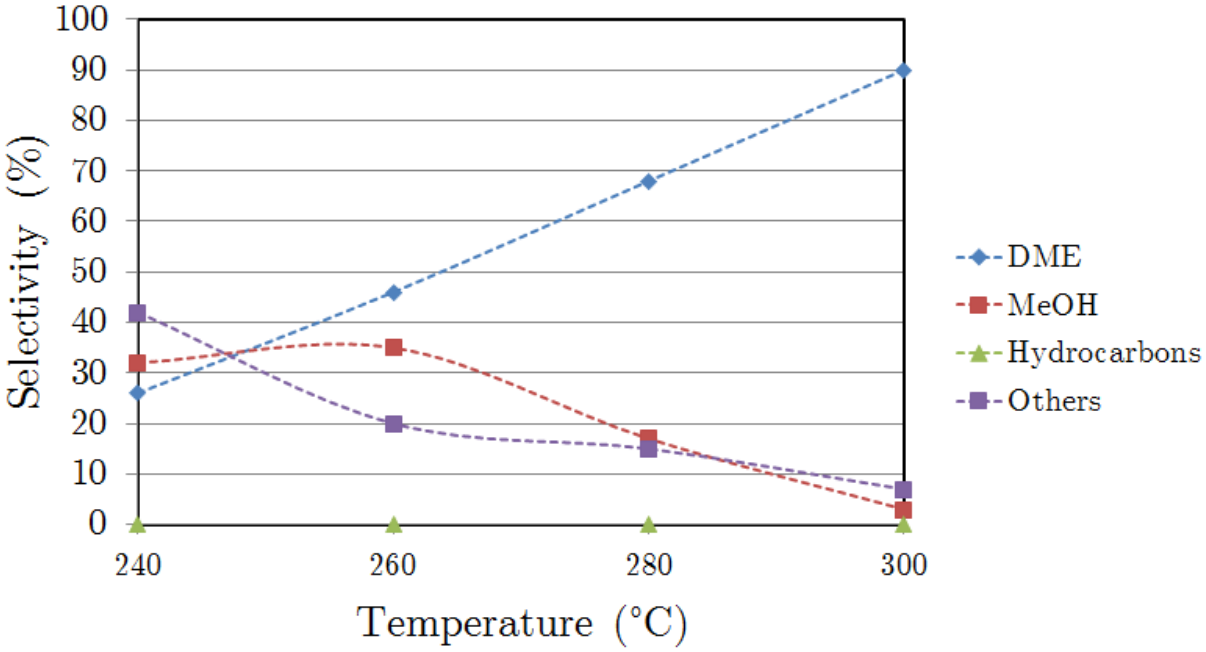

Figure 3.6: Selectivity of a physical mixtures with commercially available methanol synthesis catalyst (66.9 wt.%) and niobic acid (33.1 wt.%).

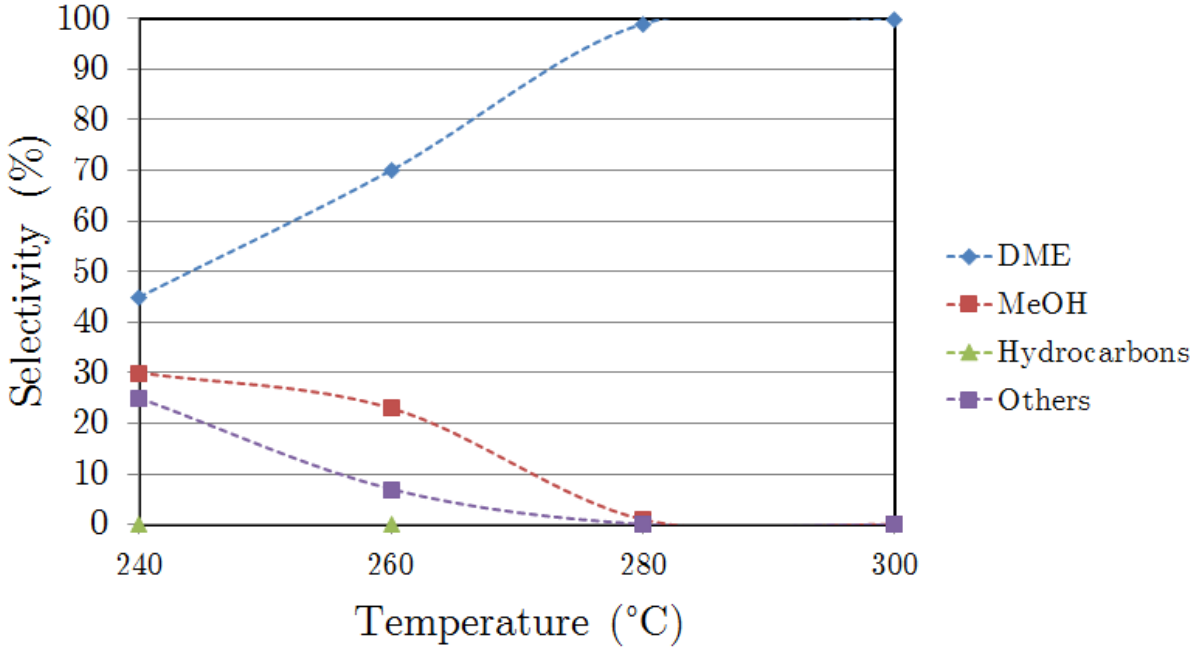

Figure 3.7: Selectivity of a physical mixtures with commercially available methanol synthesis catalyst (50 wt.%) and niobic acid (50 wt.%).

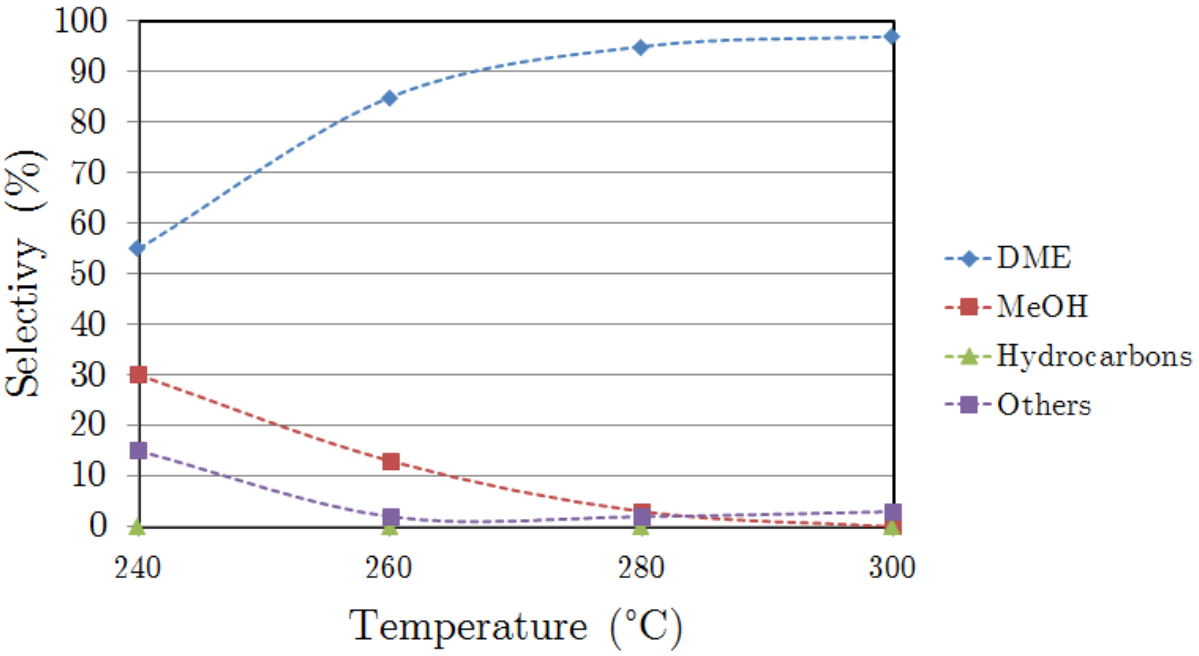

Figure 3.8: Selectivity of a physical mixtures with commercially available methanol synthesis catalyst (32.5 wt.%) and niobic acid (67.5 wt.%).

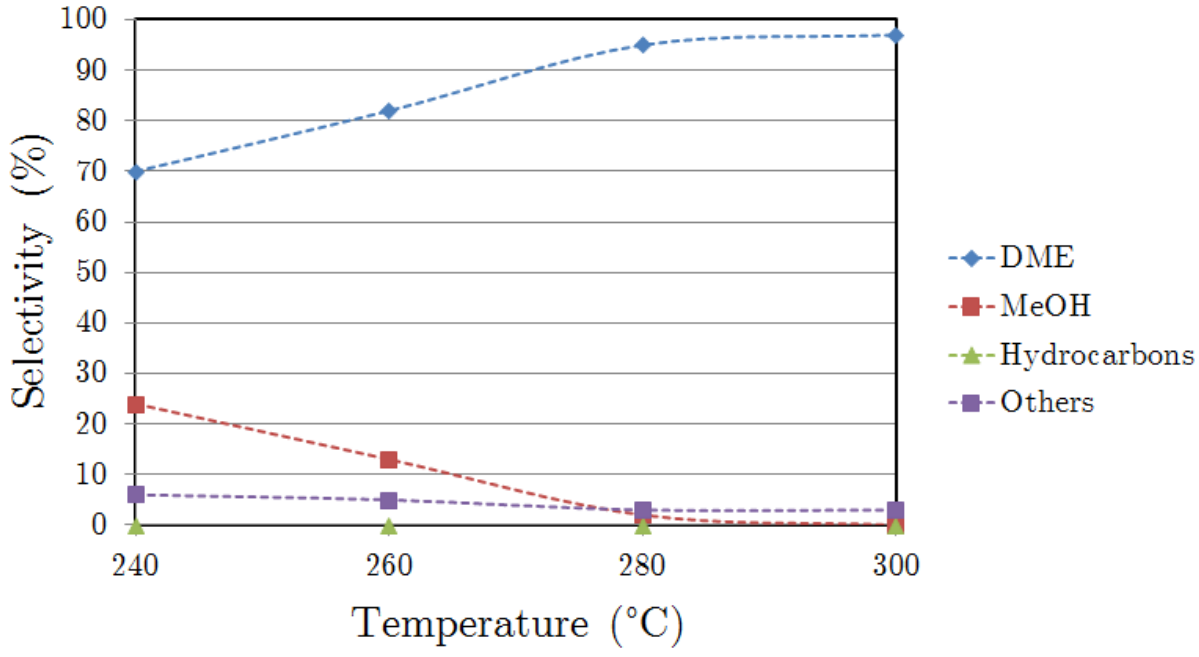

Figure 3.9: Selectivity of a physical mixtures with commercially available methanol synthesis catalyst (25 wt.%) and niobic acid (75 wt.%).

Chapter 4

Results and discussion - co-precipitation

4.1 Catalyst characterisation

Determining the composition (by weight) of various samples prepared by co-precipitation was done by ICP-MS, at the Petrology lab of Utrecht University. Aimed compositions of 10, 20, 40 and 80 wt.% of Nb_2O_5 resulted in measured values of 11, 16, 32 and 78 wt.% of Nb_2O_5. The fact that these values appear lower overall can be explained by redissolving of metal ions during the washing steps in the synthesis. However, these values should be considered with caution, as the Geolab facilities admitted having difficulty with dissolving Nb.

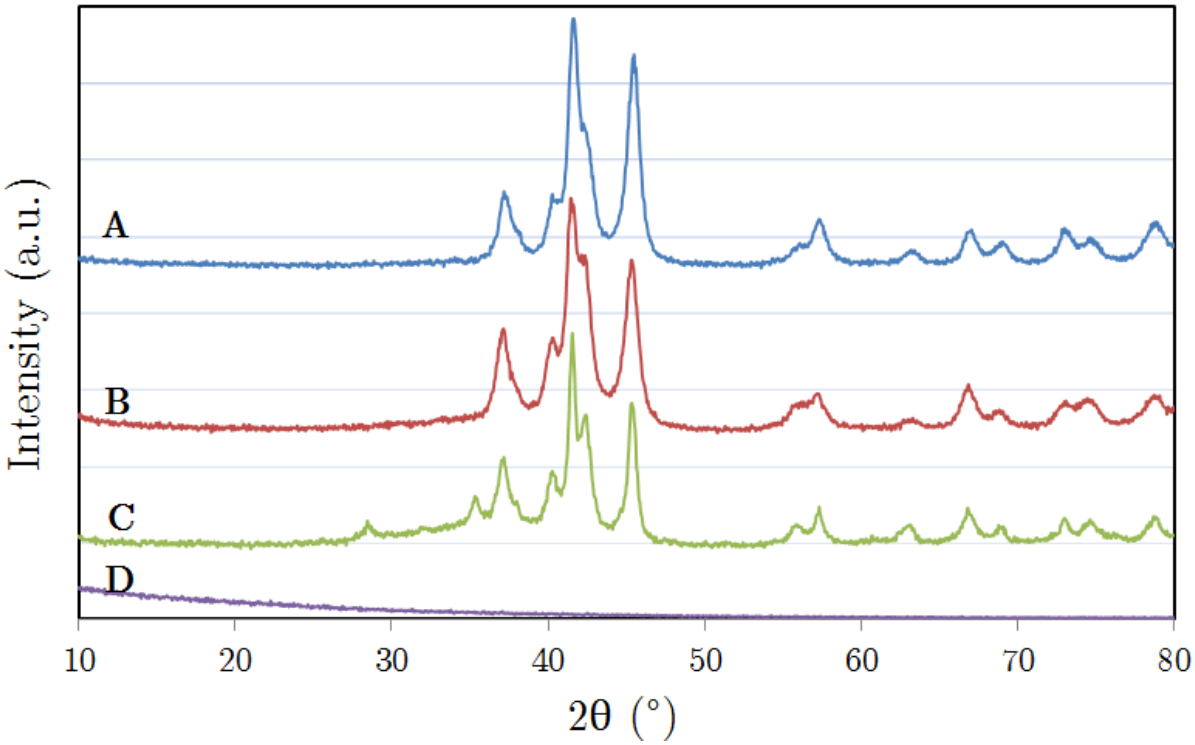

Figure 4.1: XRD of bifunctional catalysts prepared by co-precipitation with ammonium (bi)carbonate. Weight loading of: **A**) 11 wt.% Nb_2O_5, **B**) 16 wt.% Nb_2O_5, **C**) 32 wt.% Nb_2O_5, **D**) 78 wt.% Nb_2O_5.

Qualitative analysis of crystalline phases in the system was done using powder X-ray diffraction. The diffraction patterns of various catalysts prepared by co-precipitation are shown in Figure 4.1. Increasing the niobia weight loading from 11 to 16 wt.% shows no significant change in diffraction pattern. Diffraction peaks at 45.3 and 42.4 ° 2θ are the most pronounced peaks that can be ascribed to the presence of crystalline CuO and ZnO respectively. The other peaks that are due to the presence of these crystal phases are listed in Table 4.1.

Upon increasing the loading of niobia to 32 wt.%, two more species can be identified by their characteristic diffraction peaks. The most pronounced of which are at 2θ values of 28, 29 and 35.3 °, corresponding to the presence of both copper and zinc niobates (Tab. 4.1). These crystal phases are expected to be present in fewer amounts, mostly at the boundary of copper and zinc with niobium oxides. Increasing the weight loading of niobia

even further to nearly 80 wt.% results in a complete disappearance of the diffraction peaks. Cause for this is the amorphous character of niobia (Fig. 3.2). The lack of long range order indicates a fine dispersion of niobia throughout the sample.

However, co-precipitation induced by injection of aqueous solutions into a solution of oxalic acid in acetone does not result in the formation of the crystalline copper and zinc niobates, as the diffraction peaks of these crystal phases are not present in the diffractogram (Fig. 4.2).

Table 4.1: Reference values for diffraction peaks for CuO[137] , ZnO[138] , $CuNb_2O_6$[139] and $ZnNb_2O_6$[140]. Values in bold indicate the peak with highest relative intensity. For clarity only peaks with a relative intensity of 10% or more have been included in this table.

Compound	Diffraction peaks (2θ °)
CuO	38, 41.4, 41.5, **45.3**, 45.6, 57.3, 60.5, 63, 69, 72.9, 78.3, 78.8
ZnO	37.1, 40.2, **42.4**, 55.8, 66.8, 74.5
$CuNb_2O_6$	28.4, 28.7, **35.3**, 37.2, 40.6, 40.8, 42.6, 44.7, 59.5, 62, 63.5, 74.7
$ZnNb_2O_6$	28.4, 29.2, **35.3**, 36.4, 42.2, 44.5, 58.8, 60.7, 62.5, 62.9

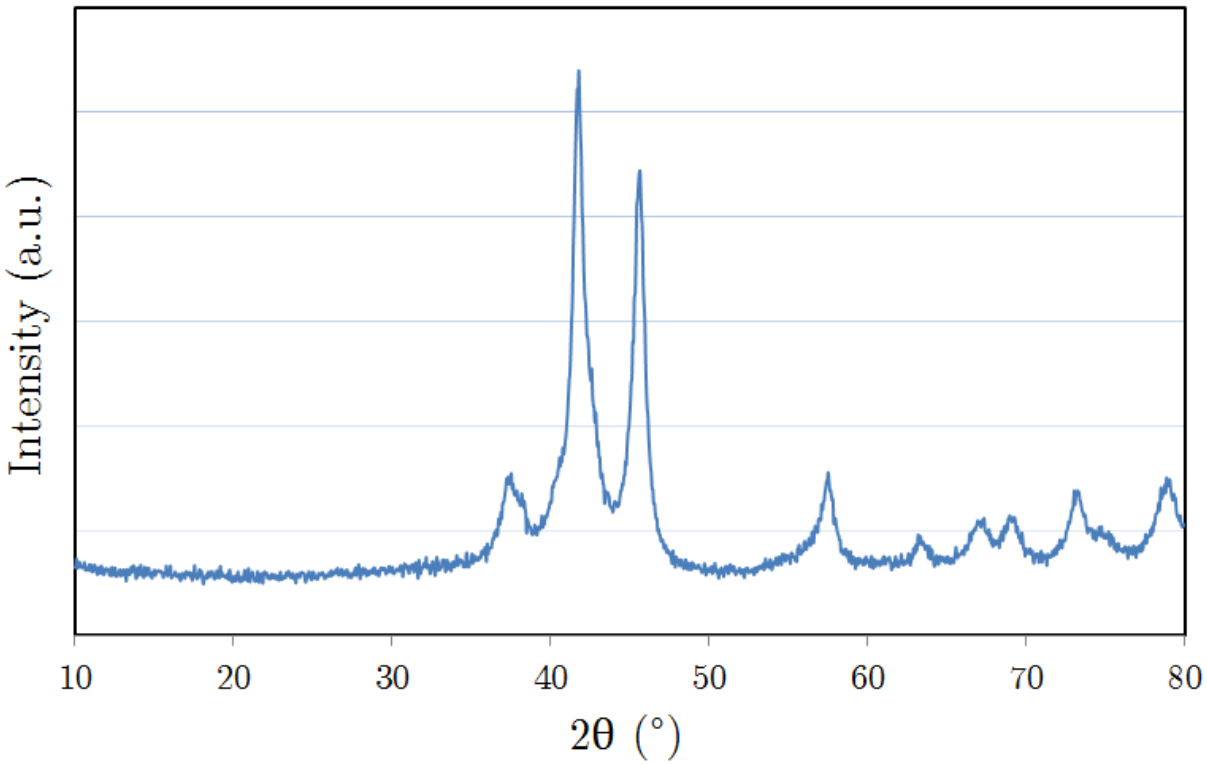

Figure 4.2: XRD of bifunctional catalysts prepared by co-precipitation using a solution of oxalic acid in acetone, with an aimed composition of 40 wt.% Nb_2O_5.

Specific surface areas (SSA) of catalysts were obtained from nitrogen physisorption data compared to niobic acid calcined at 400 °C, as shown in Table 4.2 and 4.3. Niobic acid was chosen as reference as the surface area of CZA catalysts has been shown to be dependent on many factors, such as the precipitation temperature, pH and the number of washing steps[49;53]. Both catalysts prepared by co-precipitation using an aqueous solution of ammonium carbonate or oxalic acid in acetone show very low SSA compared to commercially available niobia calcined at 400 °C. The extremely low SSA of 78 wt.% Nb_2O_5 resulted in not very reliable physisorption data, as not enough sample was available that corresponds to a measured surface of at least $10 m^2$. A sharp decrease in SSA can be seen when increasing the weight loading of niobia. This indicates that the obtained particles aggregate due to the presence of niobia, effectively losing surface area. This hypothesis was tested using electron microscopy, and will be shown later on.

Weight loading Nb_2O_5 (%)	SSA_{BET} (m^2/g)
32	53.6
78	14.5
$Nb_2O_5 \cdot nH_2O$ calcined at 400 °C	92.2

Table 4.2: Specific surface areas (SSA) of different samples prepared by co-precipitation using an aqueous solution of ammonium carbonate and of commercially available niobic acid, calcined at 400 °C.

Weight loading Nb_2O_5 (%)	SSA_{BET} (m^2/g)
10	48.6
20	57.1
40	51.1
80	27.1
$Nb_2O_5 \cdot nH_2O$ calcined at 400 °C	92.2

Table 4.3: Specific surface areas (SSA) of different samples prepared by co-precipitation using a solution of oxalic acid in acetone compared to that of commercially available niobic acid, calcined at 400 °C.

The acidic functionalities were investigated by ammonia temperature programmed desorption (NH_3-TPD). TPD profiles of catalyst prepared by co-precipitation are shown in Figure 4.3 and 4.4. A summary is given of these TPD profiles in Table 4.4 and 4.5 respectively. From the TPD profiles it can be concluded that the catalysts prepared by co-precipitation show slightly stronger acid sites, visualised by the slight shift towards higher temperatures for desorption. Precipitation by injecting both precursor solutions into a solution of acetone and oxalic acid yielded significantly more acid sites. A possible explanation for this increase in acid sites can be the catalyst structure. As no copper and zinc niobates are visible, niobia is expected to be present mostly by itself. This results in acid sites that are not blocked by surrounding copper and zinc oxides, but available for ammonia to adsorb on.

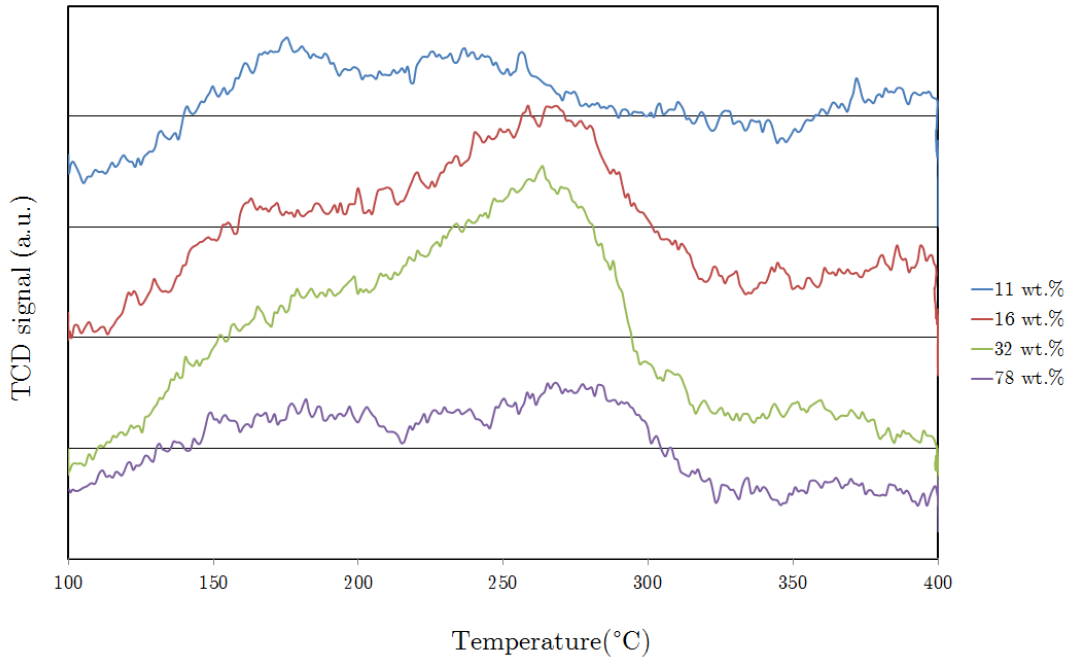

Figure 4.3: TPD profiles of various catalyst prepared by co-precipitation using an aqueous solution of ammonium carbonate.

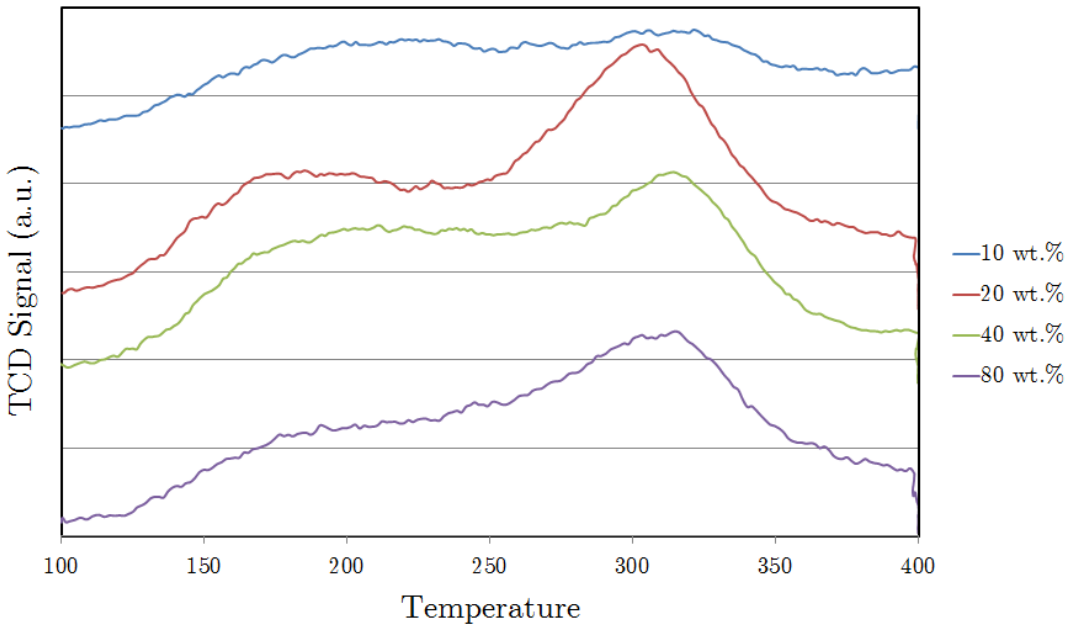

Figure 4.4: TPD profiles of various catalyst prepared by co-precipitation using a solution of oxalic acid in acetone.

Weight loading Nb_2O_5 (%)	Amount of NH_3 (mmol/g)	T at max (°C)
11	0.06	175
16	0.09	270
32	0.12	265
78	0.06	270
$Nb_2O_5 \cdot nH_2O$ calcined at 400 °C	0.78	178

Table 4.4: Ammonia TPD data of various catalyst prepared by co-precipitation using an aqueous solution of ammonium carbonate.

Weight loading Nb_2O_5 (%)	Amount of NH_3 (mmol/g)	T at max (°C)
10	0.22	315
20	0.40	300
40	0.42	315
80	0.35	315
$Nb_2O_5 \cdot nH_2O$ calcined at 400 °C	0.78	178

Table 4.5: Ammonia TPD data of various catalyst prepared by co-precipitation using a solution of oxalic acid in acetone.

Transmission electron microscopy (TEM) images (Figure 4.5) of catalyst prepared by co-precipitation induced by adding an aqueous solution of ammonium carbonate clearly show that increasing the weight loading of niobia (from **A**–**D**) results in the formation of aggregates. As hypothesized after examination of the nitrogen physisorption results. Aside from this, no clear conclusion about the elemental dispersion can be drawn from TEM images. For this EDX elemental mapping was applied. This confirmed that the presence of niobia exclusively overlapped or in very close proximity with copper and zinc (as seen in Figure 4.6 and 4.7). As seen in the XRD this results in the formation of copper and zinc niobates, or complete lack of detectable crystal phases. However these images seem to give an idea of the spatial distribution of particles and elements, electron microscopy is a local technique and does therefore not provide conclusive evidence by itself.

Co-precipitation induced by injecting the precursor solutions into a solution of oxalic acid in acetone results in a different elemental distribution, as can be seen in Figure 4.8 and 4.9. In this case, not only is the niobia much more distributed, copper and zinc seem to have spread from each other. This indicates that this catalyst will underperform in methanol synthesis, as close contact of copper to zinc oxide is preferred[26].

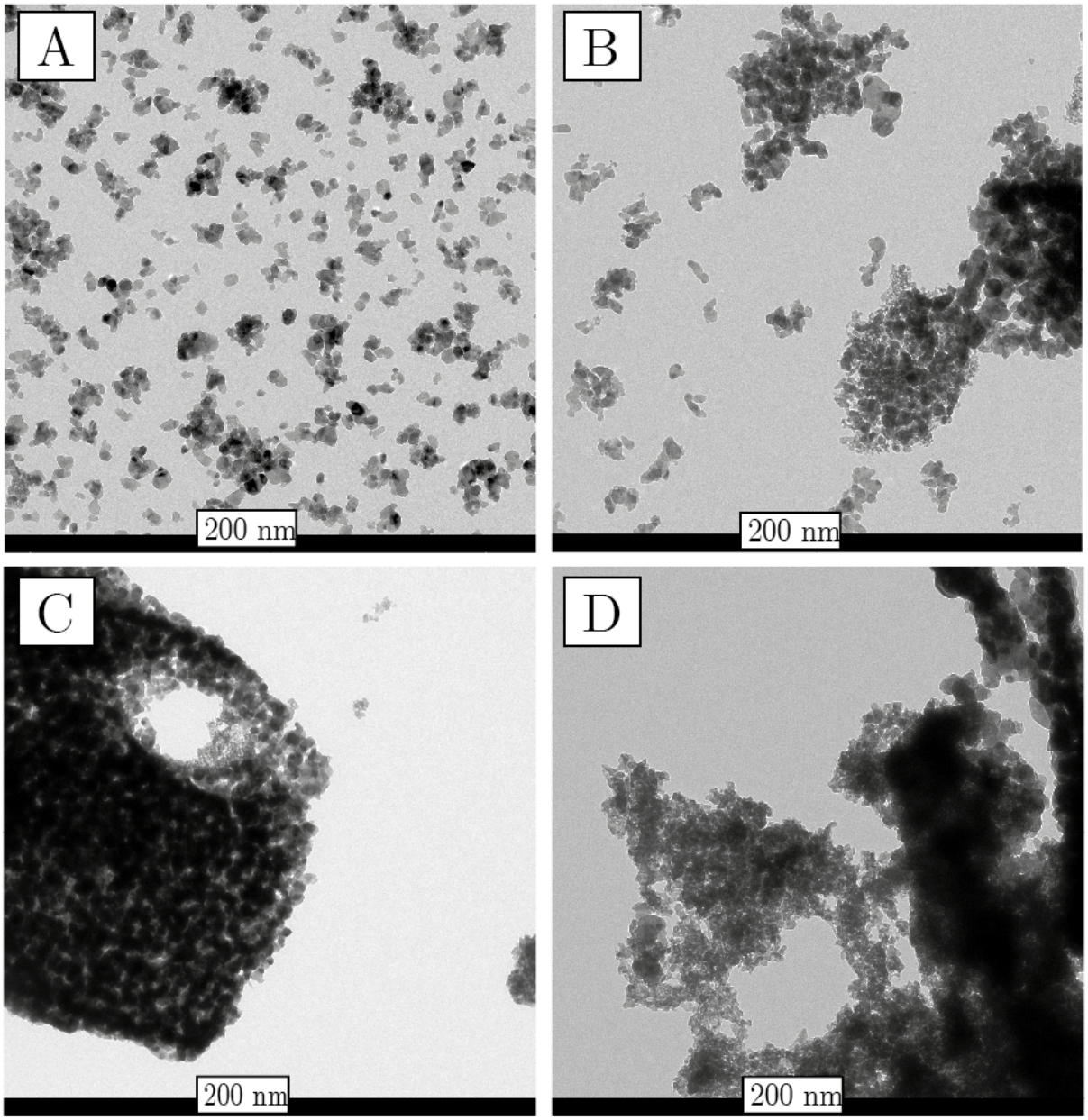

Figure 4.5: TEM images of catalyst prepared by co-precipitation using an aqueous solution of ammonium carbonate. **A**) 11 wt.% Nb_2O_5, **B**) 16 wt.% Nb_2O_5, **C**) 32 wt.% Nb_2O_5, **D**) 78 wt.% Nb_2O_5.

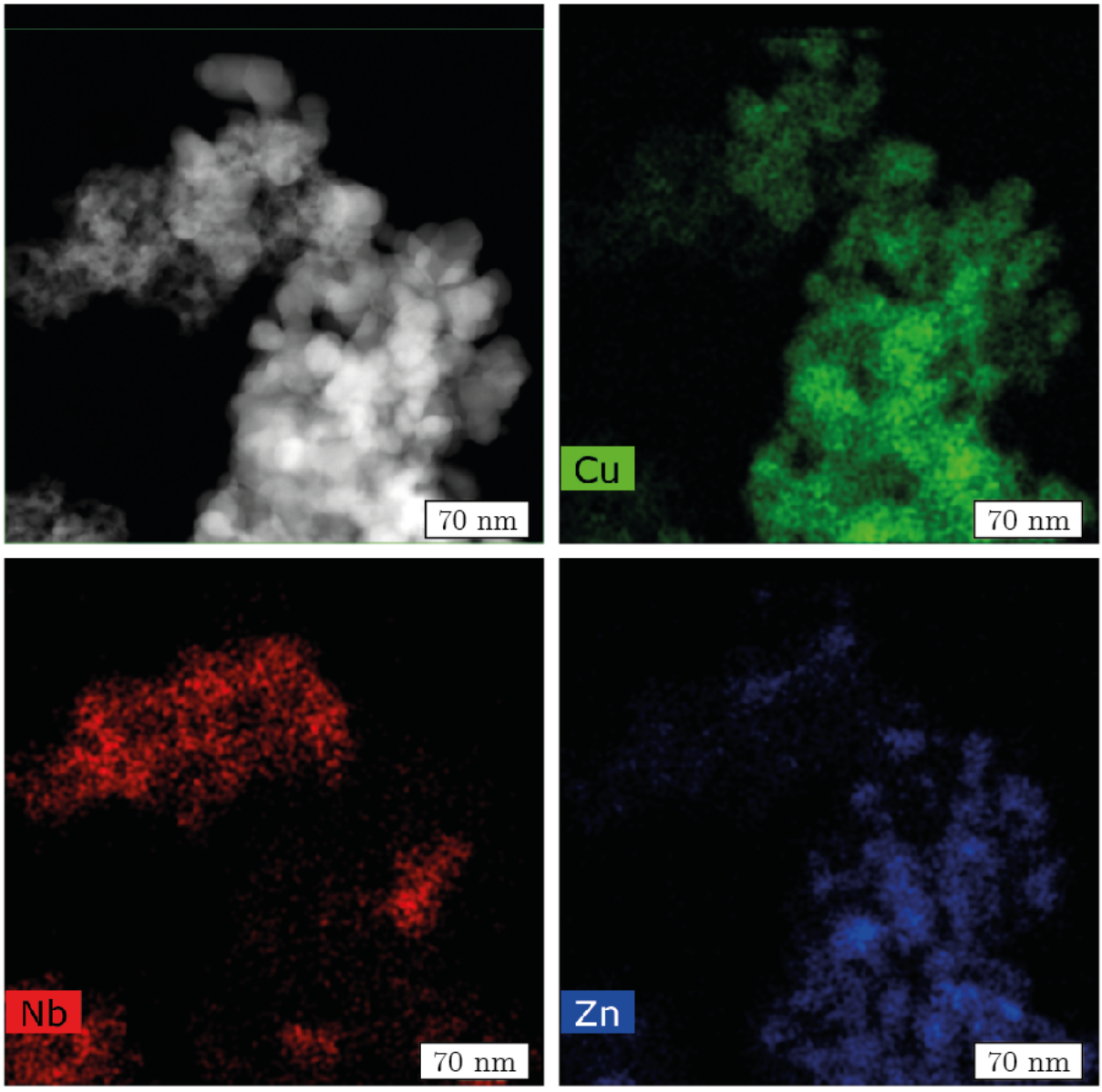

Figure 4.6: HAADF-STEM-EDX images of a sample prepared by co-precipitation using an aqueous solution of ammonium carbonate, containing 32 wt.% Nb_2O_5.

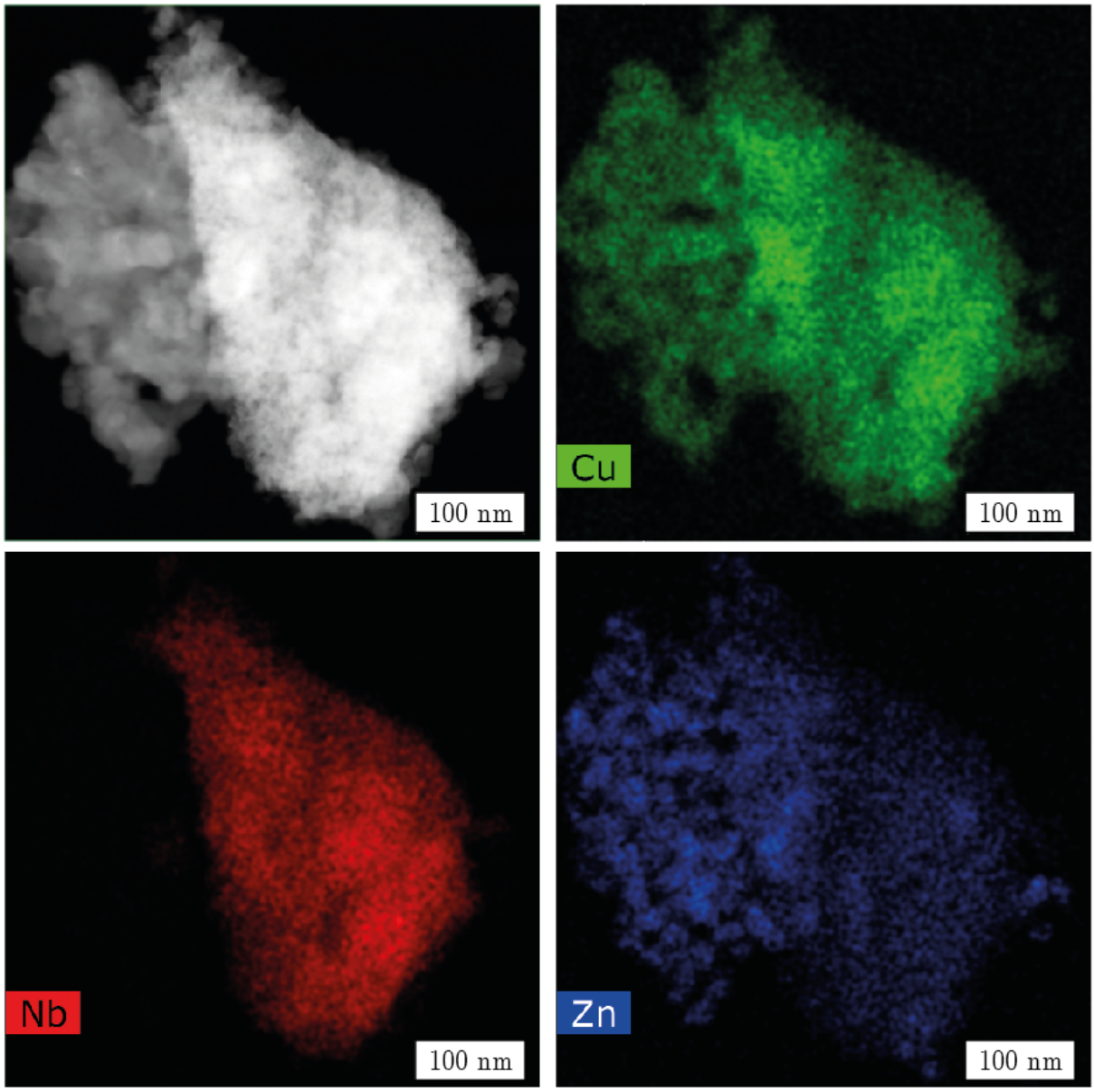

Figure 4.7: HAADF-STEM-EDX images of a sample prepared by co-precipitation using an aqueous solution of ammonium carbonate, containing 78 wt.% Nb_2O_5.

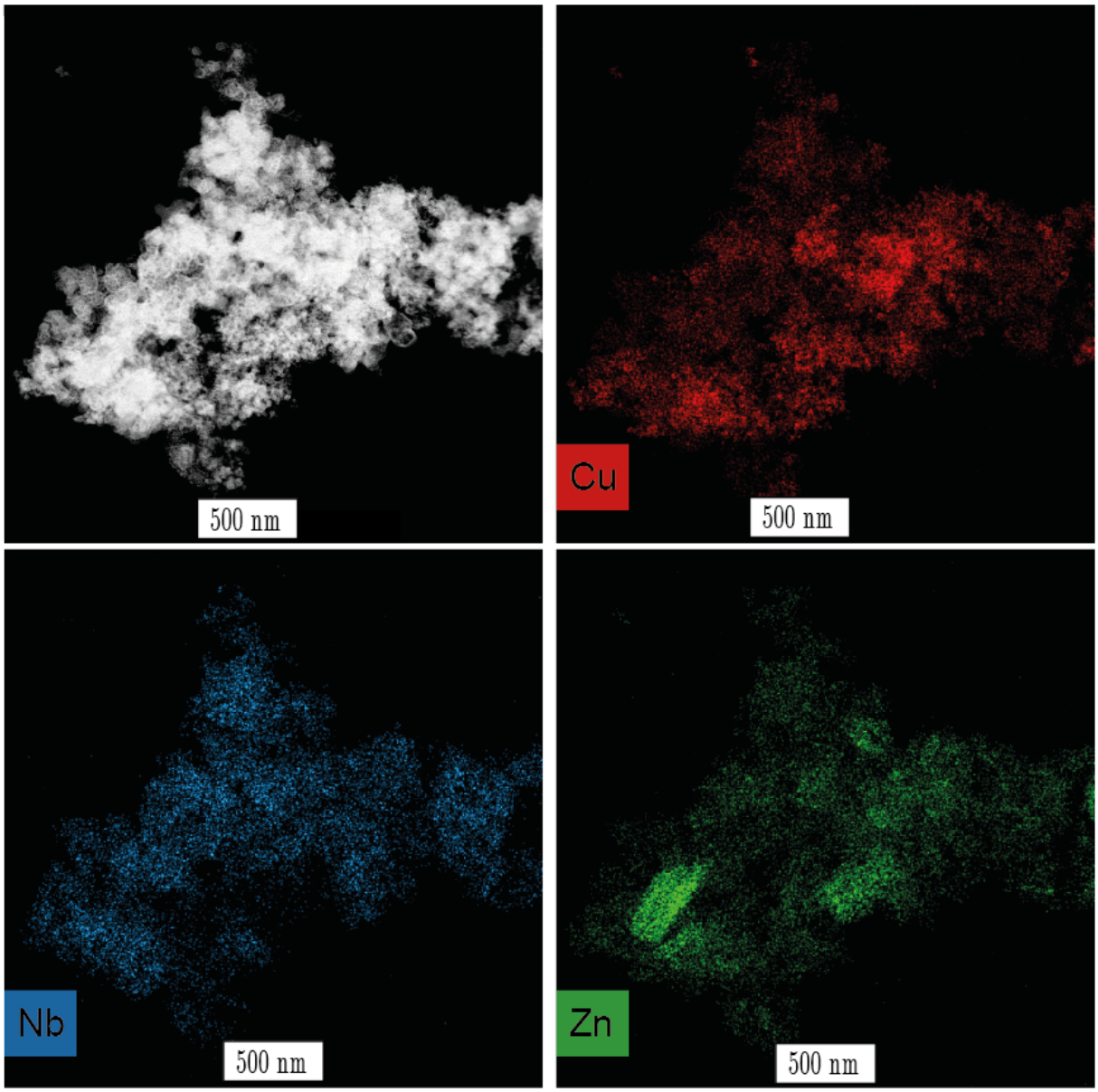

Figure 4.8: HAADF-STEM-EDX images of a sample prepared by co-precipitation using a solution of oxalic acid in acetone, containing 40 wt.% Nb_2O_5.

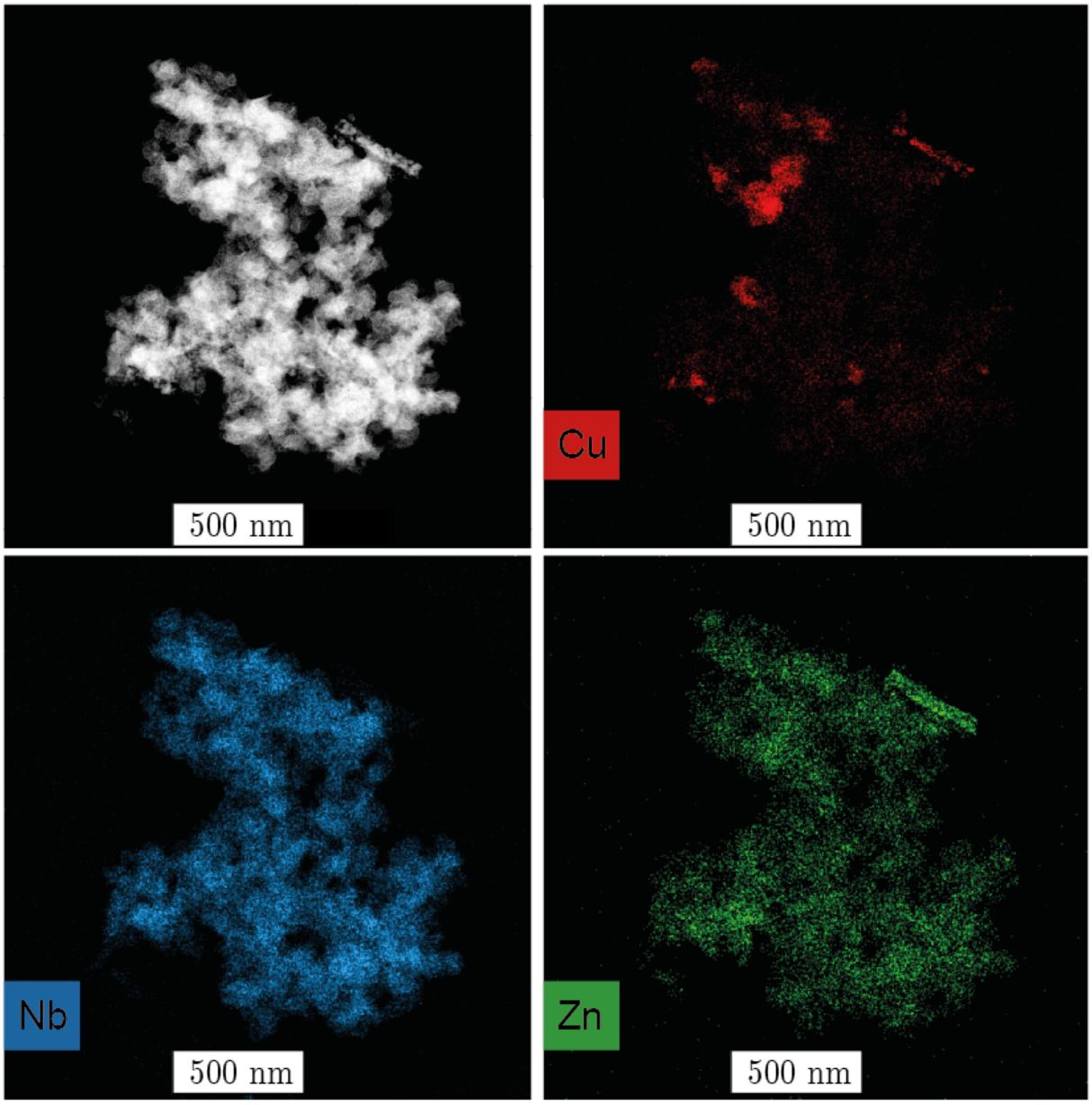

Figure 4.9: HAADF-STEM-EDX images of a sample prepared by co-precipitation using a solution of oxalic acid in acetone, containing 80 wt.% Nb_2O_5.

4.2 Catalytic performance

4.2.1 Activity

The activity of various catalysts prepared by co-precipitation was compared. The activities are plotted as CTY against TOS. In Figure 4.10 the activities of catalysts prepared by co-precipitation using an aqueous solution of ammonium carbonate are plotted. In Figure 4.11 the activities of catalysts prepared by co-precipitation by injecting the precursor solutions into a solution of oxalic acid in acetone are plotted.

In Figure 4.10 a clear activity increase can be seen upon increased niobia loadings. Although physical mixtures with corresponding ratios of niobia to methanol synthesis catalyst showed far higher CTY than the catalysts prepared by co-precipitation, also no maximum for the CTY has been reached. The nearly identical CTY of 16 and 32 wt.% Nb_2O_5 is in contrast with the sharp increase in conversion for 78 wt.% Nb_2O_5. A possible explanation for this identical behaviour can be faulty ICP data. As the Geolab facilities has admitted to experience difficulty measuring Nb.

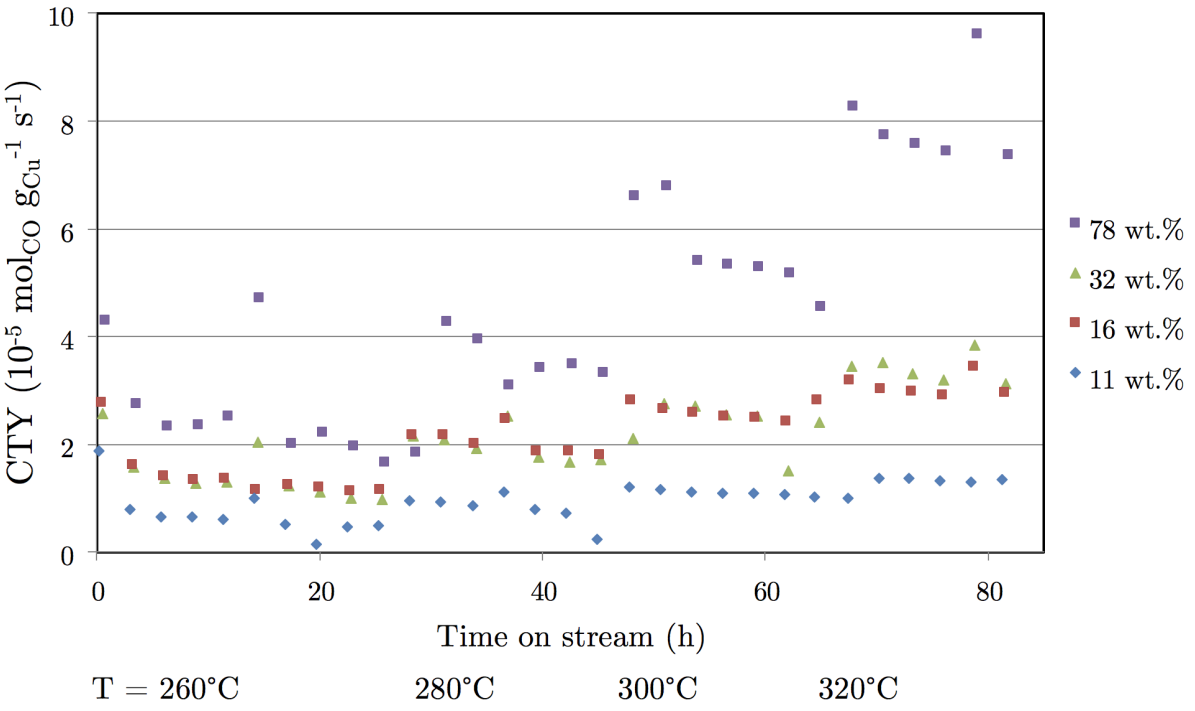

Figure 4.10: Activity of various catalysts prepared by co-precipitation using ammonium carbonate, containing various weight loadings of niobia, as determined by ICP-MS. Reaction at 260 °C, with 40 bar total pressure, a H_2/CO ratio of 2, GHSV = 3000–4000 h^{-1}. After 25 h TOS, temperatures were varied stepwise.

In Figure 4.11 the activities of catalysts prepared by co-precipitation induced by injection of precursor solutions into a solution of oxalic acid in acetone are shown. Note the different scale compared to Figure 4.10, 0–2.5 or 0–10 mol_{CO} g_{Cu}^{-1} s^{-1} respectively. The CTY was calculated using the aimed weight loading of Nb_2O_5, as no ICP-MS data was available, and therefore is likely to contain a large error margin. When the activity of these catalysts is compared to catalysts with equivalent compositions prepared by co-precipitation using an aqueous solution of ammonium carbonate, a significant drop in activity is observed. This can be explained when the HAADF-STEM-EDX images are compared. As can be seen in Figure 4.7, the observed signal for Cu and Zn overlap, indicating close proximity between copper and zinc oxide in the catalysts. Whereas in Figure 4.9, with comparable composition, shows a clear separation between the Cu and Zn signals. This dispersion indicates less proximity between copper and zinc oxide, thus leading to inherently less active methanol synthesis catalysts.

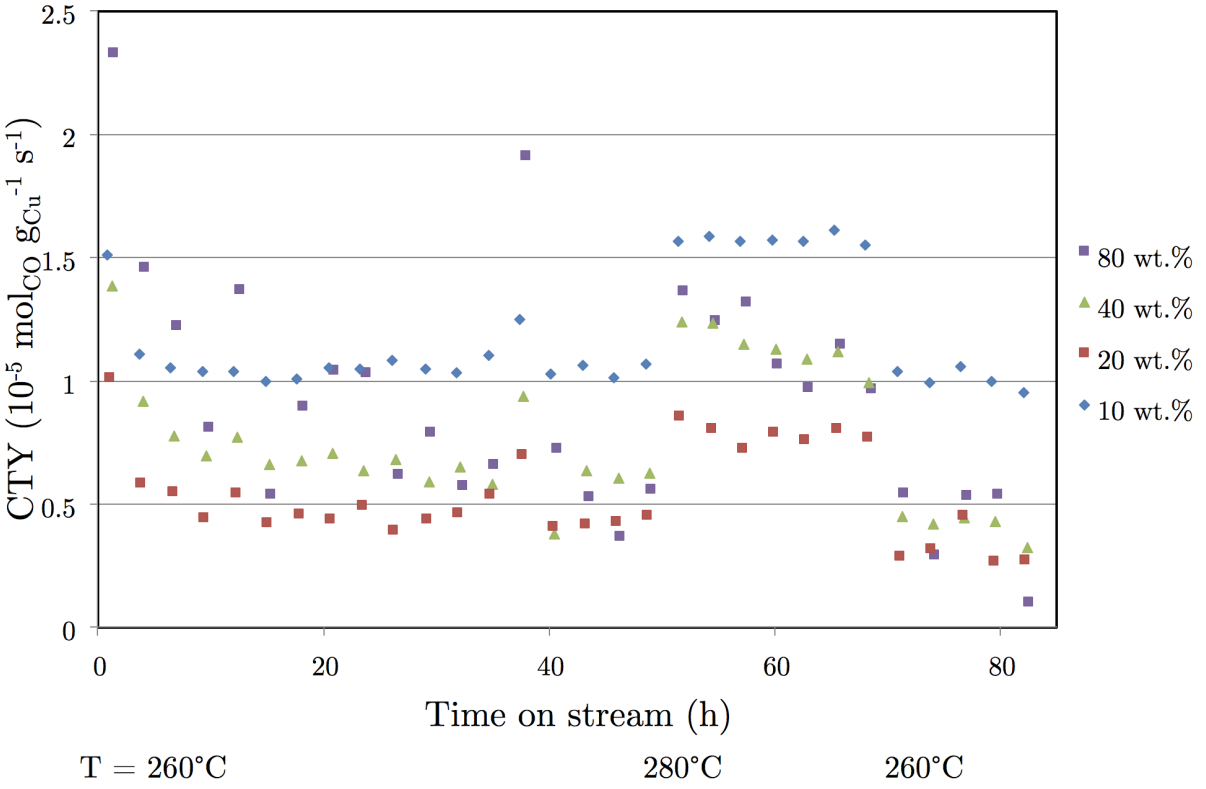

Figure 4.11: Activity of various catalysts prepared by co-precipitation using oxalic acid. Compositions listed are the aimed weight loadings of niobia. Reaction at 250 °C, with 40 bar total pressure, a H_2/CO ratio of 2, GHSV = 1300–1900 h^{-1}. After 50 h TOS, temperatures were varied stepwise.

4.2.2 Selectivity

The selectivity of catalysts prepared by co-precipitation using an aqueous solution of ammonium carbonate and injection into a solution of oxalic acid in acetone towards various products are shown in Figure 4.12–4.15 and Figure 4.16–4.19 respectively. Reaction conditions correspond to those listed with Figure 4.10 and 4.11 respectively. At low weight loadings of niobia, as can be seen in Figure 4.12 and 4.16, not all methanol was dehydrated to form DME, but significants amounts are still present in the final product distribution, mostly at low temperatures. A clear increase in selectivity towards DME can be seen upon increasing the weight loading of niobia and temperature. As with the physical mixtures, there seems to be no significant increase in methanol dehydration at temperatures above 300 °C for samples with higher weight loadings of niobia. At low weight loadings not all methanol was dehydrated and temperatures in excess of 300 °C are required, with 320 °C being sufficient already.

It can be noted that samples that contain less niobia tend to favour the formation of 'other' products that are left unidentified. At temperatures around 280–300 °C, the formation of these products is usually at its lowest, indicating that these are the favourable operating conditions for the catalysts prepared in this manner. When the catalysts are prepared by injecting the precursor solutions into a solution of oxalic acid in acetone, significant amounts of hydrocarbons are being formed. These hydrocarbons are mostly methane (CH_4), but small amounts of ethane (C_2H_6), propane (C_3H_8) and butane (C_4H_{10}) were formed, as determined by GC. Ethene, propene and butene were either not being formed, or in neligibele amounts.

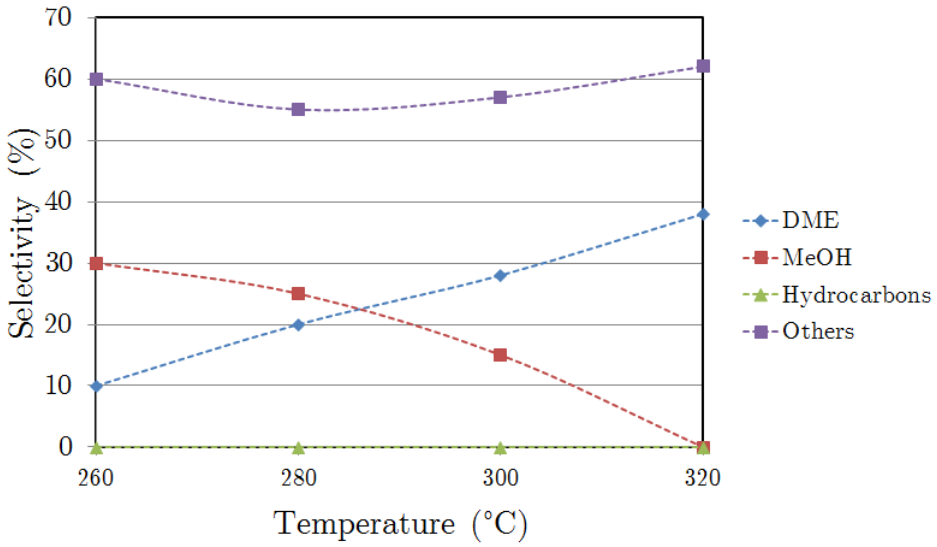

Figure 4.12: Selectivity of Cu/Zn/Nb catalyst prepared by co-precipitation, towards various products, with 11 wt.% Nb_2O_5, at temperatures ranging from 260 to 320 °C.

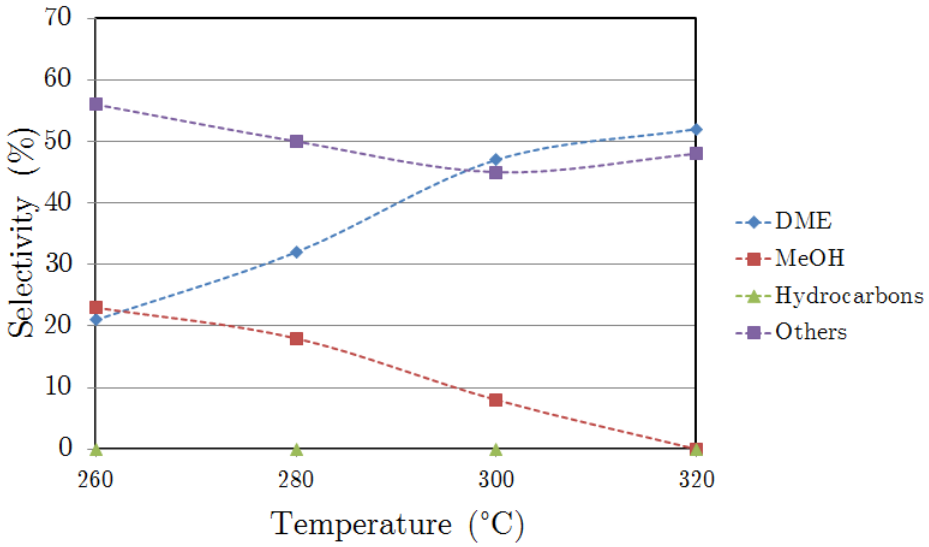

Figure 4.13: Selectivity of Cu/Zn/Nb catalyst prepared by co-precipitation, towards various products, with 16 wt.% Nb_2O_5, at temperatures ranging from 260 to 320 °C.

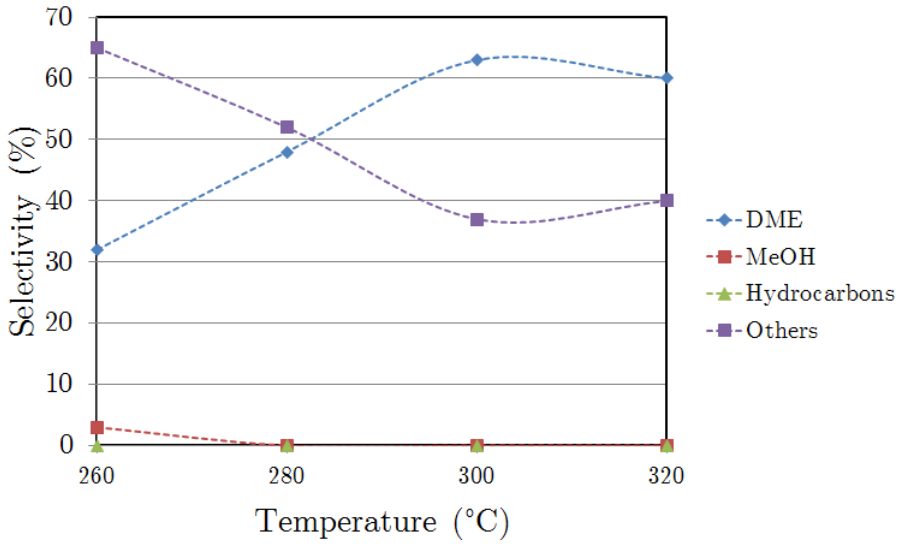

Figure 4.14: Selectivity of Cu/Zn/Nb catalyst prepared by co-precipitation, towards various products, with 32 wt.% Nb_2O_5, at temperatures ranging from 260 to 320 °C.

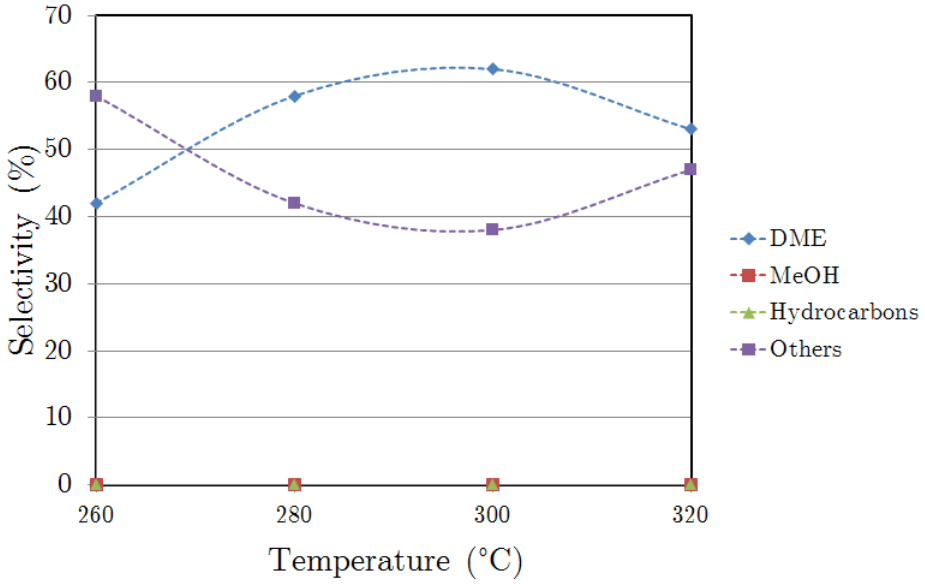

Figure 4.15: Selectivity of Cu/Zn/Nb catalyst prepared by co-precipitation, towards various products, with 78 wt.% Nb_2O_5, at temperatures ranging from 260 to 320 °C.

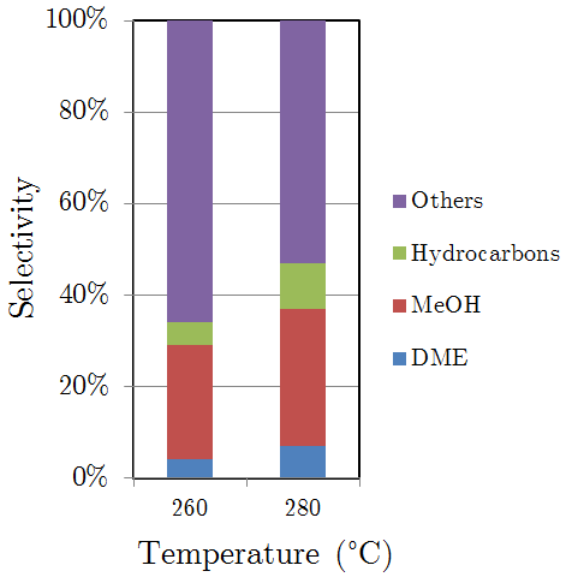

Figure 4.16: Selectivity of Cu/Zn/Nb catalyst prepared by co-precipitation with 10 wt.% Nb_2O_5 using oxalic acid and acetone.

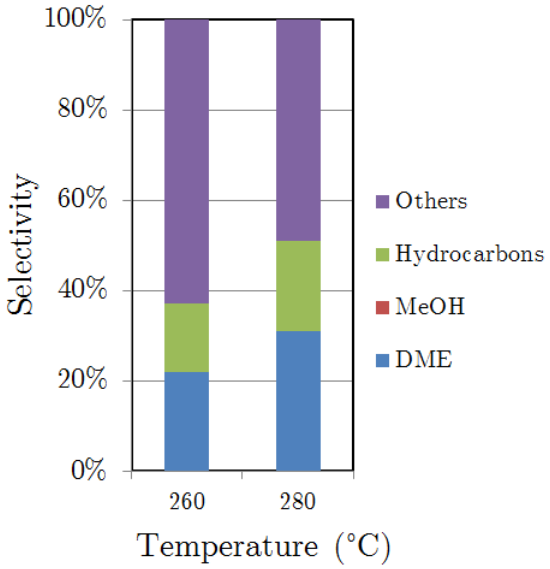

Figure 4.17: Selectivity of Cu/Zn/Nb catalyst prepared by co-precipitation with 20 wt.% Nb_2O_5 using oxalic acid and acetone.

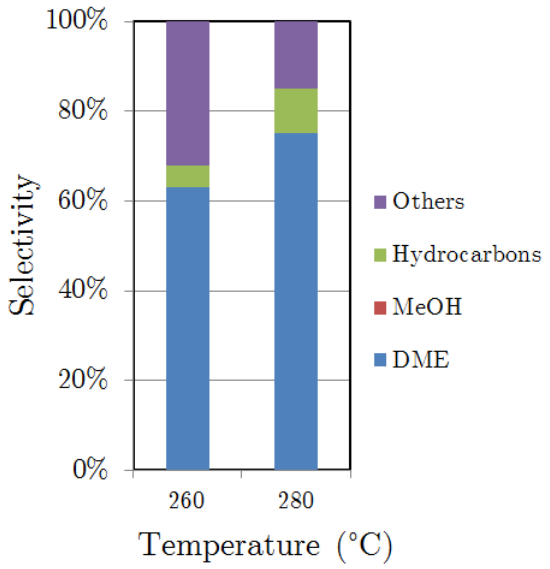

Figure 4.18: Selectivity of Cu/Zn/Nb catalyst prepared by co-precipitation with 40 wt.% Nb_2O_5 using oxalic acid and acetone.

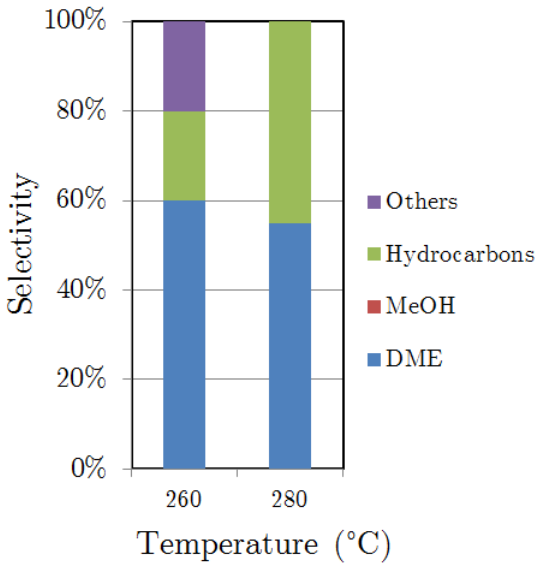

Figure 4.19: Selectivity of Cu/Zn/Nb catalyst prepared by co-precipitation with 80 wt.% Nb_2O_5 using oxalic acid and acetone..

Chapter 5

Results and discussion - sequential precipitation

5.1 Catalyst characterisation

Powder X-ray diffraction patterns of samples prepared by sequential precipitation using ammonium carbonate as a precipitating agent, show a similar trend as co-precipitate catalysts (Chapter **4.1**). At a low aimed niobia weight loading of 15%, only diffraction peaks corresponding to the presence of CuO and ZnO are visible. Increasing the aimed weight loading of niobia to 40%, diffraction peaks for copper and zinc niobates become visible (Table 4.1). Like these catalysts prepared by co-precipitation, catalysts prepared by sequential precipitation show identical peaks due to the presence of crystalline CuO and ZnO phases Figure 5.2). However, even with an aimed composition of 80 wt.%, no copper or zinc niobates can be seen. This indicates that the formation of these niobates is a direct result of the synthesis method, e.g. precipitation induced by a change of pH.

Precipitation by injection into an oxalic acid/acetone solution is a very spontaneous process, the blue colour of the copper and zinc nitrate solution fades almost instantly. Raising the pH however is far less spontaneous, as the blue colour slowly fades during the addition of the base and the ageing process. It can be expected that the different precursors, i.e. the dissolved ions, have very little or a lot of contact time depending on the precipitation process. From this, a slow precipitation can be understood to result in relatively many interactions between niobia and copper/zinc in the resulting catalyst. The formation of the metal niobates is then a direct consequence of these interactions.

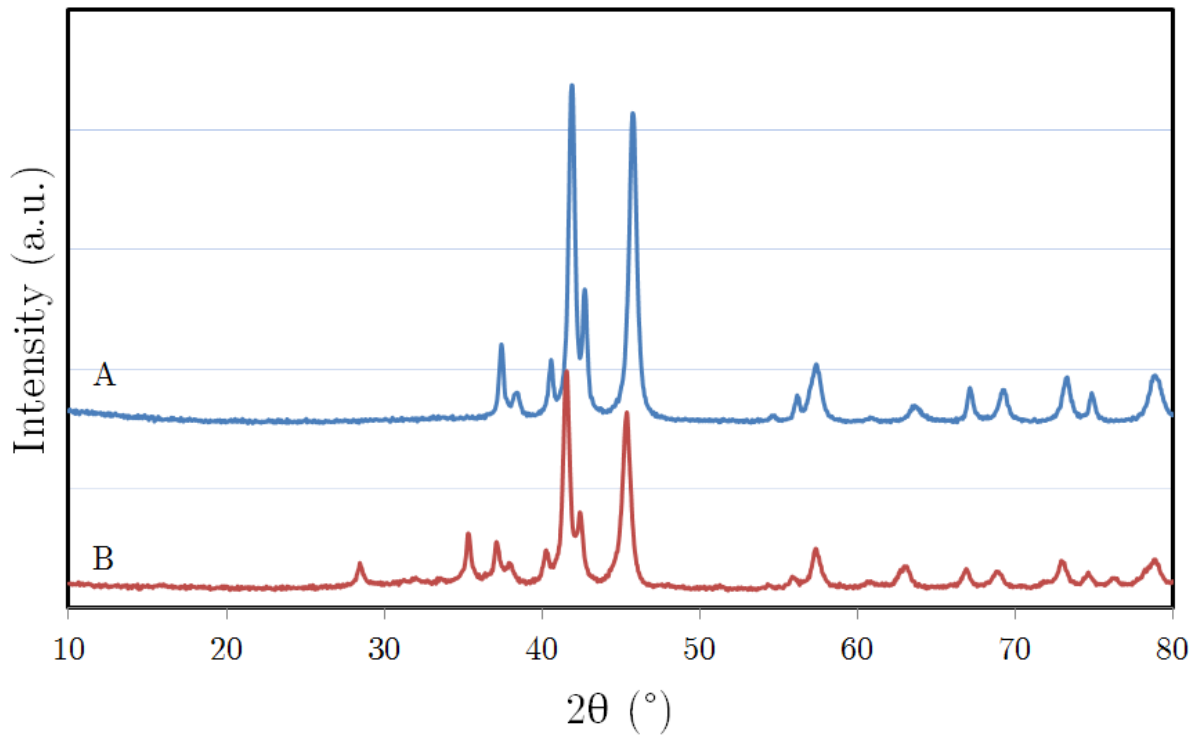

Figure 5.1: XRD of catalysts prepared by sequential precipitation using an aqueous solution of ammonium carbonate. **A**) aimed composition of 15 wt.% Nb_2O_5; **B**) aimed composition of 40 wt.% Nb_2O_5.

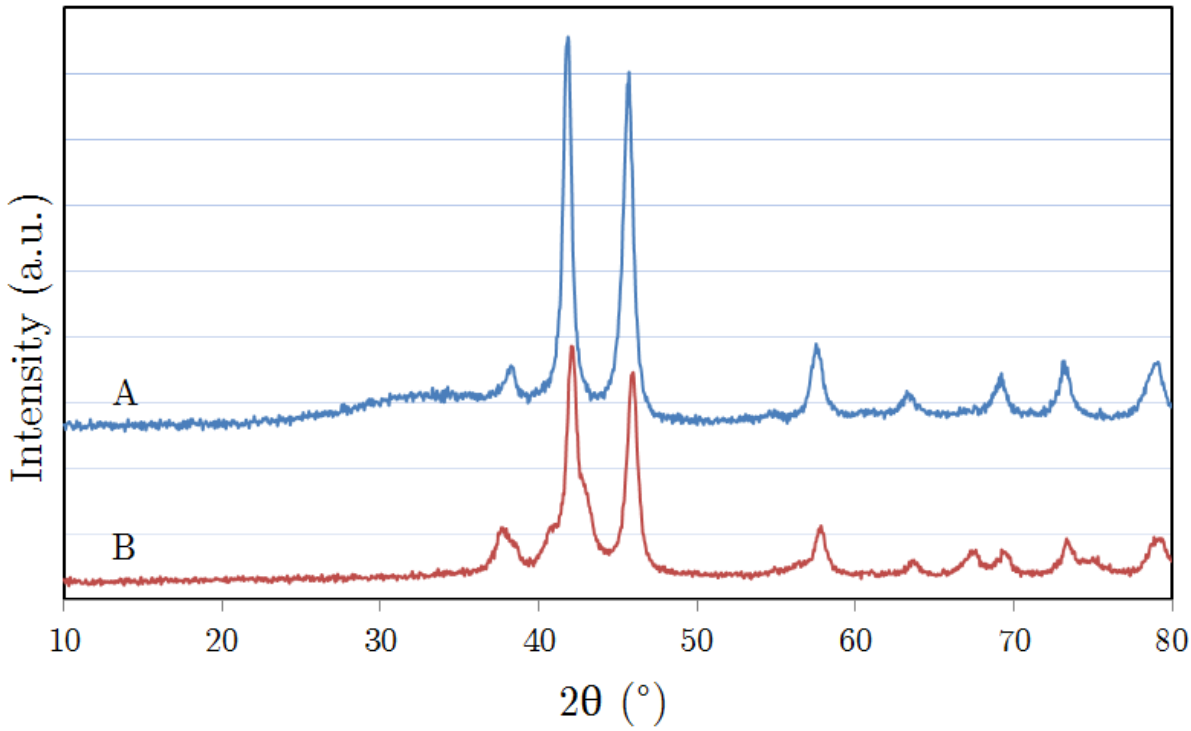

Figure 5.2: XRD of catalysts prepared by sequential precipitation prepared by using a solution of oxalic acid in acetone. **A**) aimed composition of 40 wt.% Nb_2O_5; **B**) aimed composition of 80 wt.% Nb_2O_5.

In order to evaluate the presence of these copper and zinc niobates during the actual methanol synthesis, hydrogen assisted temperature programmed reduction (H_2-TPR) experiments were performed. During these experiments, the dried sample was reduced by flowing 10% H_2 in He over the sample while heating to 1000 °C. TPR profiles are shown in Figure 5.3 for samples with aimed weight loadings of 40 and 80 wt.% niobia, either prepared by co-precipitation using a solution of ammonium carbonate or sequential precipitation by injecting both precursor solutions into a solution of oxalic acid in acetone. For catalysts prepared by co-precipitation, X-ray diffraction patterns showed a clear presence of copper and zinc niobates, whereas the catalysts prepared by sequential precipitation did not. However, it is then assumed that there are no other significant differences that might influence the reduction profiles of these catalysts. Although the TPR profiles differ significantly, from these profiles we can conclude that after reduction at 250 °C for 2.5 h, as is the usual pretreatment, no niobates are expected to be in the catalyst. As increasing the ZnO concentration in CZA catalysts is known to reduce the reduction temperature,[22] this can explain the shift visible in Figure 5.3.

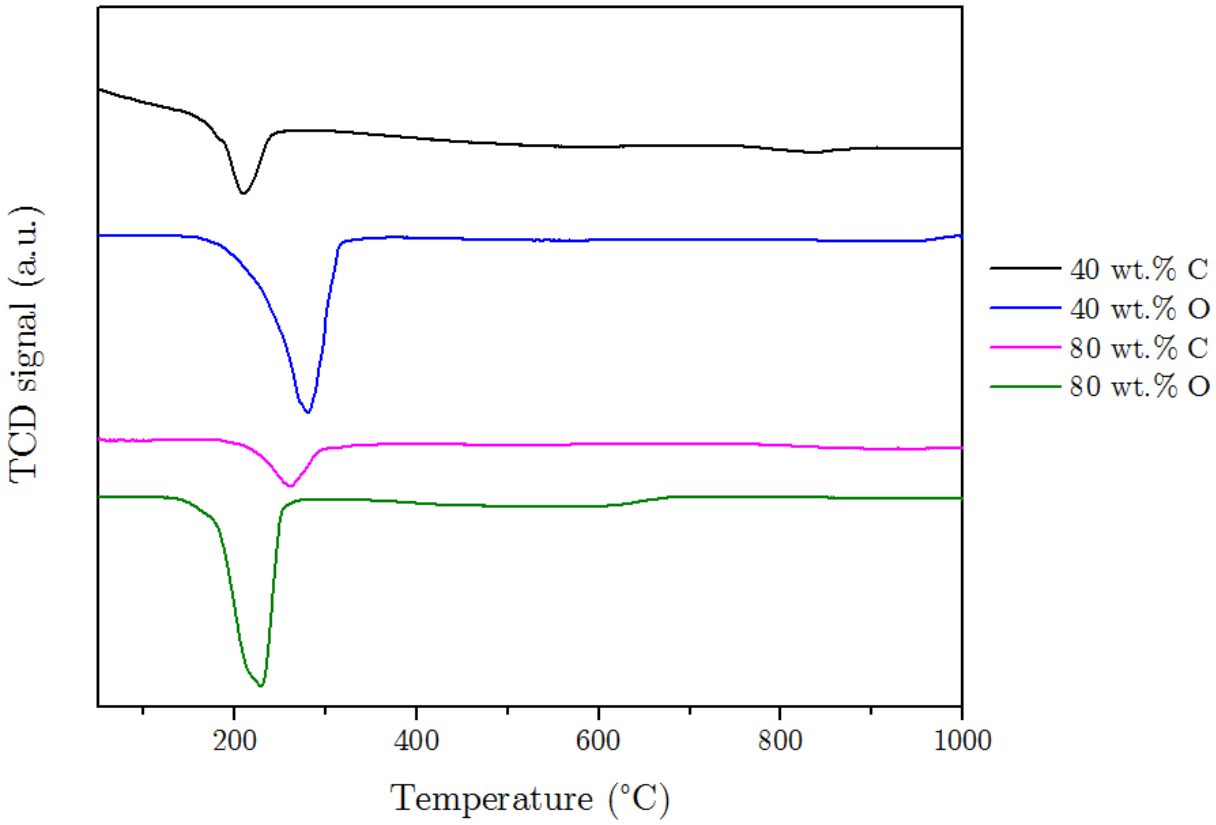

Figure 5.3: TPR profiles of various catalysts. **C** indicates catalyst prepared by co-precipitation using ammonium carbonate solution; **O** indicates catalyst prepared by sequential precipitation using oxalic acid in acetone.

The acidic functionalities were investigated by ammonia temperature programmed desorption (NH_3-TPD). A summary of these experiments is given in Table 5.1, for samples prepared by sequential precipitation using a solution of ammonium carbonate as a precipitating agent, and Table 5.2, for samples prepared by sequential injection of precursor solutions into a solution of oxalic acid in acetone. From the temperature at max desorption we can conclude that there is no significant difference in the strength of these acid sites. However, sequential precipitation into a solution of oxalic acid in acetone yields far more acid sites per gram of catalysts. An explanation for this increase in acid sites is that not all ammonium niobium oxalate (ANO) precipitates at a pH of 7, which is reached by adding ammonium carbonate. Injecting the aqueous solution of ANO into acetone however results in a much higher yield of precipitate. Therefore the actual niobia weight loadings might be slightly less than the aimed loading, in catalysts prepared by adding an aqueous ammonium carbonate solution as precipitating agent.

Table 5.1: Ammonia TPD data of various catalyst prepared by sequential precipitation using an aqueous solution of ammonium carbonate.

Weight loading Nb_2O_5 (%)	Amount of NH_3 (mmol/g)	T at max (°C)
15	0.25	280
40	0.18	290
80	0.14	305
$Nb_2O_5 \cdot nH_2O$ calcined at 400 °C	0.78	178

Table 5.2: Ammonia TPD data of various catalyst prepared by sequential precipitation using a solution of oxalic acid in acetone.

Weight loading Nb_2O_5 (%)	Amount of NH_3 (mmol/g)	T at max (°C)
10	0.31	275
20	0.40	300
40	0.41	305
80	0.32	285
$Nb_2O_5 \cdot nH_2O$ calcined at 400 °C	0.78	178

Transmission electron microscopy (TEM) images of catalysts prepared by sequential precipitation using sequential injection of the precursor solutions into a solution of oxalic acid in acetone are shown in Figure 5.4. Using the sequential precipitation the structure of these catalysts is visibly different from catalysts prepared by co-precipitation. As the co-precipitate catalysts showed the formation of large aggregates, with almost no distinguishable particles, especially at high niobia loadings (40 and 80 wt.%). Whereas the catalysts prepared by sequential precipitation do show a very open structure, even at these high niobia weight loadings. However, as no EDX maps were available of these catalysts, the spatial distribution of copper and zinc oxide with respect to niobia is unknown. EDX is essential to visualize the various metal oxides due to their near identical contrast in TEM images. Therefore no conclusions can be drawn on the proximity between these different functionalities. Although one might expect that the niobia precipitates in close proximity to the already precipitated copper and zinc precursor precipitate, and even might enclose these copper and zinc precursors. This would eventually lead to less available Cu/ZnO surface available for methanol synthesis. The larger - expected - niobia surface however, would then result in high dehydration of methanol into dimethyl ether. Effectively yielding lower activity but high selectivity.

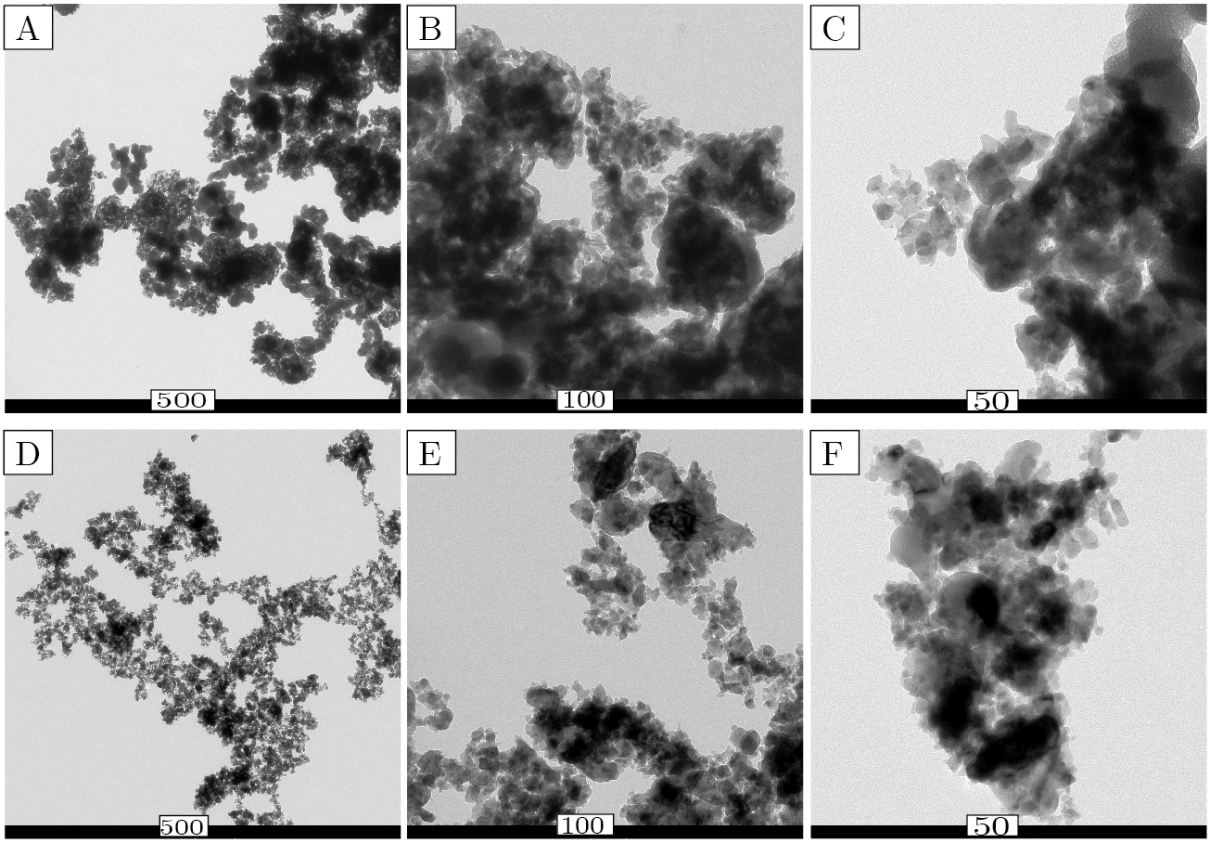

Figure 5.4: TEM images of catalyst prepared by sequential precipitation in a solution of oxalic acid in acetone. **A**, **B**, **C** have an aimed weight composition of 40 wt.% Nb_2O_5; **D**, **E**, **F** have an aimed weight composition of 80 wt.% Nb_2O_5. All scale bars are in nanometer.

5.2 Catalytic performance

5.2.1 Activity

The activity of various catalysts prepared by co-precipitation was compared. The activities are plotted as CTY against the TOS. In Figure 5.5 the activities of catalysts prepared by sequential-precipitation using an aqueous solution of ammonium carbonate are plotted, with an aimed composition of 15 and 40 wt.% Nb_2O_5. As the sample with an aimed composition of 80 wt.% Nb_2O_5 was not catalytically active at all, this was assumed to be solely Nb_2O_5. This catalyst was mixed with a commercial CZA catalyst in a 80/20 weight ratio of Nb_2O_5 to commercial CZA catalyst. The activity for this physical mixture, combined with the catalysts prepared by sequential precipitation is shown in 5.6. Activities for catalysts prepared by sequential precipitation, by injection of the precursor solutions into a solution of oxalic acid in acetone, are shown in Figure 5.7.

In Figure 5.5 a clear increase in activity can be seen upon increased niobia loadings. However, the activities are still very low, compared to a regular CZA catalyst or physical mixture (as shown in Chapter 3). This low activity can be explained by the premise that niobia precipitation occurs after the precipitation of the copper and zinc precursors, as previously mentioned. Thereby effectively blocking the active sites that convert syngas into methanol. As niobia in itself is not active in the hydrogenation of syngas, this results in a lower activity.

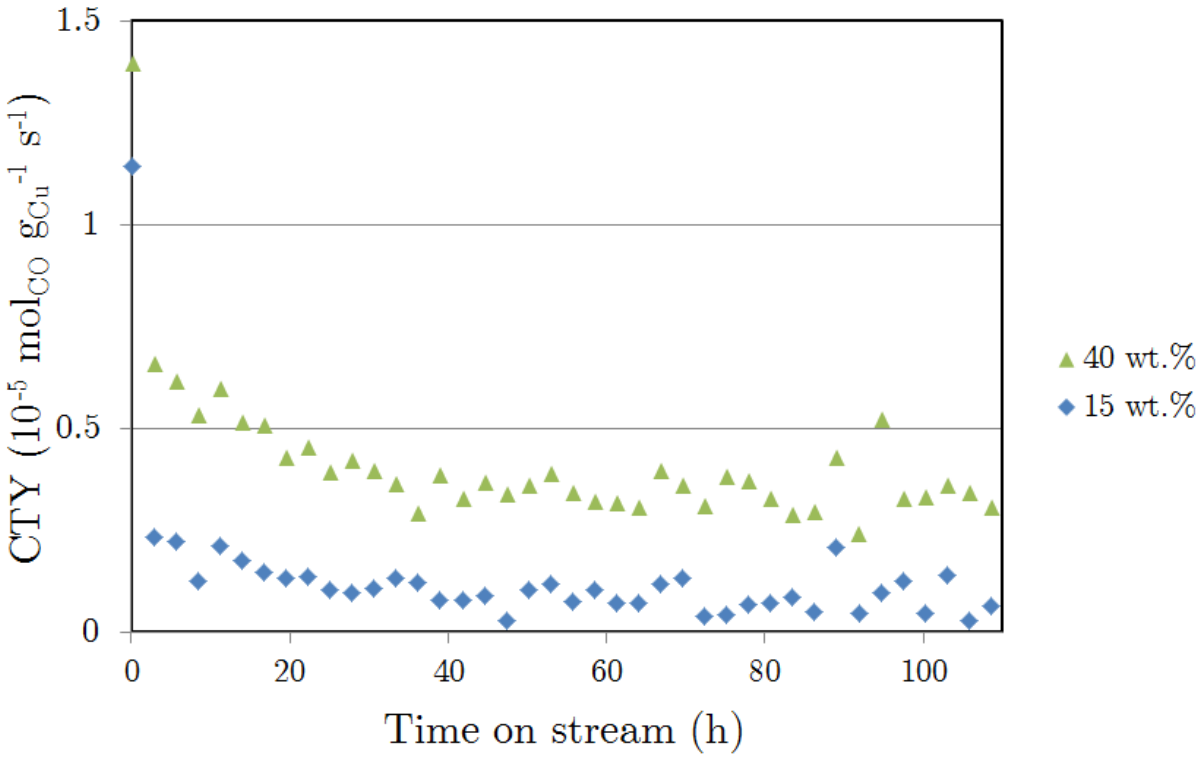

Figure 5.5: Activity of various catalysts prepared by sequential precipitation using ammonium carbonate. Reaction at 260 °C, with 40 bar total pressure, a H_2/CO ratio of 2, GHSV = 1100 and 1500 h^{-1} for the catalyst containing 15 and 40 wt.% Nb_2O_5 respectively.

The catalyst with an aimed composition of 80 wt.% Nb_2O_5, prepared by sequential precipitation, showed no activity for CO conversion. Therefore it was assumed to consist solely of Nb_2O_5, as either all copper/zinc had redissolved or blocked by the surrounding niobia. A physical mixture was prepared resulting in a final composition of 80 wt.% of the prepared Nb_2O_5 and 20 wt.% commercial CZA catalyst. This catalysts shows a significant increase in activity, although it is still not nearly as active as the physical mixtures from commercially available niobic acid (as seen in Figure 3.4). Since this catalyst is less active, we can conclude that the niobia precipitated from an aqueous ANO solution using ammonium carbonate is less active in methanol dehydration. A possible explanation for this lower activity is the significantly (more than 5 times) lower amount of acid sites, as shown in Table 5.1.

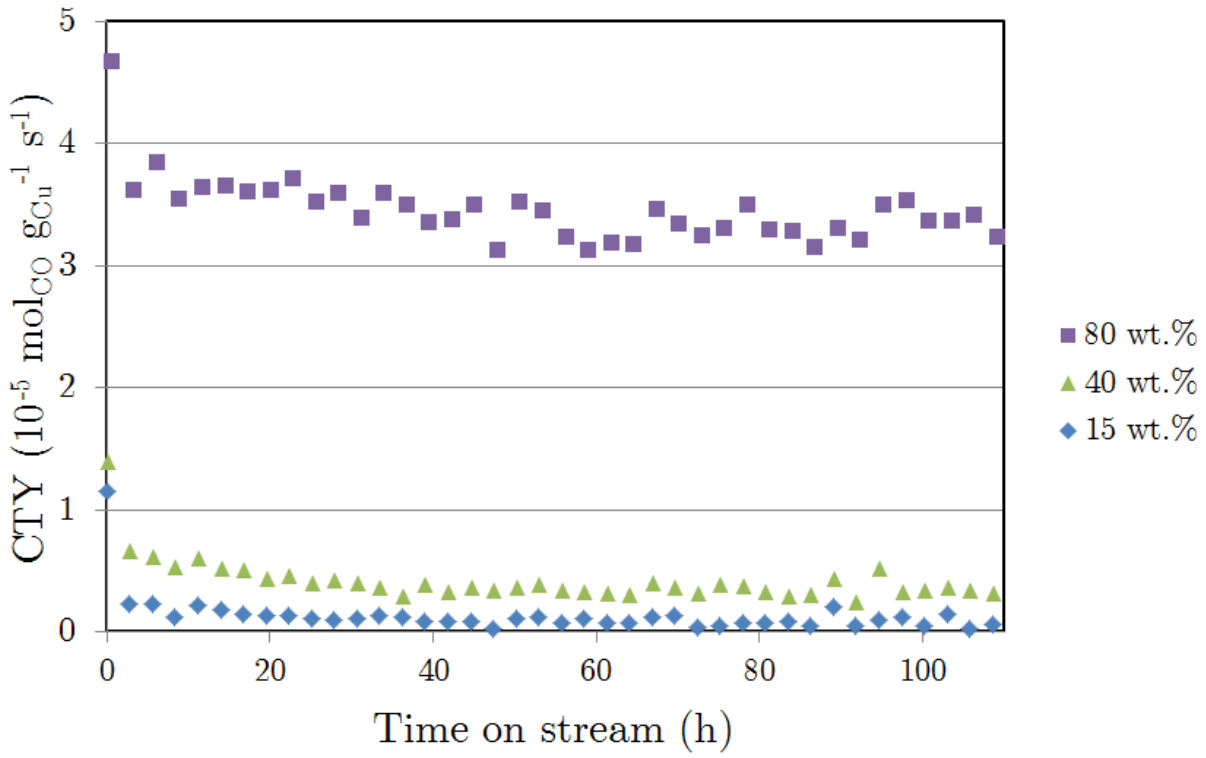

Figure 5.6: Activity of various catalysts prepared by sequential precipitation using ammonium carbonate. 80 wt.% Nb_2O_5 is a physical mixture with 20 wt.% commercial methanol synthesis catalyst. Reaction at 260 °C, with 40 bar total pressure, a H_2/CO ratio of 2, the GHSV of the physical mixture was 3500 h^{-1}.

Activities for various catalysts prepared by sequential precipitation, adapted from Xiang et al.[113] as described in Chapter 2, are shown in Figure 5.7. Although no clear increase in activity can be seen when increasing the aimed weight loading of niobia from 10 to 20 wt.%, higher niobia loadings do result in higher activity, which is consistent with our previous observations. The discrepancy between the samples aimed to contain 10 or 20 wt.% niobia and the sample aimed to contain 40 wt.% niobia can be explained to the far lower GHSV.

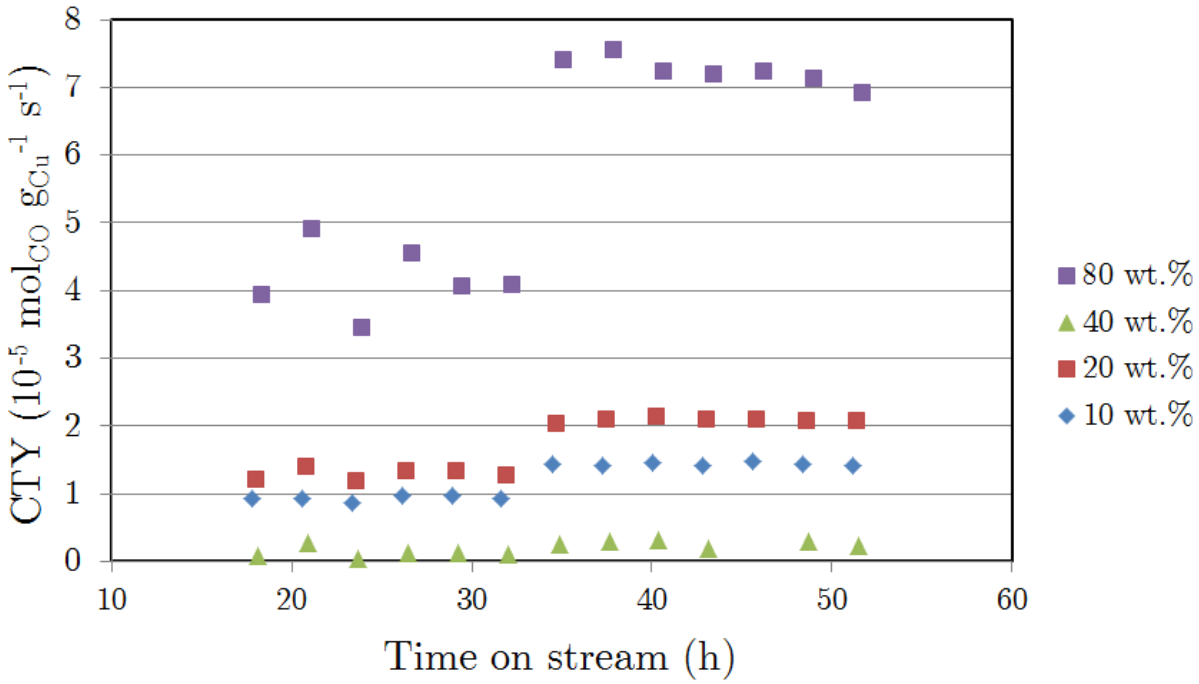

Figure 5.7: Activity of various catalysts prepared by sequential precipitation, induced by precipitation into a solution of oxalic acid in acetone. Reaction at 260 °C (0–32 h TOS) and 280 °C (33-55 h TOS), with 40 bar total pressure, a H_2/CO ratio of 2, GHSV = 3000–3600 h^{-1}, the sample aimed to contain 40 wt.% Nb_2O_5 GHSV = 1400.

5.2.2 Selectivity

As mentioned before, it is expected that the obtained catalysts contain niobia and copper/zinc oxide in a close proximity, with niobia possibly enclosing these copper/zinc oxide sites. If this were the case, relatively lower activities but higher selectivities towards DME are expected. Selectivities towards various products for catalysts prepared by sequential precipitation, using ammonium carbonate as a precipitating agent, are shown in Figure 5.8 and 5.9. Figure 8.3 shows the product distribution for the aforementioned physical mixture containing 20 wt.% commercial CZA catalyst and 80 wt.% of the sequential precipitate that was assumed to be solely niobia. The product distribution for catalysts that are prepared by sequential precipitation, by injecting of the precursor solutions into a solution of oxalic acid in acetone, are given in Figure 5.11–5.14

The hypothesis that niobia encapsulates Cu/ZnO particles works very well for the catalyst shown in Figure 5.9. Which, even at a relatively low weight loading of niobia, shows a selectivity towards DME of more than 80% at 280 °C. Catalysts prepared by sequential precipitation using an aqueous solution of ammonium carbonate as a precipitating agent, again show a relatively high selectivity towards the formation of other products. The product distribution of the physical mixture, Figure 8.3, seems to favour the formation of methanol over DME. This can be explained by the low temperature, of 260 °C, a temperature at which methanol dehydration to DME is low, as shown in Chapter 3.

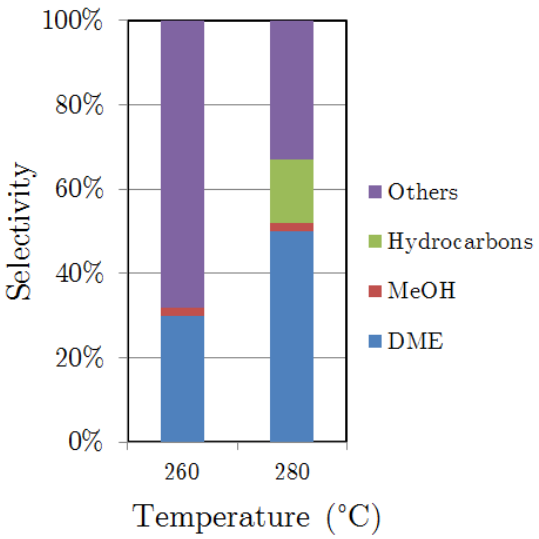

Figure 5.8: Selectivity of Cu/Zn/Nb catalyst prepared by sequential precipitation with 15 wt.% Nb_2O_5 using ammonium carbonate solution.

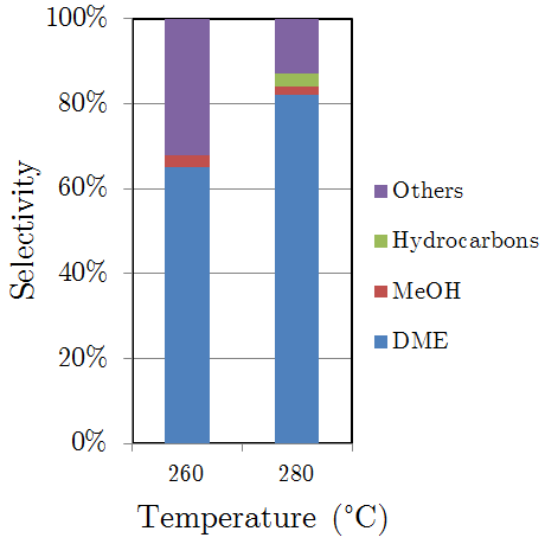

Figure 5.9: Selectivity of Cu/Zn/Nb catalyst prepared by sequential precipitation with 40 wt.% Nb_2O_5 using ammonium carbonate solution.

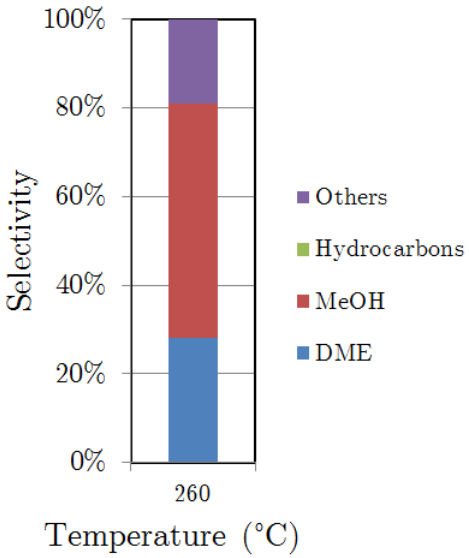

Figure 5.10: Selectivity of Cu/Zn/Nb catalyst prepared by sequential precipitation with 80 wt.% Nb_2O_5, prepared using an aqueous solution of ammonium carbonate as precipitating agent, and 20 wt.% commercial CZA catalyst.

However, this hypothesis does not hold for the catalysts shown in Figure 5.11–5.14. These catalysts all show a significant selectivity towards methanol, except for the catalyst with an aimed weight composition of 40% niobia. For this, we have already mentioned the low GHSV, which explains this increase in DME selectivity. For the catalysts that have an aimed composition of 10, 20 and 80 wt.% niobia the GHSV was quite high. This effectively results in a lower residence time in the reactor, so that there is not enough time for the formation of DME.

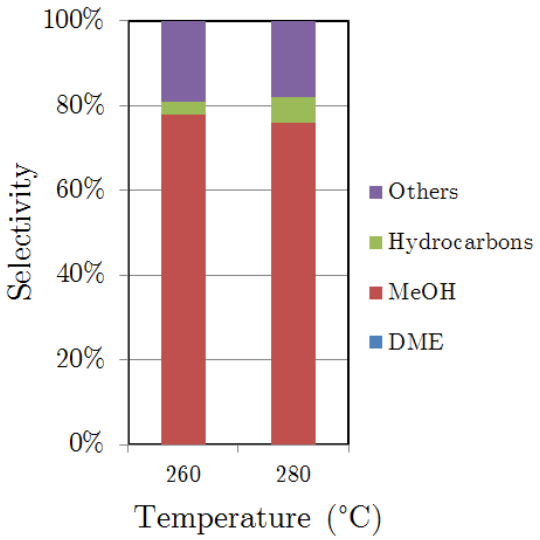

Figure 5.11: Selectivity of Cu/Zn/Nb catalyst prepared by sequential precipitation with 10 wt.% Nb_2O_5 using oxalic acid and acetone.

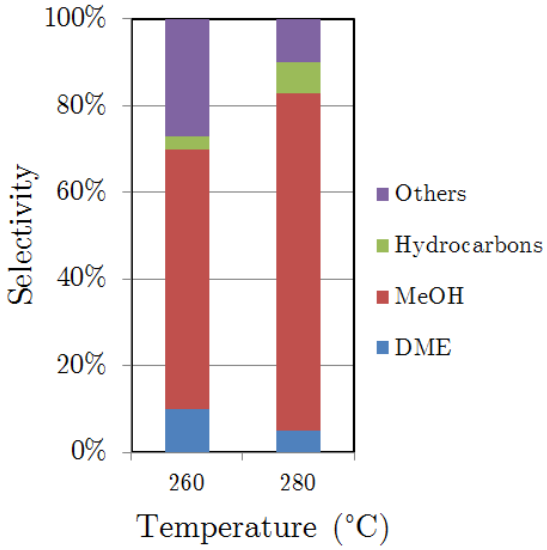

Figure 5.12: Selectivity of Cu/Zn/Nb catalyst prepared by sequential precipitation with 20 wt.% Nb_2O_5 using oxalic acid and acetone.

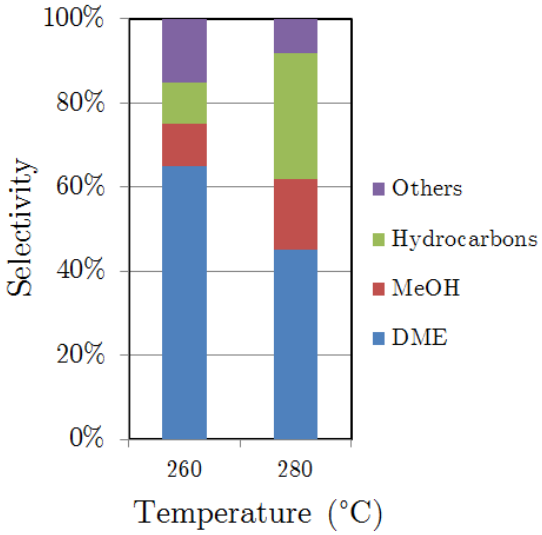

Figure 5.13: Selectivity of Cu/Zn/Nb catalyst prepared by sequential precipitation with 40 wt.% Nb_2O_5 using oxalic acid and acetone.

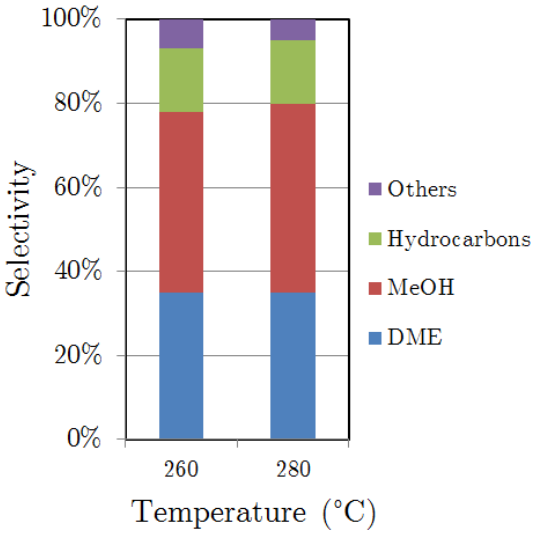

Figure 5.14: Selectivity of Cu/Zn/Nb catalyst prepared by sequential precipitation with 80 wt.% Nb_2O_5 using oxalic acid and acetone.

Chapter 6

Conclusions

6.1 General comments

Various niobium-based bifunctional catalysts for the direct conversion of synthesis gas to dimethyl ether have been synthesised, characterised, and their catalytic performance was evaluated. Catalysts were prepared by three distinct preparation methods: physical mixtures, co-precipitation and sequential precipitation. For these three methods the conclusions will be discussed separately in this chapter.

6.2 Physical mixtures

Commercially available niobic acid and methanol synthesis catalysts were physically mixed together and showed superior activity in the STD reaction. For the studied niobic acid to methanol synthesis catalysts ratios, no maximum in CTY was reached (for a 3:1 weight ratio). Indicating that higher activities can be reached upon increasing the niobic acid to methanol synthesis catalysts ratio even further. As the commercial methanol synthesis catalysts was found to lose its selectivity towards methanol at temperatures above 280 °C, catalytic performance was thereafter evaluated around this temperature. At low niobic acid to CZA catalysts, methanol was still one of the main constituents of the product distribution. Under none of the tested conditions (temperatures or weight ratios) were hydrocarbons formed by these physical mixtures. The formation of unidentified "other" products was almost negligible for catalysts with a high ratio of niobic acid to CZA catalyst or at higher (> 280 °C) temperatures.

6.3 Co-precipitation

Catalysts prepared by co-precipitation using an aqueous ammonium bicarbonate solution as precipitating agent were shown to contain copper and zinc niobates at high niobia weight loadings. Catalysts prepared by co-precipitation by injection into a solution of oxalic acid in acetone did not contain these niobates. Increasing the (aimed) niobia weight ratio resulted into an increase in acid sites, as determined by ammonia TPD. However, increasing the aimed niobia weight loading from 40 to 80 wt.% resulted in a loss of acid sites per gram sample. This effect was observed for catalysts prepared by both described co-precipitation methods. The loss in acid sites was explained by the formation of aggregates, an hypothesis that was supported by the obtained TEM images. HAADF-STEM-EDX images revealed that co-precipitation induced by the addition of ammonium bicarbonate resulted in a very close proximity between Cu/Zn and Nb (as seen in the EDX maps). However, Nb was not found separately from Cu or Zn. In catalysts prepared by injection into a solution of oxalic acid into acetone, the Nb was much more evenly distributed. In this sample the Nb, Zn and Cu signal were all much more distributed, indicating a less active methanol synthesis catalysts (as close proximity between Cu and ZnO is essential). Catalysts prepared using ammonium bicarbonate as a precipitating agent formed methanol, DME and unidentified "other" products. Selectivity towards methanol decreased with an increase in niobia weight ratio or temperature. The composition of these "other" products remains unknown, but is assumed to be mostly small oxygenates.

6.4 Sequential precipitation

Catalysts prepared by sequential precipitation using an aqueous ammonium bicarbonate solution as precipitating agent were shown to contain copper and zinc niobates at high niobia weight loadings. Catalysts prepared by sequential precipitation by injection into a solution of oxalic acid in acetone did not contain these niobates, like their co-precipitate prepared counterparts. This indicates that the formation of niobates is specific for the precipitation method used, and is not (exclusively) an effect of the ageing/decomposition process. Although copper and zinc niobates are present in the catalysts, TPR experiments show that they will be reduced prior to reaction, and thus not very significant. Sequential precipitation yields a large amount of acid sites per gram of sample, indicating that methanol synthesis catalysts will be blocked in the process. Precipitation by injection into a solution of oxalic acid in acetone yields far more acid sites than precipitation induced by the addition of an ammonium bicarbonate solution. This can be explained if the precipitation yield is higher and the actual niobium weight loadings are not exact as aimed. All catalysts prepared by sequential precipitation show very low activity in the direct STD reaction, this is explained by the model that the niobium precursor precipitates onto the methanol synthesis catalyst precursor. Effectively blocking most of the active sites of the methanol synthesis catalysts in the process. Although not very active, these catalysts show a relatively high selectivity towards DME, as most methanol that is formed is dehydrated, even at relatively low niobia weight loadings and temperatures.

Chapter 7

Outlook

Further research is needed to, accurately, determine the influence of the synthesis method on the obtained catalyst and elucidate its structure performance relationship. One of the main questions that remains unanswered is the composition of the various "other" products mentioned in this thesis. Although they are expected to be small oxygenates, this was not verified. This can be done by testing the catalysts under identical conditions, using a GC equipped with a suitable column for separating these products. Investigation of these products will give valuable insight into the performance of the tested catalysts.

Elucidating the exact elemental composition of the prepared catalysts will give us more insight into the catalytic activity. As the Geolab of Utrecht University wasn't able to accurately determine this composition by ICP-MS, certain companies might be able to do so. Knowing the exact chemical composition will be of great be of great importance in determining the activity, and correlating the amount of niobia to the amount of acid sites in the system.

As the synthesis methods used are not very constant, designing one that is will greatly improve the analysis. Eliminating human error can be done by using an automated lab set up, as described by Schumann[22], this will yield far more consistent catalysts. The synthesis method can then further be refined by systematically adjusting parameters. As a result, catalysts can be compared more effectively.

Since the prepare catalysts consist of many different phases, from the precursor salts used to the metal oxides, model systems can be designed to investigate the influence of the proximity between these different phases. For example, eliminating zinc oxide will yield a significantly less complicated catalysts already. Defined copper particles on an inert substrate can serve as a model methanol synthesis catalyst for CO hydrogenation to methanol.

As the current experimental setup did not allow for the use of syngas that contains CO_2, this can be researched in the future. As shown in the introductory section of this thesis, the Cu/ZnO catalysts are less suited for CO hydrogenation to methanol than catalysts that do not contain ZnO. Including small amounts of CO_2 in the syngas feed used will more accurately mimic the relevant conditions.

Chapter 8

Acknowledgements

C. Hernández Mejía is gratefully acknowledged for his guidance, support and teaching during this project.

Prof. dr. ir. K.P. de Jong is gratefully acknowledged for his supervision of this project and all valuable teaching moments and shared insights.

P.P. Paalanen, J.L Weber and M. Rivera Torrente are acknowledged for measuring N_2 physisorption data.

M. Versluijs-Helder is acknowledged for her instructions on using the Bruker D2 for XRD.

B. Luna Murillo and R. Oord are acknowledged for their assistance in using the Micrometrics AutoChem for ammonia TPD.

T.W. van Deelen, W.S. Lamme and L.I. van der Wal are acknowledged for their help in obtaining all (S)TEM images in this thesis.

Nearly the whole Inorganic Chemistry and Catalysis group, from students to professors, is acknowledged for their help and useful discussions during this research project.

References

[1] British Petroleum, "BP Statistical Review of World Energy 2017," *BP Statistical Review of World Energy*, no. 66, pp. 1–52, 2017.

[2] J. Furman and G. Sperling, "Reducing America's Dependence on Foreign Oil As a Strategy to Increase Economic Growth and Reduce Economic Vulnerability — whitehouse.gov," 2013.

[3] A. J. Cohen, H. R. Anderson, B. Ostro, K. D. Pandey, M. Krzyzanowski, N. Künzli, K. Gutschmidt, A. Pope, I. Romieu, J. M. Samet, and K. Smith, "The global burden of disease due to outdoor air pollution," *Journal of Toxicology and Environmental Health - Part A*, vol. 68, no. 13-14, pp. 1301–1307, 2005.

[4] H. Schulz, "Short history and present trends of FischerTropsch synthesis," *Applied Catalysis A: General*, vol. 186, no. 1-2, pp. 3–12, 1999.

[5] R. Verbeek, A. van Doorn, and M. van Walwijk, "Global assessment of Dimethylether as an automotive fuel (second edition)," tech. rep., TNO, Delft, 1996.

[6] T. A. Semelsberger, R. L. Borup, and H. L. Greene, "Dimethyl ether (DME) as an alternative fuel," *Journal of Power Sources*, vol. 156, no. 2, pp. 497–511, 2006.

[7] T. H. Fleisch, A. Basu, and R. A. Sills, "Introduction and advancement of a new clean global fuel: The status of DME developments in China and beyond," *Journal of Natural Gas Science and Engineering*, vol. 9, pp. 94–107, 2012.

[8] Z. Azizi, M. Rezaeimanesh, T. Tohidian, and M. R. Rahimpour, "Dimethyl ether: A review of technologies and production challenges," *Chemical Engineering and Processing: Process Intensification*, vol. 82, pp. 150–172, 2014.

[9] International DME Association, "About DME."

[10] Biofuels Research Advisory Council, "Biofuels in the European Union," 2006.

[11] Y. Adachi, M. Komoto, I. Watanabe, Y. Ohno, and K. Fujimoto, "Effective utilisation of remote coal through dimethyl ether synthesis," *Fuel*, vol. 79, pp. 229–234, 2000.

[12] C. Arcoumanis, C. Bae, R. Crookes, and E. Kinoshita, "The potential of di-methyl ether (DME) as an alternative fuel for compression-ignition engines: A review," *Fuel*, vol. 87, no. 7, pp. 1014–1030, 2008.

[13] E. D. Larson and H. Yang, "Dimethyl ether (DME) from coal as a household cooking fuel in China," *Energy for Sustainable Development*, vol. 8, no. 3, pp. 115–126, 2004.

[14] K. Takeishi, "Dimethyl ether and catalyst development for production from syngas," *Biofuels*, vol. 1, no. 1, pp. 217–226, 2010.

[15] G. Myhre, D. Shindell, F.-M. Bréon, W. Collins, J. Fuglestvedt, J. Huang, D. Koch, J.-F. Lamarque, D. Lee, B. Mendoza, T. Nakajima, A. Robock, G. Stephens, T. Takemura, and H. Zhang, "Anthropogenic and Natural Radiative Forcing," *Climate Change 2013: The Physical Science Basis. Contribution of Working Group I to the Fifth Assessment Report of the Intergovernmental Panel on Climate Change*, pp. 659–740, 2013.

[16] K. L. Ng, D. Chadwick, and B. A. Toseland, "Kinetics and modelling of dimethyl ether synthesis from synthesis gas," *Chemical Engineering Science*, vol. 54, no. 15-16, pp. 3587–3592, 1999.

[17] F. Hayer, H. Bakhtiary-Davijany, R. Myrstad, A. Holmen, P. Pfeifer, and H. J. Venvik, "Synthesis of dimethyl ether from syngas in a microchannel reactor-Simulation and experimental study," *Chemical Engineering Journal*, vol. 167, no. 2-3, pp. 610–615, 2011.

[18] W.-J. Shen, K.-W. Jun, H.-S. Choi, and K.-W. Lee, "Thermodynamic investigation of methanol and dimethyl ether synthesis from CO2 Hydrogenation," *Korean Journal of Chemical Engineering*, vol. 17, no. 2, pp. 210–216, 2000.

[19] Z. Nie, H. Liu, D. Liu, and W. Ying, "Intrinsic Kinetics of Dimethyl Ether Synthesis from Syngas," *Journal of Natural Gas Chemistry*, vol. 14, pp. 22–28, 2005.

[20] A. Mittasch, M. Pier, and K. Winkler, "Production of Oxygenated Organic Compounds," 1925.

[21] G. C. Chinchen, P. J. Denny, J. R. Jennings, M. S. Spencer, and K. C. Waugh, "Review - Synthesis of Methanol Part 1. Catalysts and Kinetics," *Applied Catalysis*, vol. 36, pp. 1–65, 1988.

[22] J. Schumann, *Cu , Zn-based catalysts for methanol synthesis.* PhD thesis, Technischen Universität Berlin, 2015.

[23] D. Sheldon, "Methanol Production A Technical History," *Johnson Matthey Technology Review*, vol. 61, no. 3, pp. 172–182, 2017.

[24] K. C. Waugh, "Methanol synthesis," *Catalysis Letters*, vol. 142, no. 10, pp. 1153–1166, 2012.

[25] M. Behrens, F. Studt, I. Kasatkin, S. Kuhl, M. Havecker, F. Abild-Pedersen, S. Zander, F. Girgsdies, P. Kurr, B. L. Kniep, M. Tovar, R. W. Fischer, J. K. Nørskov, and R. Schlogl, "The active site of methanol synthesis over Cu/ZnO/Al2O3 industrial catalysts," *Science*, vol. 336, no. 6083, pp. 893–897, 2012.

[26] F. Studt, M. Behrens, E. L. Kunkes, N. Thomas, S. Zander, A. Tarasov, J. Schumann, E. Frei, J. B. Varley, F. Abild-Pedersen, J. K. Nørskov, and R. Schlögl, "The Mechanism of CO and CO2 Hydrogenation to Methanol over Cu-Based Catalysts," *ChemCatChem*, vol. 7, pp. 1105–1111, 2015.

[27] G. C. Chinchen, K. C. Waugh, and D. A. Whan, "The activity and state of the copper surface in methanol synthesis catalysts," *Applied Catalysis*, vol. 25, pp. 101–107, 1986.

[28] P. Rasmussen, P. Holmblad, T. Askgaard, C. Ovesen, P. Stoltze, J. Nørskov, and I. Chorkendorff, "Methanol synthesis on Cu(100) from a binary gas mixture of CO2 and H2," *Catalysis letters*, vol. 26, no. 3-4, p. 373, 1994.

[29] V. Ponec, "Cu and Pd, two catalysts for CH3OH synthesis: the similarities and the differences," *Surface Science*, vol. 272, no. 1-3, pp. 111–117, 1992.

[30] T. Yurieva, L. Plyasova, T. Kriger, V. Zaikovskii, O. Makarova, and T. Minyukova, "State of Copper-Containing Catalyst for Methanol Synthesis in the Reaction Medium," *Reaction Kinetics and Catalysis Letters*, vol. 51, no. 2, pp. 495–500, 1993.

[31] J. Frost, "Junction effect interactions in methanol synthesis catalysts," *Nature*, vol. 334, p. 577, 1988.

[32] F. Liao, Y. Huang, J. Ge, W. Zheng, K. Tedsree, P. Collier, X. Hong, and S. C. Tsang, "Morphology-Dependent Interactions of ZnO with Cu Nanoparticles at the Materials' Interface in Selective Hydrogenation of CO2 to CH3OH," *Angewandte Chemie - International Edition*, vol. 50, no. 9, pp. 2162–2165, 2011.

[33] T. Fujitani and J. Nakamura, "The effect of ZnO in methanol synthesis catalysts on Cu dispersion and the specific activity," *Catalysis Letters*, vol. 56, no. 2-3, pp. 119–124, 1998.

[34] N. Topsøe and H. Topsøe, "On the nature of surface structural changes in Cu/ZnO methanol synthesis catalysts," *Topics in Catalysis*, vol. 8, no. 3/4, pp. 267–270, 1999.

[35] J. D. Grunwaldt, A. M. Molenbroek, N. Y. Topsøe, H. Topsøe, and B. S. Clausen, "In situ investigations of structural changes in Cu/ZnO catalysts," *Journal of Catalysis*, vol. 194, no. 2, pp. 452–460, 2000.

[36] R. Naumann d'Alnoncourt, X. Xia, J. Strunk, E. Löffler, O. Hinrichsen, and M. Muhler, "The influence of strongly reducing conditions on strong metalsupport interactions in Cu/ZnO catalysts used for methanol synthesis," *Physical Chemistry Chemical Physics*, vol. 8, no. 13, p. 1525, 2006.

[37] M. Kurtz, N. Bauer, C. Büscher, H. Wilmer, O. Hinrichsen, R. Becker, S. Rabe, K. Merz, M. Driess, R. Fischer, and M. Muhler, "New Synthetic Routes to More Active Cu/ZnO Catalysts Used for Methanol Synthesis," *Catalysis Letters*, vol. 92, no. 1, pp. 49–52, 2004.

[38] S. Polarz, F. Neues, M. W. E. Van Den Berg, W. Grünert, and L. Khodeir, "Mesosynthesis of ZnO-silica composites for methanol nanocatalysis," *Journal of the American Chemical Society*, vol. 127, no. 34, pp. 12028–12034, 2005.

[39] S. J. Tauster, "Strong Metal-Support Interactions," *Accounts of Chemical Research*, vol. 20, no. 11, pp. 389–394, 1987.

[40] C.-J. Pan, M.-C. Tsai, W.-N. Su, J. Rick, N. G. Akalework, A. K. Agegnehu, S.-Y. Cheng, and B.-J. Hwang, "Tuning/exploiting Strong Metal-Support Interaction (SMSI) in Heterogeneous Catalysis," *Journal of the Taiwan Institute of Chemical Engineers*, vol. 74, pp. 154–186, 2017.

[41] M. Spencer, "The role of zinc oxide in Cu/ZnO catalysts for methanol synthesis and the watergas shift reaction," *Topics in Catalysis*, vol. 8, pp. 259–266, 1999.

[42] J. Yoshihara and C. T. Campbell, "Methanol synthesis and reverse water-gas shift kinetics over Cu(110) model catalysts: Structural sensitivity," *Journal of Catalysis*, vol. 161, no. 2, pp. 776–782, 1996.

[43] I. Kasatkin, P. Kurr, B. Kniep, A. Trunschke, and R. Schl??gl, "Role of lattice strain and defects in copper particles on the activity of Cu/ZnO/Al2O3 catalysts for methanol synthesis," *Angewandte Chemie - International Edition*, vol. 46, no. 38, pp. 7324–7327, 2007.

[44] K. Klier, V. Chatikavanij, R. Herman, and G. Simmons, "Catalytic synthesis of methanol from CO/H2 IV. The effects of carbon dioxide," *Journal of Catalysis*, vol. 74, no. 2, pp. 343–360, 1982.

[45] Y. Amenomiya, "Methanol synthesis from CO2 + H2 II. Copper-based binary and ternary catalysts," *Applied Catalysis*, vol. 30, no. 1, pp. 57–68, 1987.

[46] G. C. Chinchen, P. J. Denny, D. G. Parker, M. S. Spencer, and D. A. Whan, "Mechanism of methanol synthesis from CO2/CO/H2 mixtures over copper/zinc oxide/alumina catalysts: use of 14C-labelled reactants," *Applied Catalysis*, vol. 30, no. 2, pp. 333–338, 1987.

[47] S. Zander, E. L. Kunkes, M. E. Schuster, J. Schumann, G. Weinberg, D. Teschner, N. Jacobsen, R. Schlögl, and M. Behrens, "The role of the oxide component in the development of copper composite catalysts for methanol synthesis," *Angewandte Chemie - International Edition*, vol. 52, no. 25, pp. 6536–6540, 2013.

[48] M. Saito and K. Murata, "Development of high performance Cu/ZnO-based catalysts for methanol synthesis and the water-gas shift reaction," *Catal. Surveys Asia*, vol. 8, no. 4, pp. 285–294, 2004.

[49] C. Baltes, S. Vukojević, and F. Schüth, "Correlations between synthesis, precursor, and catalyst structure and activity of a large set of CuO/ZnO/Al2O3 catalysts for methanol synthesis," *Journal of Catalysis*, vol. 258, no. 2, pp. 334–344, 2008.

[50] S. Kaluza, M. Behrens, N. Schiefenhövel, B. Kniep, R. Fischer, R. Schlögl, and M. Muhler, "A Novel Synthesis Route for Cu/ZnO/Al2O3 Catalysts used in Methanol Synthesis: Combining Continuous Consecutive Precipitation with Continuous Aging of the Precipitate," *ChemCatChem*, vol. 3, no. 1, pp. 189–199, 2011.

[51] S. Kühl, M. Friedrich, M. Armbrüster, and M. Behrens, "Cu,Zn,Al layered double hydroxides as precursors for copper catalysts in methanol steam reforming pH-controlled synthesis by microemulsion technique," *Journal of Materials Chemistry*, vol. 22, no. 19, p. 9632, 2012.

[52] G. Simson, E. Prasetyo, S. Reiner, and O. Hinrichsen, "Continuous precipitation of Cu/ZnO/Al2O3 catalysts for methanol synthesis in microstructured reactors with alternative precipitating agents," *Applied Catalysis A: General*, vol. 450, pp. 1–12, 2013.

[53] G. Prieto, K. P. De Jong, and P. E. De Jongh, "Towards 'greener' catalyst manufacture: Reduction of wastewater from the preparation of Cu/ZnO/Al2O3methanol synthesis catalysts," *Catalysis Today*, vol. 215, pp. 142–151, 2013.

[54] P. Munnik, P. de Jongh, and K. de Jong, "Recent Developments in the Synthesis of Supported Catalysts," *Chemical Reviews*, vol. 115, pp. 6687–6718, 2015.

[55] K. P. de Jong, *Synthesis of Solid Catalysts*. Wiley-VCH Verlag GmbH & Co. KGaA, 1st ed., 2009.

[56] M. Behrens and R. Schlögl, "How to prepare a good Cu/ZnO catalyst or the role of solid state chemistry for the synthesis of nanostructured catalysts," *Zeitschrift fur Anorganische und Allgemeine Chemie*, vol. 639, no. 15, pp. 2683–2695, 2013.

[57] M. Behrens, "Meso- and nano-structuring of industrial Cu/ZnO/(Al2O3) catalysts," *Journal of Catalysis*, vol. 267, no. 1, pp. 24–29, 2009.

[58] K.-W. Jun, W.-J. Shen, K. S. R. Rao, and K.-W. Lee, "Residual sodium effect on the catalytic activity of Cu/ZnO/Al2O3 in methanol synthesis from CO2 hydrogenation," *Applied Catalysis A: General*, vol. 174, pp. 231–238, 1998.

[59] J. L. Li and T. Inui, "Characterization of precursors of methanol synthesis catalysts, copper/zinc/aluminum oxides, precipitated at different pHs and temperatures," *Applied Catalysis A: General*, vol. 137, no. 1, pp. 105–117, 1996.

[60] S. Zander, B. Seidlhofer, and M. Behrens, "In situ EDXRD study of the chemistry of aging of co-precipitated mixed Cu,Zn hydroxycarbonates consequences for the preparation of Cu/ZnO catalysts," *Dalton Transactions*, vol. 41, no. 43, pp. 13413–13422, 2012.

[61] S. Hosseininejad, A. Afacan, and R. E. Hayes, "Catalytic and kinetic study of methanol dehydration to dimethyl ether," *Chemical Engineering Research and Design*, vol. 90, no. 6, pp. 825–833, 2012.

[62] J. J. Spivey, "Review: Dehydration catalysts for the methanol/dimethyl ether reaction," *Chemical Engineering Communications*, vol. 110, no. 1, pp. 123–142, 1991.

[63] B. C. Gates and L. N. Johanson, "Langmuir-hinshelwood kinetics of the dehydration of methanol catalyzed by cation exchange resin," *AIChE Journal*, vol. 17, pp. 981–983, jul 1971.

[64] J. Bandiera and C. Naccache, "Kinetics of methanol dehydration on dealuminated H-mordenite: Model with acid and basic active centres," *Applied Catalysis*, vol. 69, no. 1, pp. 139–148, 1991.

[65] P. K. Kiviranta-Pääkkönen, L. K. Struckmann née Rihko, J. A. Linnekoski, and A. O. I. Krause, "Dehydration of the Alcohol in the Etherification of Isoamylenes with Methanol and Ethanol," *Industrial and Engineering Chemistry Research*, vol. 37, no. 1, pp. 18–24, 1998.

[66] Z. Lei, Z. Zou, C. Dai, Q. Li, and B. Chen, "Synthesis of dimethyl ether (DME) by catalytic distillation," *Chemical Engineering Science*, vol. 66, no. 14, pp. 3195–3203, 2011.

[67] J. Jain and C. Pillai, "Dehydration of alcohols over alumina," *Journal of Catalysis*, vol. 9, pp. 322–330, 1967.

[68] J. E. Dabrowski, J. B. Butt, and H. Bliss, "Monte carlo simulation of a catalytic surface: Activity and selectivity of g-alumina for dehydration," *Journal of Catalysis*, vol. 18, no. 3, pp. 297–313, 1970.

[69] H. Knözinger, K. Kochloefl, and W. Meye, "Kinetics of the bimolecular ether formation from alcohols over alumina," *Journal of Catalysis*, vol. 28, no. 1, pp. 69–75, 1973.

[70] S. R. Blaszkowski and R. A. Van Santen, "The mechanism of dimethyl ether formation from methanol catalyzed by zeolitic protons," *Journal of the American Chemical Society*, vol. 118, no. 21, pp. 5152–5153, 1996.

[71] S. R. Blaszkowski and R. A. Van Santen, "The mechanism of dimethyl ether formation from methanol catalyzed by zeolitic protons," *Journal of Physical Chemistry B*, vol. 101, pp. 2292–2305, 1997.

[72] J. Topp-Jorgensen, "Process for the preparation of catalysts for use in ether synthesis," 1985.

[73] J. B. Hansen, F. H. Joensen, and H. F. Topsoe, "Process for preparing acetic acid, methyl acetate, acetic anhydride of mixtures thereof," 1993.

[74] V. Vishwanathan, H.-S. Roh, J.-W. Kim, and K.-W. Jun, "Surface Properties and Catalytic Activity of TiO2 ZrO2 Mixed Oxides in Dehydration of Methanol to Dimethyl Ether," *Catalysis Letters*, vol. 96, no. 1-2, pp. 23–28, 2004.

[75] Y. Fu, T. Hong, J. Chen, A. Auroux, and J. Shen, "Surface acidity and the dehydration of methanol to dimethyl ether," *Thermochimica Acta*, vol. 434, no. 1-2, pp. 22–26, 2005.

[76] M. Mollavali, F. Yaripour, S. Mohammadi-Jam, and H. Atashi, "Relationship between surface acidity and activity of solid-acid catalysts in vapour phase dehydration of methanol," *Fuel Processing Technology*, vol. 90, no. 9, pp. 1093–1098, 2009.

[77] C. W. Seo, K. D. Jung, K. Y. Lee, and K. S. Yoo, "Dehydration of methanol over Nordstrandite based catalysts for dimethyl ether synthesis," *Journal of Industrial and Engineering Chemistry*, vol. 15, no. 5, pp. 649–652, 2009.

[78] Z. Hosseini, M. Taghizadeh, and F. Yaripour, "Synthesis of nanocrystalline g-Al2O3 by sol-gel and precipitation methods for methanol dehydration to dimethyl ether," *Journal of Natural Gas Chemistry*, vol. 20, no. 2, pp. 128–134, 2011.

[79] W. H. Chen, B. J. Lin, H. M. Lee, and M. H. Huang, "One-step synthesis of dimethyl ether from the gas mixture containing CO2 with high space velocity," *Applied Energy*, vol. 98, pp. 92–101, 2012.

[80] J. C. Woodhouse, "Process for the preparation of methyl ether," 1935.

[81] S. Hosseini, M. Taghizadeh, and A. Eliassi, "Optimization of hydrothermal synthesis of H-ZSM-5 zeolite for dehydration of methanol to dimethyl ether using full factorial design," *Journal of Natural Gas Chemistry*, vol. 21, no. 3, pp. 344–351, 2012.

[82] J. M. Campelo, A. Garcia, J. F. Herencia, D. Luna, J. M. Marinas, and A. A. Romero, "Conversion of Alcohols (alpha-Methylated Series) on AlPO4 Catalysts," *Journal of Catalysis*, vol. 151, pp. 307–314, 1995.

[83] F. Yaripour, F. Baghaei, I. Schmidt, and J. Perregaarad, "Synthesis of dimethyl ether from methanol over aluminium phosphate and silica-titania catalysts," *Catalysis Communications*, vol. 6, no. 8, pp. 542–549, 2005.

[84] V. Siva Kumar, A. H. Padmasri, C. V. Satyanarayana, I. Ajit Kumar Reddy, B. David Raju, and K. S. Rama Rao, "Nature and mode of addition of phosphate precursor in the synthesis of aluminum phosphate and its influence on methanol dehydration to dimethyl ether," *Catalysis Communications*, vol. 7, no. 10, pp. 745–751, 2006.

[85] K. Lertjiamratn, P. Praserthdam, M. Arai, and J. Panpranot, "Modification of acid properties and catalytic properties of AlPO4 by hydrothermal pretreatment for methanol dehydration to dimethyl ether," *Applied Catalysis A: General*, vol. 378, no. 1, pp. 119–123, 2010.

[86] K. Nakajima, Y. Baba, R. Noma, M. Kitano, J. N. Kondo, S. Hayashi, and M. Hara, "Nb2O5nH2O as a Heterogeneous Catalyst with Water-Tolerant Lewis Acid Sites," *Journal of the American Chemical Society*, vol. 133, pp. 4224–4227, mar 2011.

[87] Z.-h. Chen, T. Iizuka, and K. Tanabe, "Niobic acid as an efficient catalyst for vapor phase esterification of ehtyl alcohol with acetic acid," *Chemistry Letters*, vol. 13, no. 7, pp. 1085–1088, 1984.

[88] K. Tanabe, "Niobic acid as an unusual acidic solid material," *Materials Chemistry and Physics*, vol. 17, no. 1-2, pp. 217–225, 1987.

[89] K. Tanabe and S. Okazaki, "Various reactions catalyzed by niobium compounds and materials," *Applied Catalysis A, General*, vol. 133, no. 2, pp. 191–218, 1995.

[90] Q. Sun, Y. Fu, H. Yang, A. Auroux, and J. Shen, "Dehydration of methanol to dimethyl ether over Nb2O5 and NbOPO4 catalysts: Microcalorimetric and FT-IR studies," *Journal of Molecular Catalysis A: Chemical*, vol. 275, no. 1-2, pp. 183–193, 2007.

[91] R. Ladera, E. Finocchio, S. Rojas, J. L. G. Fierro, and M. Ojeda, "Supported niobium catalysts for methanol dehydration to dimethyl ether: FTIR studies of acid properties," *Catalysis Today*, vol. 192, no. 1, pp. 136–143, 2012.

[92] A. S. Rocha, A. M. Aline, E. R. Lachter, E. F. Sousa-Aguiar, and A. C. Faro, "Niobia-modified aluminas prepared by impregnation with niobium peroxo complexes for dimethyl ether production," *Catalysis Today*, vol. 192, no. 1, pp. 104–111, 2012.

[93] S. H. Lima, A. M. S. Forrester, L. A. Palacio, and A. C. Faro, "Niobia-alumina as methanol dehydration component in mixed catalyst systems for dimethyl ether production from syngas," *Applied Catalysis A: General*, vol. 488, pp. 19–27, 2014.

[94] R. J. Da Silva, A. F. Pimentel, R. S. Monteiro, and C. J. A. Mota, "Synthesis of methanol and dimethyl ether from the CO2 hydrogenation over Cu.ZnO supported on Al2O3 and Nb2O5," *Journal of CO2 Utilization*, vol. 15, pp. 83–88, 2016.

[95] M. Xu, J. H. Lunsford, D. Goodman, and A. Bhattacharyya, "Synthesis of dimethyl ether (DME) from methanol over solid-acid catalysts," *Applied Catalysis A: General*, vol. 149, no. 2, pp. 289–301, 1997.

[96] V. Vishwanathan, K. W. Jun, J. W. Kim, and H. S. Roh, "Vapour phase dehydration of crude methanol to dimethyl ether over Na-modified H-ZSM-5 catalysts," *Applied Catalysis A: General*, vol. 276, no. 1-2, pp. 251–255, 2004.

[97] F. Raoof, M. Taghizadeh, A. Eliassi, and F. Yaripour, "Effects of temperature and feed composition on catalytic dehydration of methanol to dimethyl ether over gamma-alumina," *Fuel*, vol. 87, no. 13-14, pp. 2967–2971, 2008.

[98] K. Tanabe, "Catalytic application of niobium compounds," *Catalysis Today*, vol. 78, pp. 65–77, 2003.

[99] I. Nowak and M. Ziolek, "Niobium Compounds: Preparation, Characterization, and Application in Heterogeneous Catalysis," *Chemical Review*, vol. 99, pp. 3603–3624, 1999.

[100] T. Iizuka, K. Ogasawara, and K. Tanabe, "Acidic and Catalytic Properties of Niobium Pentaoxide.," 1983.

[101] J. R. H. Ross, R. H. H. Smits, and K. Seshan, "The use of niobia in oxidation catalysis," *Catalysis Today*, vol. 16, no. 3-4, pp. 503–511, 1993.

[102] P. Carniti, A. Gervasini, S. Biella, and A. Auroux, "Niobic acid and niobium phosphate as highly acidic viable catalysts in aqueous medium: Fructose dehydration reaction," *Catalysis Today*, vol. 118, no. 3-4 SPEC. ISS., pp. 373–378, 2006.

[103] K. Ogasawara, T. Iizuka, and K. Tanabe, "Ethylene hydration over niobic acid catalysts," *Chemistry Letters*, vol. 13, pp. 645–648, 1984.

[104] T. Ushikubo, "Recent topics of research and development of catalysis by niobium and tantalum oxides," *Catalysis Today*, vol. 57, pp. 331–338, 2000.

[105] D. M. Antonelli, A. Nakahira, and J. Y. Ying, "Ligand-Assisted Liquid Crystal Templating in Mesoporous Niobium Oxide Molecular Sieves," *Inorganic Chemistry*, vol. 35, no. 11, pp. 3126–3136, 1996.

[106] D. M. Antonelli and J. Y. Ying, "Synthesis of a stable hexagonally packed Mesoporous niobium oxide molecular sieve through a novel ligand-assisted templating mechanism," *Angewandte Chemie International Edition*, vol. 35, no. 4, pp. 426–430, 1996.

[107] K. Okumura, T. Tomiyama, S. Shirakawa, S. Ishida, T. Sanada, M. Arao, and M. Niwa, "Hydrothermal synthesis and catalysis of Nb2O5WOx nanofiber crystal," *Journal of Materials Chemistry*, vol. 21, no. 1, p. 229, 2011.

[108] T. Murayama, J. Chen, J. Hirata, K. Matsumoto, and W. Ueda, "Hydrothermal synthesis of octahedra-based layered niobium oxide and its catalytic activity as a solid acid," *Catalysis Science & Technology*, vol. 4, pp. 4250–4257, 2014.

[109] C. L. T. Da Silva, V. L. L. Camorim, J. L. Zotin, M. L. R. Duarte Pereira, and A. d. C. Faro, "Surface acidic properties of alumina-supported niobia prepared by chemical vapour deposition and hydrolysis of niobium pentachloride," *Catalysis Today*, vol. 57, no. 3-4, pp. 209–217, 2000.

[110] T. Kitano, T. Shishido, K. Teramura, and T. Tanaka, "Brønsted Acid Property of Alumina-Supported Niobium Oxide Calcined at High Temperatures: Characterization by Acid-Catalyzed Reactions and Spectroscopic Methods," *Journal of Physical Chemistry C*, vol. 116, pp. 11615–11625, 2012.

[111] T. Kitano, T. Shishido, K. Teramura, and T. Tanaka, "Acid property of Nb2O5/Al2O3 prepared by impregnation method by using niobium oxalate solution: Effect of pH on the structure and acid property," *Catalysis Today*, vol. 226, pp. 97–102, 2014.

[112] F. M. T. Mendes, C. A. C. Perez, F. B. Noronha, C. D. D. Souza, D. V. Cesar, H. J. Freund, and M. Schmal, "Fischer-Tropsch synthesis on anchored Co/Nb2O5/Al2O3 catalysts: the nature of the surface and the effect on chain growth.," *The Journal of Physical Chemistry B*, vol. 110, no. 18, pp. 9155–9163, 2006.

[113] Y. Xiang, R. Barbosa, X. Li, and N. Kruse, "Ternary Cobalt-Copper-Niobium Catalysts for the Selective CO Hydrogenation to Higher Alcohols," *ACS Catalysis*, vol. 5, no. 5, pp. 2929–2934, 2015.

[114] C. Hernández Mejía, J. H. den Otter, J. L. Weber, and K. P. de Jong, "Crystalline niobia with tailored porosity as support for cobalt catalysts for the FischerTropsch synthesis," *Applied Catalysis A: General*, vol. 548, no. July, pp. 143–149, 2017.

[115] J. Sun, G. Yang, Y. Yoneyama, and N. Tsubaki, "Catalysis chemistry of dimethyl ether synthesis," *ACS Catalysis*, vol. 4, no. 10, pp. 3346–3356, 2014.

[116] F. Dadgar, R. Myrstad, P. Pfeifer, A. Holmen, and H. J. Venvik, "Direct dimethyl ether synthesis from synthesis gas: The influence of methanol dehydration on methanol synthesis reaction.," *Catalysis Today*, vol. 270, pp. 76–84, 2015.

[117] J. Wu, M. Saito, M. Takeuchi, and T. Watanabe, "The stability of Cu/ZnO-based catalysts in methanol synthesis from a CO2-rich feed and from a CO-rich feed," *Applied Catalysis A: General*, vol. 218, no. 1-2, pp. 235–240, 2001.

[118] Y. Luan, H. Xu, C. Yu, W. Li, and S. Hou, "Effects and control of steam in the systems of methanol and DME synthesis from syngas over Cu-based catalysts," *Catalysis Letters*, vol. 125, no. 3-4, pp. 271–276, 2008.

[119] F. Dadgar, R. Myrstad, P. Pfeifer, A. Holmen, and H. J. Venvik, "Catalyst Deactivation During One-Step Dimethyl Ether Synthesis from Synthesis Gas," *Catalysis Letters*, vol. 147, no. 4, pp. 865–879, 2017.

[120] P. B. Weisz, "Polyfunctional Heterogeneous Catalysis," *Advances in Catalysis*, vol. 13, no. C, pp. 137–190, 1962.

[121] F. A. Cavalcanti, A. Y. Stakheev, and W. M. Sachtler, "Direct synthesis of methanol, dimethyl ether, and paraffins from syngas over Pd/zeolite Y catalysts," *Journal of Catalysis*, vol. 134, no. 1, pp. 226–241, 1992.

[122] J. Francis, E. Guillon, N. Bats, C. Pichon, A. Corma, and L. J. Simon, "Design of improved hydrocracking catalysts by increasing the proximity between acid and metallic sites," *Applied Catalysis A: General*, vol. 409-410, pp. 140–147, 2011.

[123] N. Batalha, L. Pinard, C. Bouchy, E. Guillon, and M. Guisnet, "N-Hexadecane hydroisomerization over Pt-HBEA catalysts. Quantification and effect of the intimacy between metal and protonic sites," *Journal of Catalysis*, vol. 307, pp. 122–131, 2013.

[124] J. Kim, W. Kim, Y. Seo, J. C. Kim, and R. Ryoo, "N-Heptane hydroisomerization over Pt/MFI zeolite nanosheets: Effects of zeolite crystal thickness and platinum location," *Journal of Catalysis*, vol. 301, pp. 187–197, 2013.

[125] K. Cheng, B. Gu, X. Liu, J. Kang, Q. Zhang, and Y. Wang, "Direct and Highly Selective Conversion of Synthesis Gas into Lower Olefins: Design of a Bifunctional Catalyst Combining Methanol Synthesis and Carbon-Carbon Coupling," *Angewandte Chemie - International Edition*, vol. 55, no. 15, pp. 4725–4728, 2016.

[126] M. Guisnet, "Ideal bifunctional catalysis over Pt-acid zeolites," *Catalysis Today*, vol. 218-219, pp. 123–134, 2013.

[127] J. Zecevic, G. Vanbutsele, K. P. de Jong, and J. A. Martens, "Nanoscale intimacy in bifunctional catalysts for selective conversion of hydrocarbons," *Nature*, vol. 528, no. 7581, pp. 245–248, 2015.

[128] A. Telhado Pereira, K. Alves de Oliveira, R. de Souza Monteiro, and Companhia Brasileira de Metalurgia e Mineração, "Process of Production of Ammonium Niobium Oxalate, Ammonium Niobium Oxalate and use of the same," 2006.

[129] T. T. Su, Y. C. Zhai, H. Jiang, and H. Gong, "Studies on the thermal decomposition kinetics and mechanism of ammonium niobium oxalate," *Journal of Thermal Analysis and Calorimetry*, vol. 98, no. 2, pp. 449–455, 2009.

[130] C. Jeong, H. Ham, J. W. Bae, D.-C. Kang, C.-H. Shin, J. H. Baik, and Y.-W. Suh, "Facile Structure Tuning of a Methanol Synthesis Catalyst Towards Direct Synthesis of Dimethyl Ether from Syngas," *ChemCatChem*, vol. 9, no. 24, pp. 4484–4489, 2017.

[131] W. Bragg and W. Bragg, "The Reflection of X-rays by Crystals," *Proceedings of the Royal Society of London. Series A, Containing Papers of a Mathematical and Physical Character*, vol. 88, pp. 428–438, 1913.

[132] I. Chorkendorff and J. W. Niemantsverdriet, *Concepts of Modern Catalysis and Kinetics*. Weinheim: Wiley-VCH Verlag GmbH & Co. KGaA, 2003.

[133] M. Thommes, K. Kaneko, A. V. Neimark, J. P. Olivier, F. Rodriguez-Reinoso, J. Rouquerol, and K. S. W. Sing, "Physisorption of gases, with special reference to the evaluation of surface area and pore size distribution (IUPAC Technical Report)," *Pure and Applied Chemistry*, vol. 87, no. 9-10, pp. 1051–1069, 2015.

[134] R. Erni, M. D. Rossell, C. Kisielowski, and U. Dahmen, "Atomic-Resolution Imaging with a Sub-50-pm Electron Probe," *Physical Review Letters*, vol. 102, no. 9, pp. 1–4, 2009.

[135] R. E. Russo, X. L. Mao, H. C. Liu, J. H. Yoo, and S. S. Mao, "Time-resolved plasma diagnostics and mass removal during single-pulse laser ablation," *Applied Physics A: Materials Science and Processing, Supplement 1*, vol. 69, no. 7, pp. S887–S894, 1999.

[136] P. Mason and H. de Waard, "Laser ablation ICP-MS - Petrology - Universiteit Utrecht," 2017.

[137] S. Asbrink and L.-J. Norrby, "A Refinement of the Crystal Structure of Copper(II) Oxide with a Discussion of Some Exceptional E.s.d.'s," *Acta Crystallographica Section B Structural Science*, vol. 26, pp. 8–15, 1970.

[138] E. Kisi and M. Elcombe, "u Parameters for the Wurtzite Structure of ZnS and ZnO using Powder Neutron Diffraction," *Acta Crystallographica Section C Crystal Structure Communications*, vol. 45, pp. 1867–1870, 1989.

[139] E. Felten, "The Preparation of CuNb2O6 and CuTa2O6," *Journal of Inorganic and Nuclear Chemistry*, vol. 29, pp. 1168–1171, 1967.

[140] D. Pfoertsch and R. Schwartz, "ICDD Grant-in-Aid," 1986.

Appendices

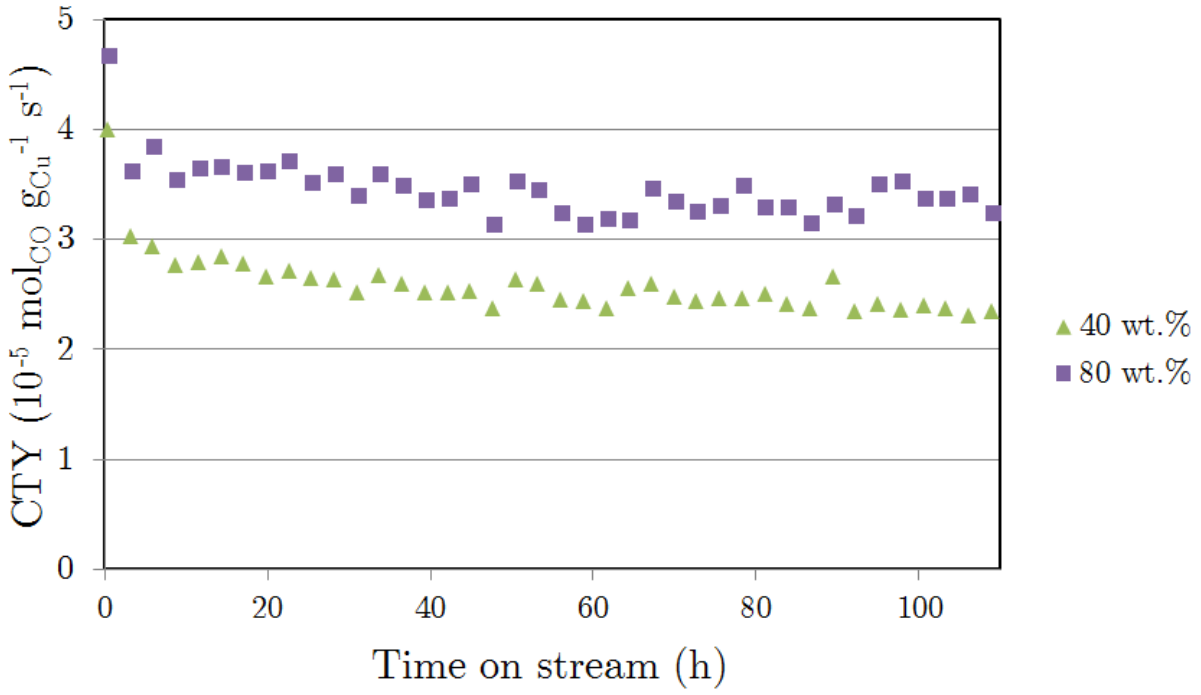

Figure 8.1: Activity of various physical mixtures with commercially available methanol synthesis catalyst and niobic acid precipitated using ammonium carbonate.

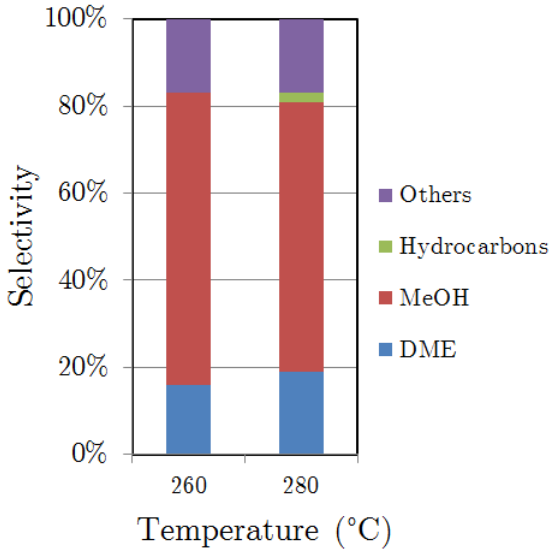

Figure 8.2: Selectivity of a physical mixtures with 60 wt.% commercially available methanol synthesis catalyst and 40 wt.% niobic acid precipitated using ammonium carbonate.

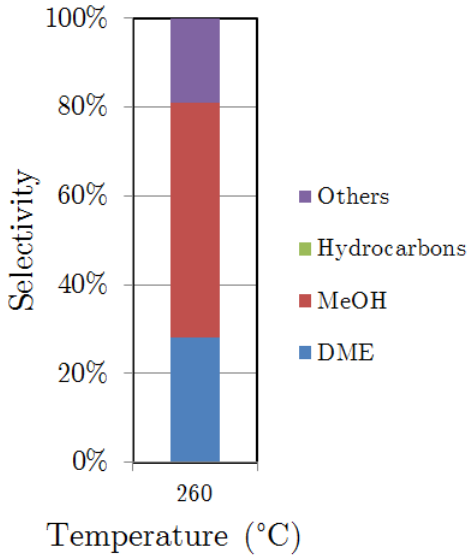

Figure 8.3: Selectivity of a physical mixtures with 20 wt.% commercially available methanol synthesis catalyst and 80 wt.% niobic acid precipitated using ammonium carbonate.

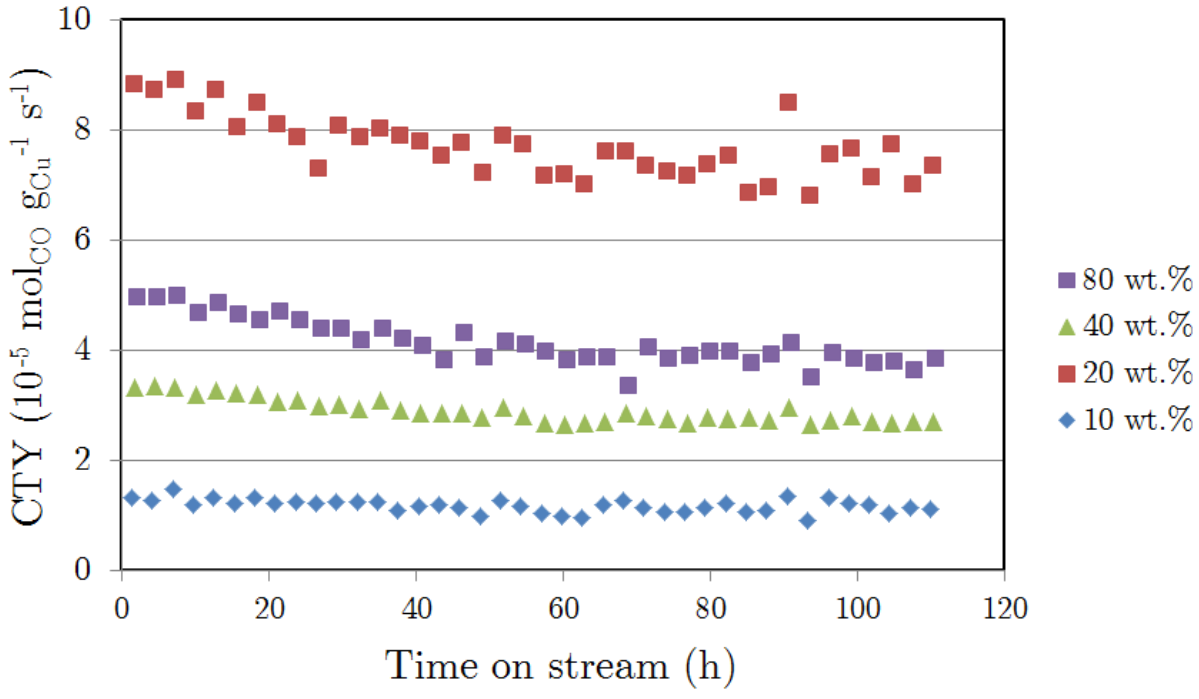

Figure 8.4: Activity of various physical mixtures with Cu/Zn based methanol synthesis catalyst, prepared from precipitation using oxalic acid, and commercially available niobic acid.

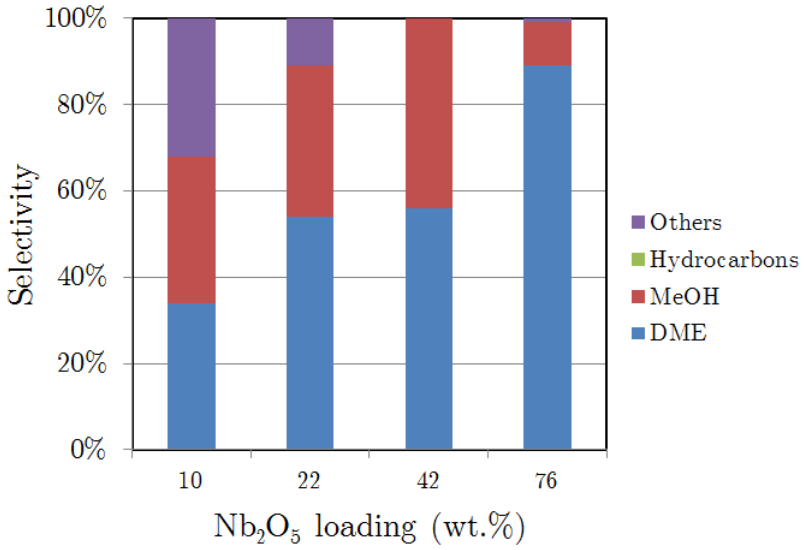

Figure 8.5: Selectivity of physical mixtures. using using Cu/Zn catalyst prepared by precipitation using a solution of oxalic acid in acetone and commercially available niobic acid.

Weight loading Nb_2O_5 (%)	Amount of NH_3 (mmol/g)	T at max (°C)
40	2.1	340
80	0.87	330
$Nb_2O_5 \cdot nH_2O$ calcined at 400 °C	0.78	178

Table 8.1: Ammonia TPD data of various physical mixture of commercial CZA catalyst and niobia prepared by precipitation using an aqueous solution of ammonium carbonate.

Weight loading Nb_2O_5 (%)	Amount of NH_3 (mmol/g)	T at max (°C)
10	0.27	260
20	0.33	275
40	0.54	285
80	0.78	315
$Nb_2O_5 \cdot nH_2O$ calcined at 400 °C	0.78	178

Table 8.2: Ammonia TPD data of a various physical mixture of a Cu/Zn catalyst prepared by precipitation using a solution of oxalic acid in acetone and commercially available niobia.

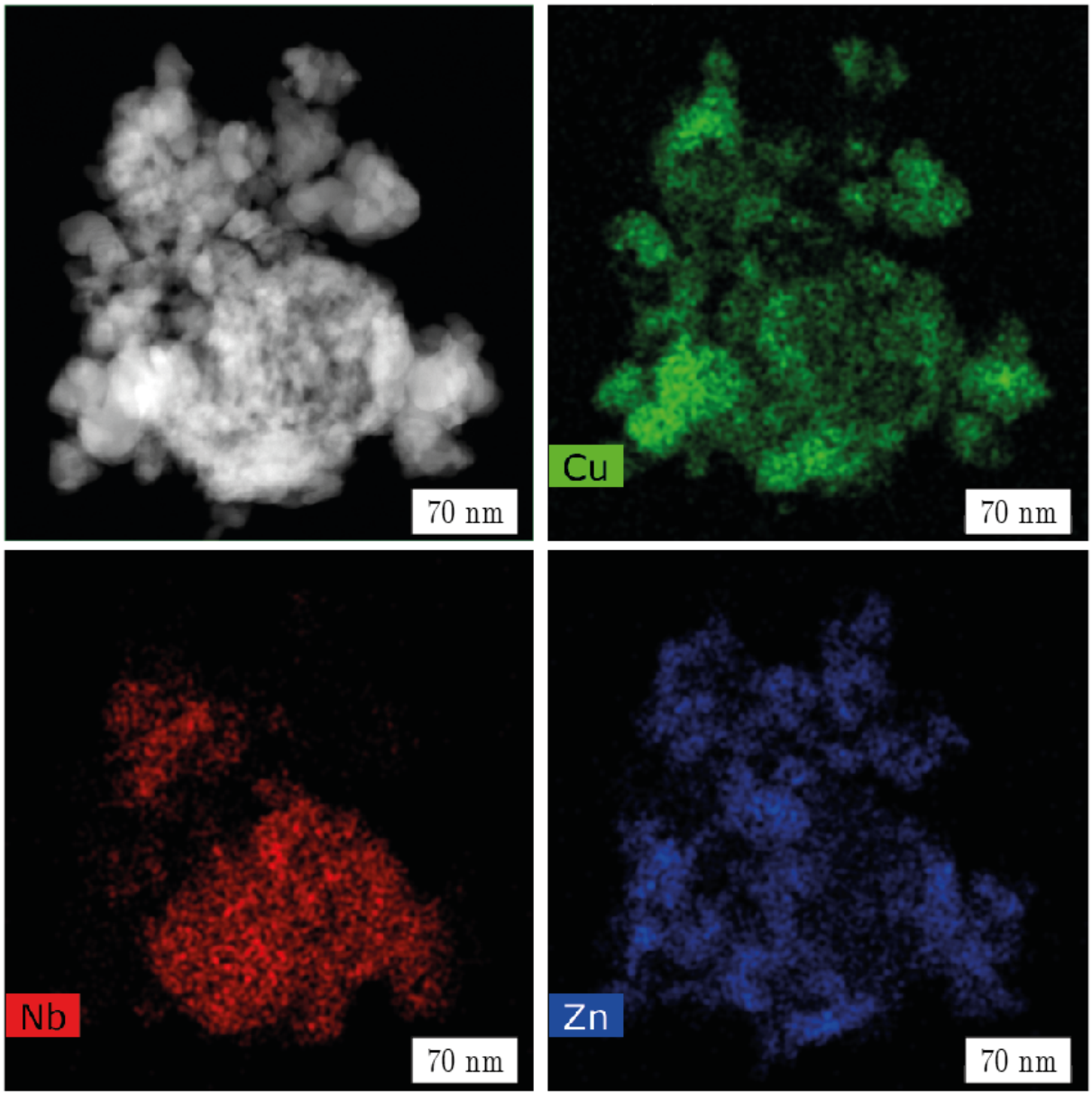

Figure 8.6: Additional HAADF-STEM-EDX images of a sample prepared by co-precipitation using an aqueous solution of ammonium carbonate, containing 32 wt.% Nb_2O_5.

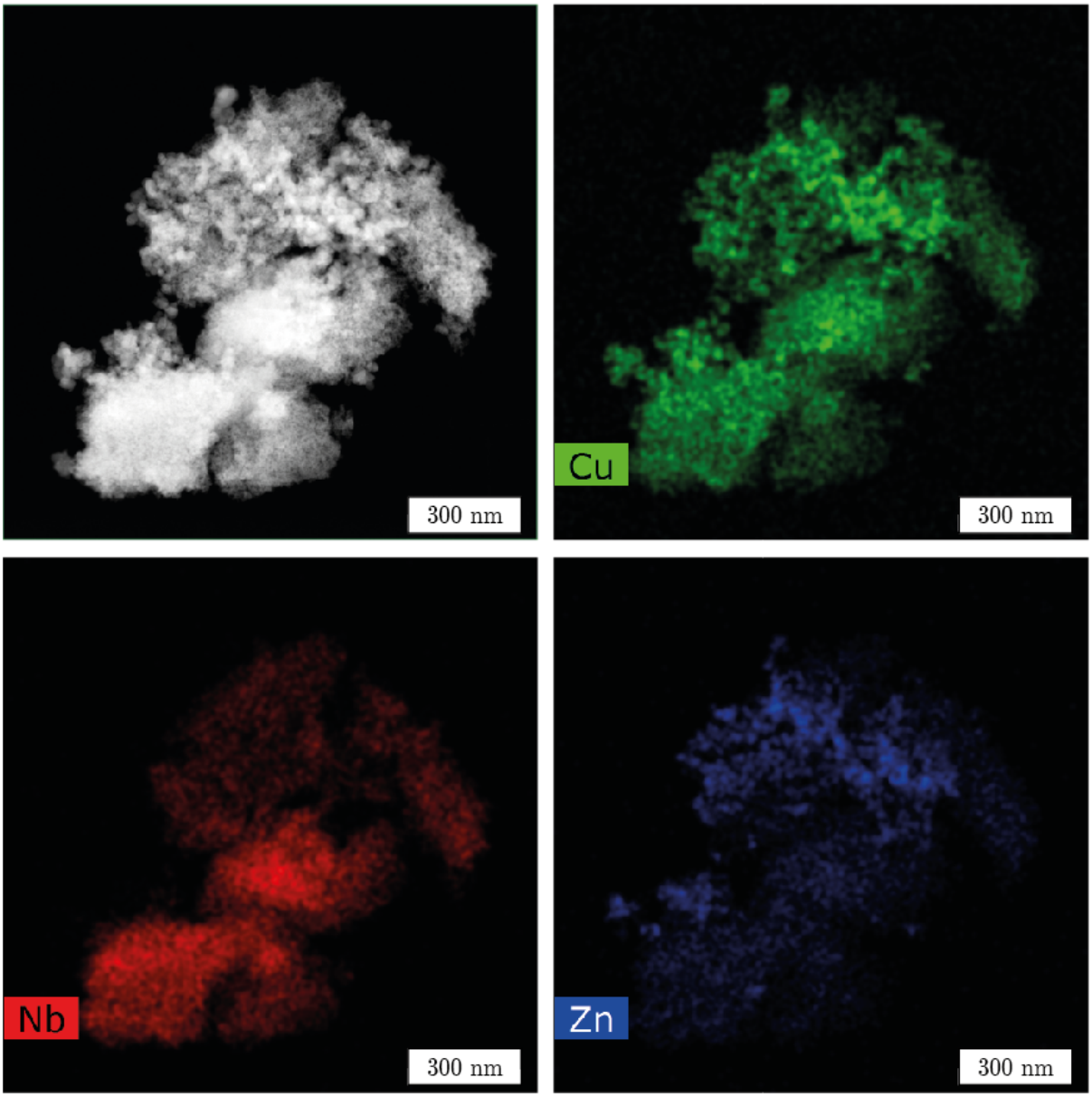

Figure 8.7: Additional HAADF-STEM-EDX images of a sample prepared by co-precipitation using an aqueous solution of ammonium carbonate, containing 32 wt.% Nb_2O_5.

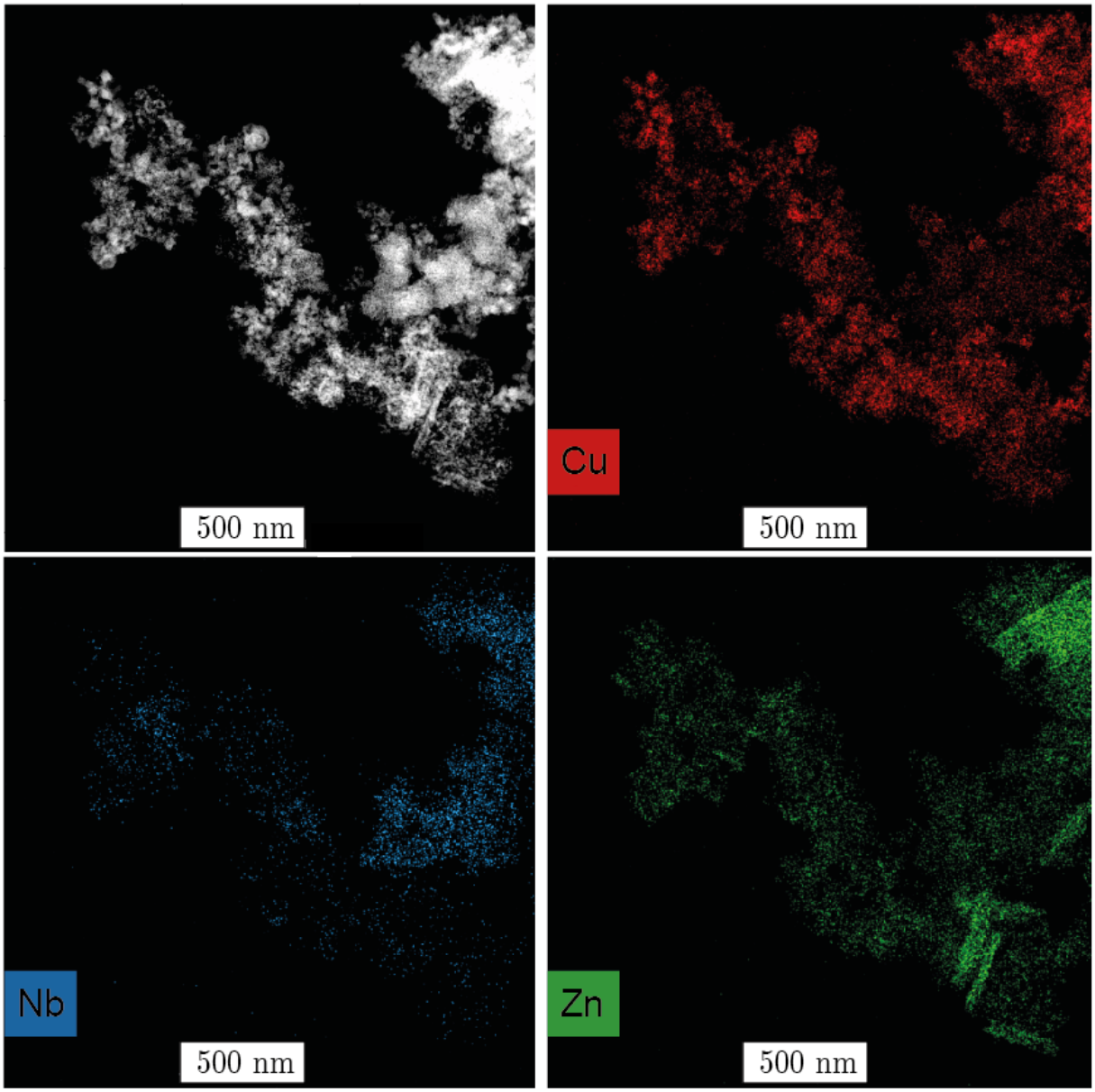

Figure 8.8: Additional HAADF-STEM-EDX images of a sample prepared by sequential precipitation using a solution of oxalic acid in acetone, containing 40 wt.% Nb_2O_5.

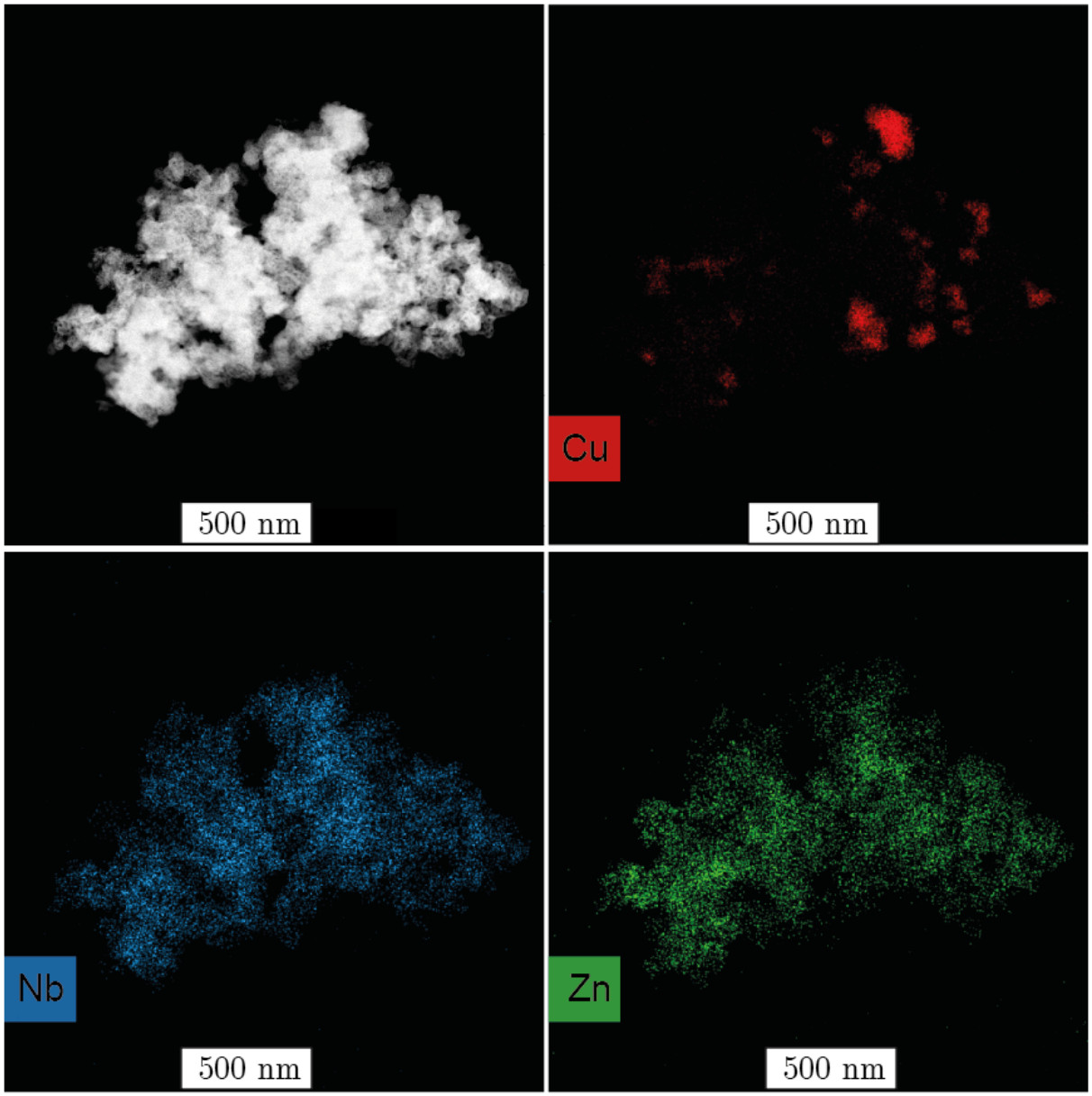

Figure 8.9: Additional HAADF-STEM-EDX images of a sample prepared by sequential precipitation using a solution of oxalic acid in acetone, containing 80 wt.% Nb_2O_5.